Spring 1993

Unreinforced masonry structures : nonlinear analysis and evaluation of some rehab schemes

Sanjay Mehta
New Jersey Institute of Technology

Copyright Warning & Restrictions

The copyright law of the United States (Title 17, United States Code) governs the making of photocopies or other reproductions of copyrighted material.

Under certain conditions specified in the law, libraries and archives are authorized to furnish a photocopy or other reproduction. One of these specified conditions is that the photocopy or reproduction is not to be "used for any purpose other than private study, scholarship, or research." If a, user makes a request for, or later uses, a photocopy or reproduction for purposes in excess of "fair use" that user may be liable for copyright infringement,

This institution reserves the right to refuse to accept a copying order if, in its judgment, fulfillment of the order would involve violation of copyright law.

Please Note: The author retains the copyright while the New Jersey Institute of Technology reserves the right to distribute this thesis or dissertation

Printing note: If you do not wish to print this page, then select "Pages from: first page # to: last page #" on the print dialog screen

Order Number 9401734

Unreinforced masonry structures: Nonlinear analysis and evaluation of some rehab schemes

Mehta, Sanjay S., Ph.D.

New Jersey Institute of Technology, 1993

U·M·I

300 N. Zeeb Rd.
Ann Arbor, MI 48106

UNREINFORCED MASONRY STRUCTURES: NONLINEAR ANALYSIS AND EVALUATION OF SOME REHAB SCHEMES

by
Sanjay Mehta

A Dissertation
Submitted to the Faculty of
New Jersey Institute of Technology
in Partial Fulfillment of the Requirements for the Degree of
Doctor of Philosophy

Department of Civil and Environmental Engineering

May 1993

ABSTRACT

UNREINFORCED MASONRY STRUCTURES: NONLINEAR ANALYSIS AND EVALUATION OF SOME REHAB SCHEMES

by

Sanjay Mehta

Unreinforced masonry (URM) structures have been a common type of construction in the past and are still used in regions of low seismicity. Retrofitting of these structures is necessary because of two reasons: Firstly, observed damage after earthquakes reveals that URM construction is one of the most hazardous constructions even in the region of low seismicity; secondly, reclassification of seismic zones would require retrofitting of existing structures to comply with new guidelines for earthquake design.

Retrofitting measures require that the response of original and new structural systems as well as their interaction be considered. It is therefore important to correctly understand and predict the response of URM structures before implementing any strengthening scheme. Special techniques for analysis of URM structures are necessary because mortar joints act as planes of weakness.

In this thesis a new approach for analytical modeling of URM structures is presented with a special emphasis on nonlinear behavior of mortar joints. This approach is included in a general purpose finite element software so that various options of the software can be effectively utilized for linear and nonlinear analysis of different structural systems under static and dynamic loading conditions.

The analytical scheme is verified at element as well as structure level by comparison with available experimental and analytical results. Two rehabilitation schemes commonly used to strengthen existing URM structures are analyzed and their effectiveness in increasing strength and stiffness is discussed. Finally, nonlinear dynamic analysis is performed to study the effect of ground motion on URM walls and rehabilitation schemes.

APPROVAL PAGE

UNREINFORCED MASONRY STRUCTURES: NONLINEAR ANALYSIS AND EVALUATION OF SOME REHAB SCHEMES

Sanjay Mehta

Dr. M. Ala Saadeghvaziri, Thesis Advisor (date)

Assistant Professor of Civil and Environmental Engineering, NJIT

Dr. W. R. Spillers, Committee Member (date)

Chairperson and Professor of Civil and Environmental Engineering, NJIT

Dr. C. T. Thomas Hsu, Committee Member (date)

Professor of Civil and Environmental Engineering, NJIT

E. G. Dauenheimer, Committee Member (date)

Professor of Civil and Environmental Engineering, NJIT

Dr. Rajesh Dave, Committee Member (date)

Associate Professor of Mechanical Engineering, NJIT

BIOGRAPHICAL SKETCH

Author: Sanjay Mehta

Degree: Doctor of Philosophy in Civil Engineering

Date: May 1993

Undergraduate and Graduate Education:

- Doctor of Philosophy in Civil Engineering,
  New Jersey Institute of Technology, Newark, NJ, 1993.

- Master of Engineering in Civil Engineering,
  Victoria Jubilee Technical Institute, Bombay, India, 1989.

- Bachelor of Engineering in Civil Engineering,
  Victoria Jubilee Technical Institute, Bombay, India, 1987.

Major: Civil Engineering

Presentations and Publications:

Saadeghvaziri, M. A., and Mehta, S. S., "Finite Element Model for Unreinforced Masonry Structures," Conference on Nonlinear Engineering Computations, Swansea, U. K., September 1991.

Mehta, S. S., and Saadeghvaziri, M. A., "Analytical Evaluation of Joint Stiffness in Unreinforced Masonry Structures," Sixth Canadian Conference on Masonry Structures, Canada, June 1992.

Saadeghvaziri, M. A. and Mehta, S. S., "Analytical Model for Unreinforced Masonry Structures," Accepted for Publication, Sixth North American Masonry Conference, Philadelphia, Pennsylvania, June 1993 (will be published, peer reviewed).

ACKNOWLEDGMENT

This report is based on the work done by Sanjay Mehta towards a Doctoral Degree in Civil Engineering. The research was conducted under the guidance of M. Ala Saadeghvaziri, whose technical advice and moral support are greatly appreciated. Thanks are due to the members of the doctoral committee: Profs. W. R. Spillers, C. T. Hsu, E. G. Dauenheimer, R. Dave for their expert opinion during the research work.

The financial support for this work came in part from the Department of Civil and Environmental Engineering at the New Jersey Institute of Technology and from the National Science Foundation under grant BCS-9109115. This support is greatly appreciated. The results, opinions, and conclusions expressed in this report are solely those of the author and do not necessarily reflect those of sponsors.

Numerical computations were done on SPARC workstation. Unlimited computer time, large amount of disk space, and excellent networking provided by Computer Aided Engineering Laboratory and Civil Engineering Computer Laboratory is very greatly appreciated. Thanks are also due to Dr. D. Perel and system administrators in Computer Laboratories for their help in system maintenance.

TABLE OF CONTENTS

Chapter **Page**

LIST OF TABLES

Table **Page**

LIST OF FIGURES

Figure **Page**

CHAPTER 1

INTRODUCTION

In this chapter the necessity for repair and retrofit of URM structures is discussed. An overview of various experimental projects is presented followed by the need for analytical studies and objectives of the present study.

1.1 Background

Observed damage after earthquakes reveals that unreinforced masonry (URM) construction is one of the most hazardous constructions in seismic regions. In 1981, to better protect its residents from seismic hazards, the City of Los Angeles adopted an earthquake safety ordinance that requires the strengthening of URM buildings constructed prior to 1934 [33]. The purpose of this ordinance is twofold: (1) to provide a minimum level of seismic resistance for URM buildings, approximately 60 to 70 percent of the lateral load resistance for new low-rise structures and, (2) to reduce the risk of death and injury during an earthquake.

The Whittier Narrows Earthquake of October 1987 provided an excellent opportunity to evaluate the current guidelines for repair and rehabilitation of URM structures. Although there was no loss of life nor serious injury due to the relatively low magnitude of the earthquake (5.9 on the Richter scale), observed damage demonstrated a clear-cut need to improve certain aspects of the code design standards for strengthening URM buildings [18].

In October 1989, a large number of URM structures were damaged and suffered partial collapse during the Loma Prieta Earthquake near San Francisco (7.1 on the Richter scale) [3]. There was ample evidence of inplane shear cracking

of URM walls. The out of plane failure of parapet walls resulted in substantial damage to adjacent structure and, in several instances, casualties.

One of the most interesting cases of damage was the Hotel Oakland (Fig. 1.2). The building was "reinforced to prevent collapse and to minimize life safety hazards in a major earthquake". All interior clay tile partitions were removed and replaced by studs and plasterboard. When the earthquake struck, the hotel was the only frame building from which large pieces of masonry facade dropped onto sidewalk below. This partially strengthened building sustained considerably more damage to its facade than any of the unstrengthened buildings in the area [32]. Thus, partial strengthening might have exacerbated the performance of the building.

In December, 1989, the City of Newcastle, Australia experienced an earthquake of magnitude 5.6 on the Richter scale. Once again it was found that despite the relatively low magnitude of the earthquake, URM structures suffered heavy damage [45].

Investigations after these earthquakes revealed that much of the damage resulted from the lack of consideration of earthquake loading in design. This is because building construction using URM predates the development of seismic criteria that guide the design and construction of present-day buildings. Most of the existing URM buildings have been designed for gravity loading. The fact that URM structures have been able to transfer gravity loads for several decades without sustaining any damage proves their capability under vertical stress. However, for lateral loadings the converse is true because the probability of exceeding the return period of an extreme environmental event increases with the age of the building. Therefore, evaluation studies should be directed towards the ability

of the structural system to resist lateral loads rather than vertical loads. With increasing awareness of the hazard posed by existing URM construction, many research projects have been initiated to develop and improve the methodology for repair and retrofit of existing URM structures.

1.2 Recent Studies

ABK, a joint venture consisting of three firms (Agbabian Associates, S. B. Berns and Associates, and Kariotis and Associates all in the Los Angeles area), prepared several reports for the National Science Foundation attempting to develop a methodology for the mitigation of seismic hazards in existing unreinforced masonry buildings. URM walls were subjected to dynamic out-of-plane motions in order (1) to establish bounds on the resistance of URM walls to collapse, (2) to provide data for the development of guidelines and criteria for determining the resistance of this type of wall to collapse, and (3) to evaluate the effectiveness of retrofit procedures for increasing their collapse resistance. The tests were designed to account, as closely as possible, for the nonlinear dynamic interaction between the walls and diaphragms of typical URM buildings. This interaction was included in the test by defining the kinematic environment at the top and base of the walls. Dynamic analyses were performed using lumped parameter model to obtain the kinematic environment at the top and the base of the walls. The lumped parameter models included nonlinear hysteretic characteristics of the diaphragm and the diaphragm/wall mass system. The kinematic environments were obtained for buildings with both stiff and soft diaphragms, for single-story buildings and for walls at various levels in multistory buildings. Various parameters considered in the experimental programs included specimen thickness, height,

unit weight of URM walls, overburden weight and input motions. Based on the experimental results, a methodology was developed for strengthening of existing URM construction. Federal Emergency Management Agency (ATC-22) has adopted ABK recommendations for seismic evaluation and hazard reductions of existing URM structures [2].

In an investigation motivated by U.S. Department of Housing & Urban Development (HUD) in Arizona, Gulkan and others tested single story masonry houses. The objective was to determine the maximum earthquake ground motion intensity that could be resisted by an URM house and to evaluate the additional resistance that would be provided by partial reinforcement for UBC seismic zone 2. It was concluded that if certain construction requirements are satisfied, single story unreinforced masonry houses may be built in seismic zone 2. Although these structures cannot be expected to remain uncracked or undamaged when subjected to zone 2 motions, they will not collapse or endanger life. Design recommendations and formulae were developed for determination of size and strength of shear resisting components [24].

The U. S. - TCCMAR (Technical Coordinating Committee on Masonry Research) program represents a comprehensive coordinated research effort to provide a solid knowledge base on the behavior of reinforced masonry buildings under seismic loadings of various intensities. It is based on the concepts that (1) large or full scale tests are needed to validate analytical models, (2) individual, self contained test modules have to be identified which maximize nation wide utilization of expertise and facilities, and (3) all the experimental modules are interconnected through the common analytical effort to allow the complex synthesis process. Both analytical and experimental investigations at the material, com-

ponent, subassemblage and full-scale prototype building level would be used to provide a broad database for the definition of principal behavioral characteristics and the derivation of design models for reinforced masonry buildings. Tests on a five story full scale prototype reinforced concrete masonry building were planned and carried out as a part of this project which has the ultimate goal of updating and revising reinforced masonry design code. An analytical model for reinforced masonry has been developed using isoparametric elements in which reinforcement and masonry are treated separately but are tied together by compatibility requirements. The constitutive behavior of the fully grouted masonry is based on an orthogonally anisotropic material model and smeared crack theory. Reinforcement can be treated as a discrete or smeared overlay in the horizontal and vertical directions. The analytical model was successfully used to provide monotonic load deformation envelopes for cyclic single-story wall tests. The model was subsequently calibrated using the experimental results and will be used to predict the behavior of components and subassemblages of the 5–story full-scale TCCMAR research building [55].

Epperson and Abrams tested five unreinforced masonry panels extracted from a building constructed in 1917. The objectives of the study were: (1) to verify the accuracy of insitu test for estimating vertical compressive stress and elastic moduli, (2) to study the failure mechanisms for unreinforced brick masonry walls in shear, and to verify the accuracy of insitu tests for estimating inplane shear strength, (3) to explore the general topic of nondestructive evaluation of masonry structures so that basic research needs could be identified for further study. It was found that (1) vertical stress on URM walls could be very well estimated (within 5% error) using single flat jack tests, (2) when masonry was compressed

between two flat jacks, the elastic modulus of the masonry could be measured to within 90 percent of values obtained from the prism tests. However, when test walls were subjected to vertical compressive stress larger than 100 psi, estimates using flat jacks exceeded prism values by as much as 60 percent, (3) estimates of shear strength based on results of shove test, modified by commonly used reduction factors, exceeded the actual ultimate shear strength of test walls by 40 to 70 percent, (4) the ultimate strength of the test walls exceeded flexural cracking strengths by as much as 70 percent. The test walls were observed to deflect substantially after flexural cracking, as the resultant of vertical stress shifted towards the extreme compression face indicating significant stress redistribution, (5) sonic wave velocity tests showed less scatter of measured data than ultrasonic tests because of longer wavelength. In general it was concluded that shear strength is significantly affected by the flexural cracking at the base of the wall and a better failure theory for unreinforced masonry in shear needs to be developed so that estimates of wall capacity can be made more rationally in terms of non-destructive test measurements [22].

As full scale testing of masonry structures is very expensive, researchers at the Drexel University have studied the feasibility of using direct modeling techniques for concrete block masonry. Using the theory of dimensional analysis, the set of necessary scaling model requirements were derived for masonry. Correlations between model and prototype results in basic strength characteristics such as axial compression, joint shear, splitting tension etc., were studied. In general, it was concluded that direct modeling of concrete block masonry is a viable and powerful method to study and improve understanding of the complex behavior of masonry systems [1].

Page [43] studied behavior of clay masonry walls subjected to vertical inplane loading. It was realized that mortar joints act as planes of weakness in URM structures and have strong influence on the strength of URM walls. Dhanasekar and Page developed failure criteria for the brick masonry considering the biaxial state of stress. A series of biaxial compression-compression and compression-tension tests involving 180 panels were carried out on half-scale brick masonry specimens. Using Ramsberg-Osgood formulation, incremental plastic stress-strain relations were developed [20]. Later Ali and Page developed failure criteria for bond failure of mortar joints under combined shear stress and tensile stress [7].

Woodward and Klyde tested several unreinforced masonry walls with an objective of defining the shear capacity of shear-dominated URM walls. The research project was initiated based on the conclusion by the NBS/BSSC review committee for the Applied Technology Council, ATC-06, that research was needed to substantiate and improve the current design recommendations for the shear capacity. Effects of various parameters such as aspect ratio, vertical compression, etc. on the strength of URM walls were studied in a series of experiments [28–30]. It was concluded that (1) the maximum lateral load resistance was affected by the aspect ratio for higher levels of axial compressive stress and, (2) longer walls developed maximum lateral load resistance greater than the resistance associated with diagonal cracking due to shear friction along horizontal cracks in highly compressed regions of the walls [28].

Naraine and Sinha tested 45 half scale brick masonry specimens to study the cyclic behavior of unreinforced brick masonry under biaxial stress conditions. As a conclusion, a failure criterion for masonry in terms of stress invariant was suggested and general empirical equations were proposed for envelope stress-

strain curves, common point curves and stability curves. The common point curve is a locus of points where the reloading portion of any cycle crosses the unloading portion of previous cycle. Stresses above the common point will produce additional strain. Stresses below the common point will result in stress-strain path going into a loop causing the common point to descend to a lower bound called the stability point. The locus of stability points is known as the stability point curve. An exponential relationship involving the axial stress, the axial strain, and the plastic strain was found to be appropriate to represent reloading and unloading curves. It was shown that reloading curves can be mathematically represented by a family of parabolas and unloading curves can be similarly represented by a family of straight lines. Equations of a parent parabola and a parent straight line were used to generate family of parabolas and family of straight lines respectively. Comparisons of model predictions with experimental reloading and unloading curves showed very good agreement [40].

1.3 The Need for Analytical Studies

Experimental projects mentioned in the previous section have generated sufficient information to carry out development of analytical models for URM structures. As suggested by the National Science Foundation (NSF) during a workshop on repair and retrofit of existing buildings [50], analytical models developed based on mechanics of material behavior and verified using experimental results can be very useful tools for detail analysis of many complex structural systems. Such models should be easy to use and should be able to simulate the most important modes of failure of the system under consideration, such as bond failure in case of URM structures. Analytical studies are particularly important in rehabilitation projects

because the problem of strength and stiffness evaluation for rehab projects is more involved than design of new structures. There is a philosophical difference between *design* and *evaluation*.

In design, the buildings are treated as elastic systems with stresses proportional to strains [9]. The design lateral forces obtained from base-shear formula includes response modification factor, R. Associated with R factor is the requirement of ductility. Larger R factor implies more ductility requirements and vice versa. Earthquake forces will stress buildings beyond elastic limit, depending on R factor. If ductility requirement is satisfied (using proper detailing), the building survives the earthquake by dissipating energy through yielding of different components. Thus there is trade-off between strength and ductility in the design of structures.

Evaluation, on the other hand, is related to performance of the structural system. What are the weak links? What is the ultimate strength? What is the mode of failure? Existing structures can not be evaluated based on design criteria. Consider for instance, the design of shear walls. As mentioned in ATC-22 [9], "There is a capacity reduction factor, when considering shearing stresses. The purpose of this provision is to force ductile bending failure instead of brittle shear failure by providing more shear strength. But existing wall may have, for number of reasons, a moment capacity greater than the current code requirements and the shear associated with this moment capacity may be greater even than the design shear capacity. In such a case, the wall design meets the code, but in the event envisioned by the code it can suffer the brittle failure that the code tried to prevent." Furthermore, for economic feasibility of any strengthening scheme, the ABK Methodology permits considering the resistance of existing structural

components, including unreinforced masonry, in evaluation of increase in strength and stiffness [18]. Thus response of original and new structural systems as well as their interaction needs to be considered. Although the guidelines for specific strengthening schemes may be available, their relative merits will depend on the specific case under consideration. Analytical models can be of great help in comparing the effectiveness of various retrofitting options available.

1.4 Objectives

Keeping in mind the need for analytical studies in URM structures, the first task would be to discuss available analytical approaches. It would be a worthwhile effort to continue further studies based on the synthesis of previous efforts to formulate analytical scheme for URM structures. Thus, the objectives of the present study are:

1). To evaluate the state-of-the-art models for inplane behavior of URM structures with particular emphasis on joint bond failure and address the need for further development in analytical modeling of joints.

2). To develop an analytical approach for modeling joint behavior and verify the same at element level as well as structure level.

3). To use the developed model for predicting and explaining the behavior of URM walls under combined action of vertical compression and lateral force.

4). To analyze some of the retrofitting schemes used in practice and evaluate their effectiveness in increasing strength and stiffness of URM walls.

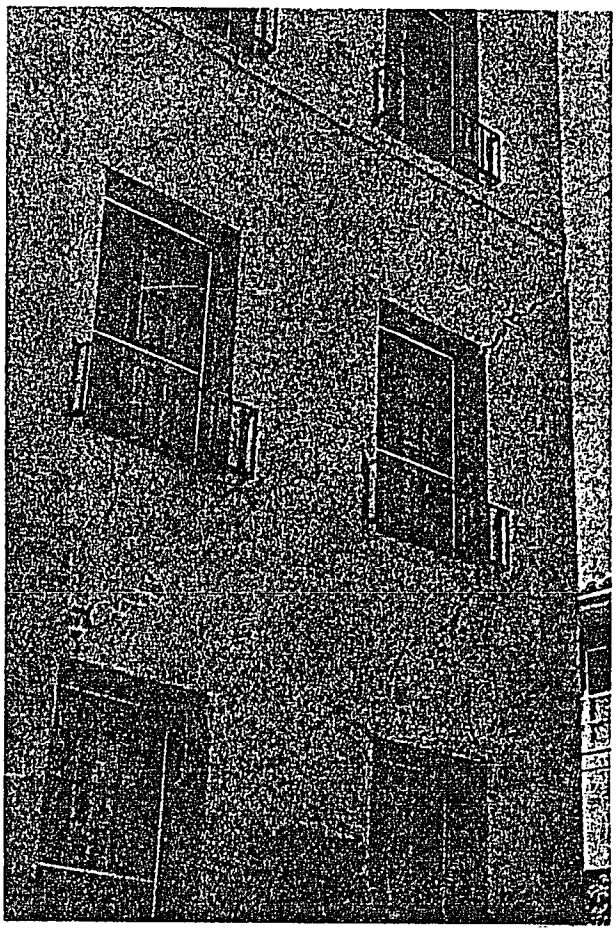

Figure 1.1 Shear Failure at URM Piers During the Whittier Narrows Earthquake, 1987 [18]

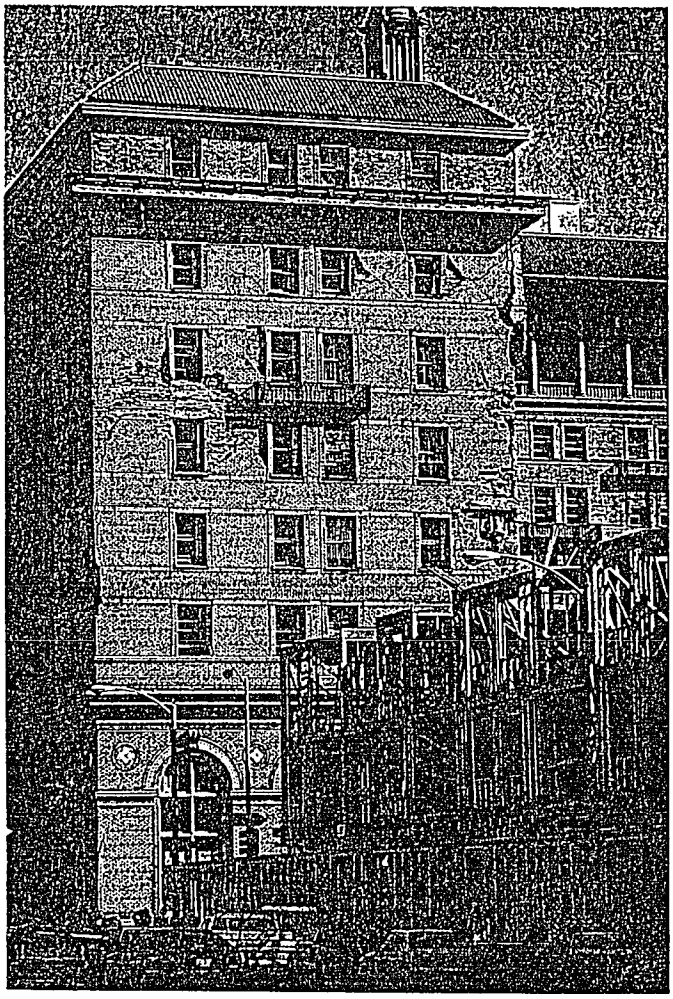

Figure 1.2 Damage to Hotel Oakland During the Loma Prieta Earthquake, 1989 [32]

CHAPTER 2

ANALYTICAL MODELS

This chapter is devoted to the discussion on various models to predict the joint failure followed by the analytical approach developed for the present study. A brief discussion of modeling of bricks is also presented.

Analytical models for URM structures should be able to represent nonlinearity due to both material failure and bond failure. However, most of the nonlinear behavior in URM structures can be attributed to mortar joint bond failure. In 1986, Dhanasekar and Page [21], after studying effects of various parameters affecting the behavior of URM structures, concluded that tensile and shear bond strength of mortar joints are the most critical factor governing the ultimate strength of URM walls. Considering the effect of bond failure on ultimate strength of URM structures, Ali and Page [7] studied the behavior of tensile and shear bond strength between mortar joints and bricks. In the following section, various models for predicting the joint bond failure are discussed.

2.1 Models for Joints

Joint models are classified into two categories, smeared models and discrete models.

2.1.1 Smeared Models

In smeared modelling, the presence of joints is smeared over adjacent brick elements. Thus, failure of joint will result in stiffness reduction of surrounding elements.

Zienkiewicz and Pande [60] developed such a model to simulate the behavior of discontinuous rock mass and can be applied to URM structures. In this model

it is assumed that the material is traversed by "n" families of "weak" planes. The "weak" planes have failure parameters significantly smaller as compared to the basic material matrix. The state of stress at any point can be related to stresses in these planes of weakness through series of transformation. Smearing the failure of weak planes over the basic material matrix will result in highly anisotropic behavior which can represent realistic situations reasonably well. The assumptions in this modeling technique are justified because joints are randomly distributed in the underground rock masses. Although such joints significantly reduce the strength, they can not completely define the failure path of the jointed rock masses.

Pande et al. [46] presented an equivalent material approach for the computation of the elastic properties of brick masonry. A concept of brick-mortar system consisting of a series of parallel layers which will behave elastically is introduced. This concept is extended such that masonry with two sets of mortar joints (bed and head joints) can be represented by an equivalent elastic material. It is assumed that 1) no slippage occurs between mortar layers and, 2) brick units and head joints are continuous.

Mengi and McNiven [39] derived a mixture model considering interaction between mortar joints and brick elements to predict linear dynamic response of URM walls. This model was further simplified assuming isotropic behavior to study nonlinear dynamic response of URM walls.

Dhanasekar and Page [21] analyzed infilled frames considering nonlinearities for the masonry infill under monotonic loading. Failure envelope for material failure was derived based on compression-compression and tension-compression tests on several URM panels. Nonlinearities due to bond failure were smeared over the adjacent blocks. The solution of nonlinear problem proceeded as follows:

At a particular load level an iterative solution was performed till all the material nonlinearities converged. After convergence of material nonlinearities check was performed for bond failure. If bond failure occurred, its effect would be smeared by changing material properties of the element encompassing the joint and problem would be solved again at the same load step. The process was continued until convergence was achieved at a particular load level. If the bond failure is the most important factor governing the strength of URM structures then iterative solution for bond failure, similar to the iterative solution for material nonlinearities, should be performed for precise representation of progressive joint bond failure. This is because stress redistribution is highly dependent on the location of stress release. The solution scheme described earlier [21, 23, 43] implies that the problem would be re-solved after changing material properties to account for bond failure. Such a solution scheme will redistribute total load based on new element stiffness matrices. It will not permit redistribution corresponding to stress release which occurs with bond failure, at the location of failure. Actual redistribution should occur with change in material properties as well as stress-release at the location of bond failure. In fact, initial stress method developed by Zienkiewicz [61], does not require even the reformulation of stiffness matrix because nonlinearities can be represented as unbalanced nodal forces corresponding to stress release.

Furthermore, smeared models are good to study global response, but can not be used when the behavior is dictated by bond failure. Bond failure is a localized phenomenon. In real situations material properties of adjacent brick elements may not at all be affected by bond failure. In such cases it will be necessary to have discrete representation of joints for precise representation of the joint bond failure.

2.1.2 Discrete Models

In discrete models, both blocks and joints are treated as separate elements. The failure of one will not change the material properties of the other.

Finite element model using 4 noded isoparametric elements is the most reliable way for plane stress analysis of walls. Nonlinearities due to both material behavior and bond failure can be incorporated. Ali and Page [7] performed finite element analysis of masonry walls subjected to concentrated vertical force using 4 noded elements. The wall was divided into two regions based on the assumption that: (1) Nonlinearities due to vertical concentrated load would be restricted to the region around the concentrated load and, (2) Crack would propagate in vertical direction starting from the concentrated load. The first region modeled using very coarse finite element mesh was treated as an elastic region. The second region in the vicinity of concentrated load was treated as an inelastic portion and a very fine finite element mesh was used to account for nonlinearities. A very fine mesh was necessary because joints were very thin as compared to adjacent bricks. General guidelines for finite element mesh layout suggest that aspect ratio of elements should not exceed three for good stress results. When joints are very thin as compared to adjacent blocks, more elements will be necessary to meet the restriction of aspect ratio. If specific region of nonlinear behavior can not be identified, nonlinear analysis of entire structure using such a fine mesh will be very costly and cumbersome making its regular use impractical.

In the last decade much attention has been devoted to the development of contact surface elements. Such a formulation is based on Coulomb's friction and requires knowledge of only one quantity, friction. Katona [27] presented a finite element formulation in which contact conditions are modeled using constraint

equations. The element has two nodes and uses Coulomb's friction law to check the contact conditions. This element will have convergence problem when contact conditions are changing rapidly. Moreover, one point node to node contact may not give correct estimate of stresses.

Bathe and Chaudhary [11] developed an improved version of this contact element. The surface traction between the nodal points are used to check the contact conditions instead of concentrated forces at nodal point of contact. Also, to avoid oscillation of contact elements, the gap closing is achieved in two steps. This contact element has been incorporated in a commercial software ADINA [5]. However, the contact formulation requires that different parts in the structural systems be stable when contacts are removed. The restriction is because of constraint equations used to formulate the contact matrices. The stiffness matrices of different structural parts are coupled through contact matrices derived using constraint of compatible boundary displacements. When contact is open, different parts in structural system become isolated. If the only constraint for each part is through the contact conditions then the opening of contact permits rigid body motion in the structural systems i.e. singular stiffness matrix. In URM structures each block is connected to the adjacent ones through joints only. Tension bond failure of joints will isolate certain blocks, permitting rigid body motion. Fig. 2.1 shows this case. In fact the program detects this point even before assembling the stiffness matrix and analysis terminates with an error message. Thus, in the present form, use of contact surfaces in ADINA is not possible for modeling joint failure in URM structures.

ANSYS [8], another commercial software has an interface element with two nodes. Uncoupled springs are used to simulate the contact conditions. Small

stiffness is used to prevent the numerical problems arising due to local failure of the interface. Additional input parameter is the specification of gap or overlap. The interface checking is based on concentrated forces at nodes. As done in contact elements, tension is not permitted. The stiffness of springs should be higher than that of adjacent blocks by an order or two. This element does not perform well when a simple cantilever beam with a point load at the free end (Fig. 2.2) is analyzed. In Table 2.1, exact maximum deflection is compared with computed value. It can be seen that the computed value is eight times the exact value. In fact, the actual beam of depth 1.5in is split into two beams of depth 0.75in because of the failure of all joints along the longitudinal centerline of the beam. This happens because shear strength of the joints is proportional to the normal stress, i.e. $\tau = \alpha\sigma$. If normal stress is equal to zero (i.e. σ=0) for the joint element, which is the case for the present problem, then shear strength, τ=0, resulting in the failure of all the joint elements for infinitesimally small point load at the free end. Such a behavior is not very realistic as joints may have initial bond strength. Also, convergence problems may arise due to rapid change in contact conditions.

From the foregoing discussion it is clear that although some of the first discrete joint representations were derived quite some time ago [23], there is still a great deal of effort necessary for the development of a reliable, general and cost-effective algorithm for the *practical analysis* of such problems. In light of repair and retrofit need for URM structures, similar conclusion was drawn by masonry task group during a symposium on repair and retrofit of existing structures sponsored by NSF [50]. It was concluded, "With increased computer facilities, engineering offices can now have the capabilities to perform nonlinear dynamic analysis on simple systems. Software needs to be developed for this purpose and scope." It is therefore necessary that efforts be directed towards implementation of

fundamental concepts of contact mechanics and joint behavior to obtain efficient numerical model for analysis of URM structures.

2.2 Proposed Analytical Approach for Modeling of Joints

2.2.1 Element Formulation

Ngo and Scordilis [41] used uncoupled springs to model bond failure in reinforced concrete beams. Similar concept can be used for modeling of joints in URM structures if stiffness of springs can be derived from material and geometric properties of mortar joints. Alternatively, truss links can also be used to model joints. The inclined components of link model transfer shear stress and horizontal components transfer normal stress. Fig. 2.3 shows a typical joint element and its idealization using the spring model and the link model. Analytical evaluation will give normal stiffness K_n equal to 1 / 2 (E $\times$ L / b) and shear stiffness K_s equal to 1 / 2 (G $\times$ L / b), where E is modulus of elasticity, G is shear modulus, L is length of joint element, and b is thickness of the joint element. Alternatively, the stiffness of springs (links) can be determined experimentally as suggested by Page [43] and Goodman et al [23]. Three examples are solved to check the performance of two idealization of joints.

1) Transverse Joints: This example considers only transverse joints i.e. joints parallel to load. Consider the cantilever beam shown as in Fig. 2.4. Joints along the length of the beam are modeled using the link model.

The beam is 10.3in long with 1.0in x 1.0in of cross section. Modulus of elasticity is 2.0E06psi and Poisson ratio is 0.2 for both blocks and joints. Hence, normal stiffness K_n is 1.0E07lb/in and shear stiffness K_s is 4.167E06lb/in. Concentrated

load of 2000lb is applied at the free end. From Table 2.2 it can be seen that deflection and stresses in joints are in good agreement with the answers obtained using theory of elasticity for bending of beams.

2) Transverse Joints and Staggered Longitudinal Joints: A simply supported beam shown in Fig. 2.5 is analyzed. Transverse joints are modeled with the link model and longitudinal joints with the spring model. The beam length is 19.6in with cross section of 1.0inx 2.1in. Modulus of elasticity is 2.0E06psi and Poisson ratio is 0.0, for both blocks and joints. Thus K_n is 1.0E07lb/in and K_s is 5.0E06lb/in, for both the link model and the spring model. From Table 2.3 it can be seen that the shear stress in longitudinal joints is very much different as compared to the correct value. It was found that this difference is because of staggered nature of the longitudinal joints. Horizontal displacements of nodes 55, 58 and 59 (Fig. 2.5) are not independent of each other but are related to each other as: $(U_{55} - U_{59} = U_{55} - U_{58})$ in order to maintain equilibrium at the ends of staggered joint. This restriction could be avoided if joints in longitudinal directions are continued into the brick elements. This point is illustrated through another example that follows

3) Continuous Joints in Both Directions: A cantilever beam shown in Fig. 2.6 is analyzed. Load of 2000lb (500lb at each of 4 nodes) at free end is applied. Transverse joints are modeled with truss links and longitudinal joints with springs. The beam length is 21.9in with 1.0in x 2.0in cross section. Modulus of elasticity is 2.0E06psi and Poisson ratio is 0.0, for both blocks and joints. Hence K_n is 1.0E07lb/in and K_s is 5.0e06lb/in. Calculated deflection and stresses compare well with exact answers, as can be seen from Table 2.4.

Thus it can be concluded that the joints must be continuous in both directions in order to obtain correct normal as well as shear stresses in joints. In actual URM structures when mortar joints are staggered, similar elements in brick should be considered, of course, using material properties of bricks. Such an element will be referred to as *pseudo joint* hereafter.

It is essential to discuss several points on the determination of stresses in the joint. Shear stresses are determined based on the average shear force in the springs at two ends of the joint. The average shear force divided by the area of joint (A) gives the average shear stress in joints. Linear distribution along the cross section is assumed to determine flexural stresses in transverse joints. That is, normal force in the spring is equated to the total compressive or tensile force on the section based on linear stress variation. However, when there are large number of transverse joints along the cross section, average normal stress will be calculated similar to the average shear stress calculation. Thus, stresses in joints will be the average of forces in springs at two ends of joint divided by the length of the joint element.

The link model shown in Fig. 2.3 has a restriction. It can not be used for the case shown in Fig. 2.7. In such a case distribution of compressive force between blocks and joint will not be correct because inclined links have shear stiffness instead of axial stiffness. Using spring model in such a case will give correct stresses in blocks (assuming zero axial stiffness of joints) because shear springs will not be stressed under uniform compression. Thus for further analysis spring model will be used.

Once joints are modeled with desired accuracy, bond failure can be modeled using one of the available bond failure surfaces.

2.2.2 Bond Failure Surfaces

Corresponding to the element formulation discussed in the previous section, bond failure surface used to check the joint bond failure should be in terms of normal stress and shear stress in the joint.

Zienkiewicz and Pande [60] used Mohr-Coulomb failure surface in the study of failure of jointed rock masses. In compression-shear zone, shear strength will linearly increase with increase in compression. Intercept of failure curve on τ-axis (Fig. 2.8) represents cohesion, C. In tension-shear zone the concept of "tension cut-off" was used. That is, small tension will result in failure of joints, the effect of which is smeared. Thus, the yield criterion, F, can be expressed as:

$$\begin{aligned} F &= |\tau| - \sigma tan(\alpha) - C = 0 \quad for \;\; compression - shear \;\; zone \\ F &= 0 \qquad\qquad\qquad\qquad\qquad\qquad for \; tension - shear \; zone \end{aligned} \tag{2.1}$$

Page [43] developed bond failure surface in terms of normal stress and shear stress in joints. Several masonry panels were tested under combined shear and normal stress on mortar joints. In compression-shear zone, shear strength was characterized using bilinear curve. In tension-shear zone shear strength would decrease linearly with increase in tension as shown in Fig. 2.9. The failure criterion can be written as:

$$\begin{aligned} Region \;\; 1: \;\; \tau &= 0.66\sigma + 0.19 \\ Region \;\; 2: \;\; \tau &= 0.87\sigma + 0.19 \\ Region \;\; 3: \;\; \tau &= 0.11\sigma + 1.91 \end{aligned} \tag{2.2}$$

The failure envelope used by Sharma and Desai [57] is shown in Fig. 2.10. The yield criterion F can be expressed in terms of shear stress and normal stress

as:

$$F = \left(\frac{\tau}{p_a}\right)^2 + \alpha\left(\frac{\sigma}{p_a}\right)^n + \gamma\left(\frac{\sigma}{p_a}\right)^2 = 0 \qquad (2.3)$$

Where γ is ultimate function, α is hardening function, n is phase change parameter, p_a is atmospheric pressure.

For the present study, bond failure surface shown in Fig. 2.11 will be used. In compression-shear zone the first failure of joints will be governed by "initial failure curve" which is the same as that used by Zienkiewicz. Initial failure curve permits modeling of initial bond strength of joints. Once the joint element fails, initial bond strength will not be available for resisting additional shear stresses developed in the joint [59]. Thereafter the failure will be governed by "subsequent failure curve" which is based on Coulomb's friction law. In tension-shear zone shear resistance decreases with increase in tension and failure envelope in this region is similar to region 1 suggested by Page. No shear resistance is available in this zone after initial failure of joint. Hence "subsequent failure curve" in tension-shear zone reduces to a point at the origin.

To achieve convergence in the case of rapidly changing contact conditions, gap closing can be achieved in two stages. Suppose that the converged solution with proper knowledge of all the joint elements is available. Incremental load/displacement is then applied. Status of all the joint elements is checked. If open interface has closed (a decision based on normal stress), elastic stiffness is assigned to the element but no forces are transmitted across the joint. In subsequent iterations forces will be transferred across the joint if the joint element remains closed.

To avoid the numerical problems because of local failure of joint elements, small stiffness is assigned to joints after failure. Generally stiffness should be smaller than elastic stiffness by the factor of 1000 to 10000.

2.3 Models for Blocks

Considering the geometry of blocks, two dimensional rectangular finite elements can be used for blocks. Two dimensional elements could either be four noded (linear) or eight noded (parabolic) isoparametric elements. Eight noded isoparametric elements are useful for modeling structures with complex geometry. Parabolic elements have more unknowns as compared to linear elements and hence computation of element stiffness matrix for eight noded elements is more involved and expensive as compared to four noded elements. Linear elements are very stiff. Consequently, number of linear elements required to model a cantilever beam, which has a very simple geometry, will be significantly more as compared to parabolic elements. The performance of four noded element improves greatly if extra shape function (nodeless variable) permitting parabolic displacement variation are added to the linear formulation. Special procedure is required for the evaluation of nodeless variables in order to avoid displacement incompatibility along the edges. The implementation of this procedure is discussed in reference [8]. Four noded hybrid finite element developed by Pian [48] gives the same stiffness matrix as obtained by linear elements with extra shape function. Hybrid formulation is based on an equilibrating stress field within the element and linear displacements along the element boundaries. Integrals involved in hybrid formulation are easier to evaluate but one matrix inversion is required at an element level to get the element stiffness matrix.

In the present study four noded isoparametric elements with extra shape

functions and linear material model will be used for modeling blocks. Two elements will be required for one block because of compatibility requirements and the resulting mesh will be fine enough for use of four noded elements. The nonlinear concrete models available in the general purpose software ANSYS (in which the developed element has been incorporated), can be used for describing material behavior of blocks if desired.

The finite element implementation of the suggested analytical approach will be discussed in the next chapter.

Table 2.1
Comparison of Maximum Deflection (Fig. 2.2)

Computed (in)	Exact (in), Using Beam Theory
32.00	4.00

Table 2.2
Cantilever Beam with Transverse Joints (Fig. 2.4)

Title	Deflection (in)	SS[a] (psi)	NS[b] (psi)
Exact	4.37	2010.00	29000.00
Model	4.31	2000.00	29000.00

a. Shear Stress based on Shear Force in Links 4-19 and 5-18
b. Normal Stress based on Normal Force in Links 4-5 and 18-19

Table 2.3
SSB with Staggered Longitudinal Joints (Fig. 2.5)

	Deflection (in) (free end)	Transverse Joints		Longitudinal Joints (staggered)	
		SS[a] (psi)	NS[b] (psi)	SS[c] (psi)	NS[d] (psi)
Exact	0.40	952.38	17400.00	1428.00	0.00
Model	0.41	956.69	17500.00	525.00	0.00

a. Shear Stress based on Shear Force in Springs: 55-60, 56-59, 54-58, 55-57
b. Normal Stress based on Normal Force in Springs: 56-60, 55-59, 55-58, 54-57
c. Shear Stress for all Longitudinal Joints.
d. Normal Stress for all Longitudinal Joints.

Table 2.4.
Cantilever with Continuous Joints in Both Directions (Fig. 2.6)

Title	Deflection (in) (free end)	Transverse Joints		Longitudinal Joints (continuous)	
		SS[a] (psi)	NS[b] (psi)	SS[c] (psi)	NS[d] (psi)
Exact	5.25	1000.00	28600.00	1428.00	0.00
Model	5.17	1005.00	28480.00	1455.00	0.00

a. Shear Stress Based on Shear Force in Links : 55-60, 56-59, 53-58, 54-57
b. Based on Normal Force in Links : 53-57, 54-58, 55-59, 56-60
c. Shear Stress for all Longitudinal Joints.
d. Normal Stress for all Longitudinal Joints.

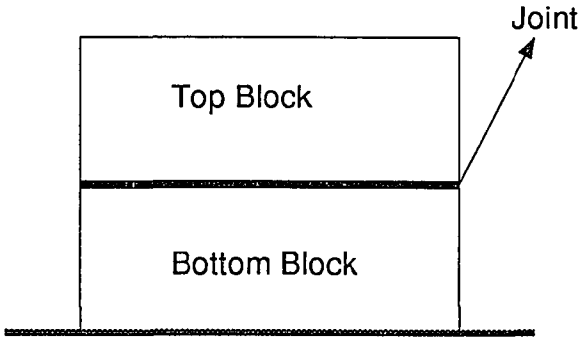

Tension failure of joint
will permit rigid body motioin
of the top block if contact surface
in ADINA is used to model the joint.

Figure 2.1 Modeling of Joint using Contact Surface in ADINA

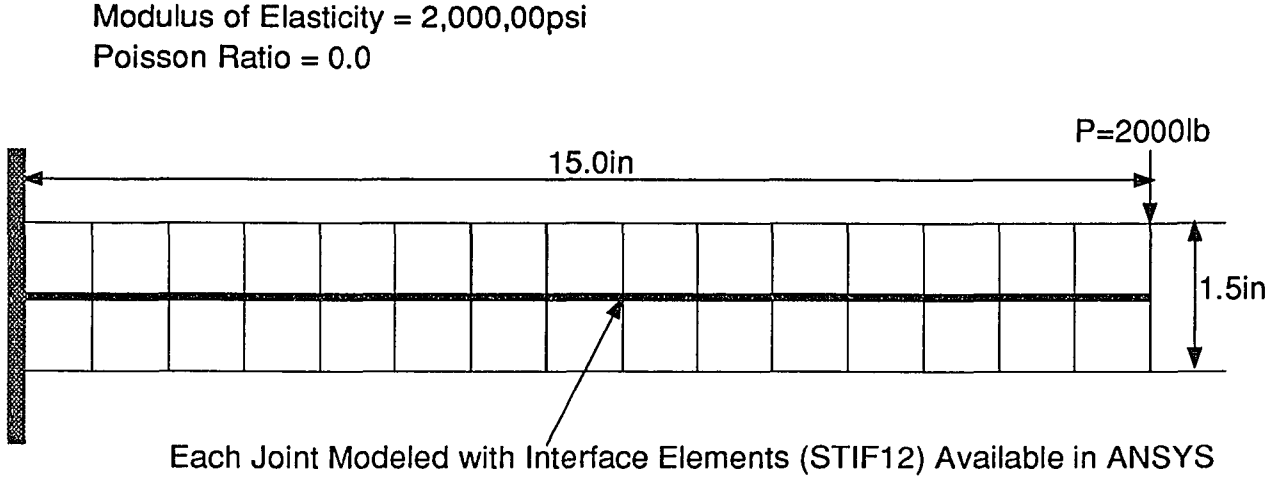

Figure 2.2 Cantilever Beam with Joints along Centerline

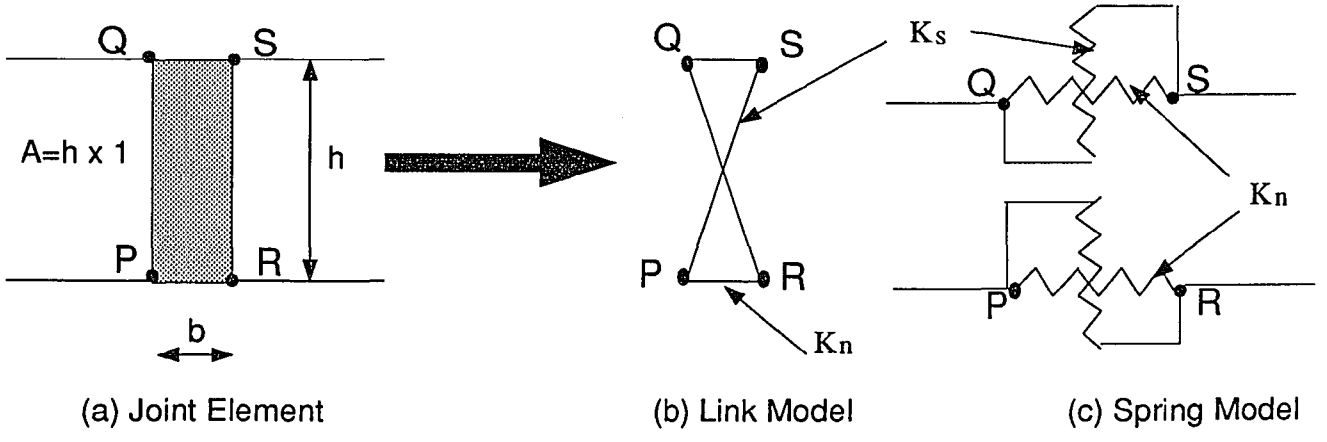

Figure 2.3 Joint Element and its Idealization

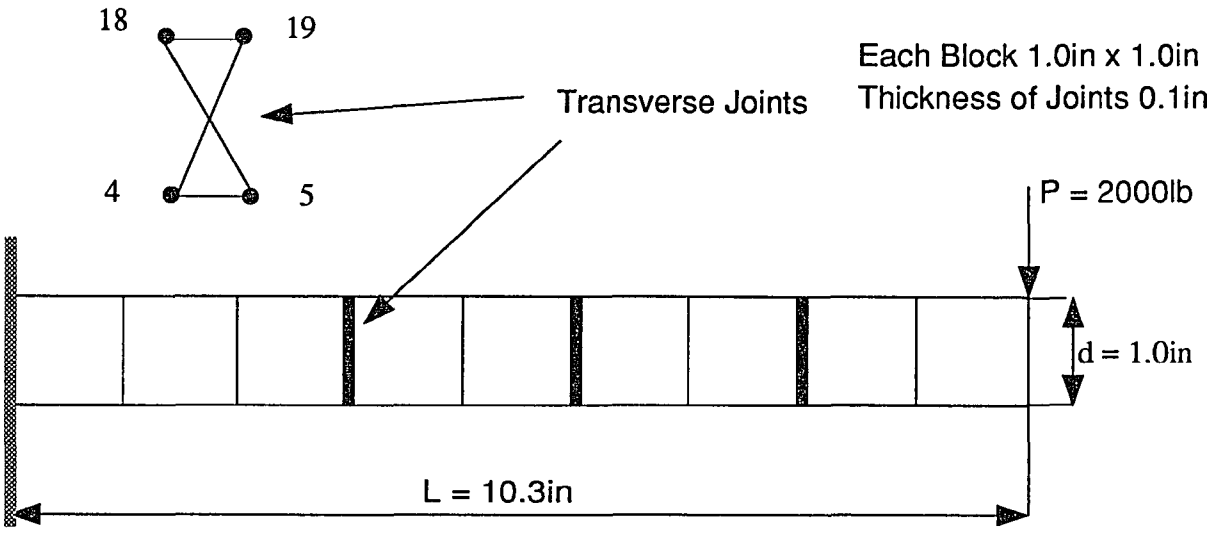

Figure 2.4 Cantilever Beam with Transverse Joints, Example 1

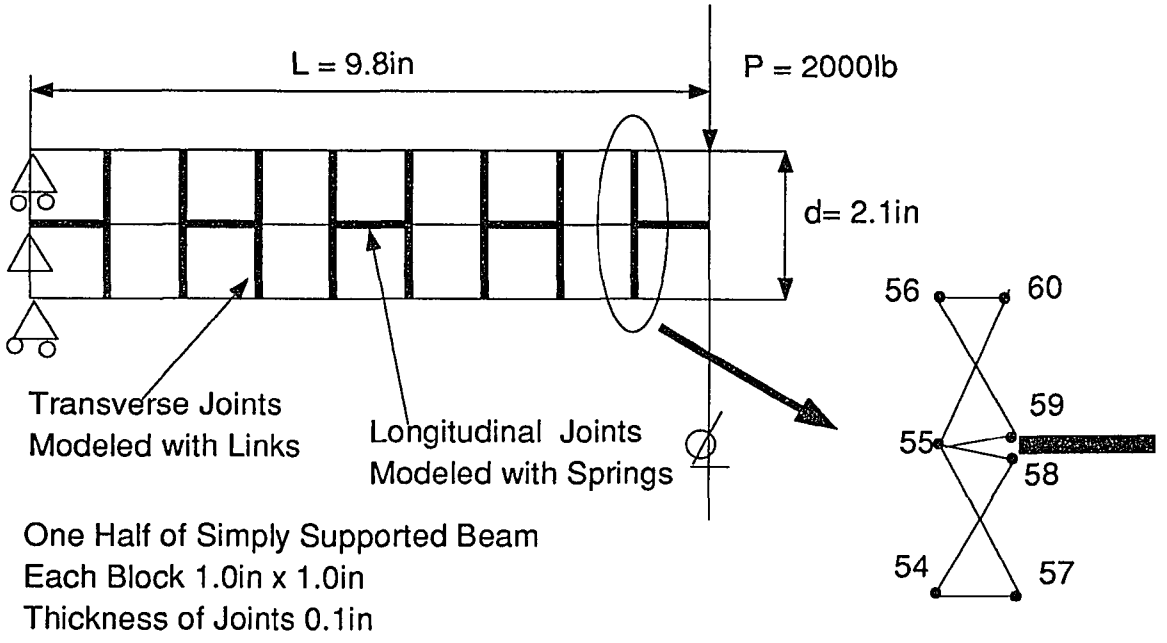

Figure 2.5 Simply Supported Beam for Example 2

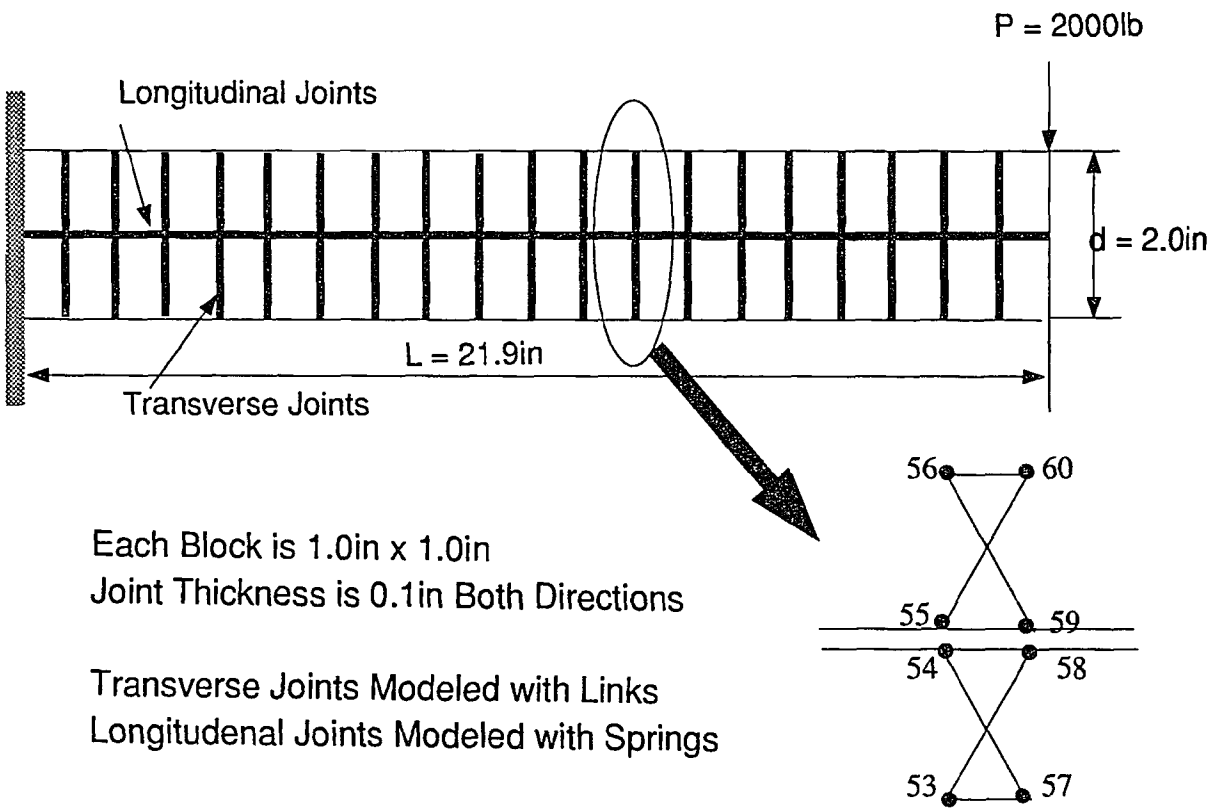

Figure 2.6 Cantilever Beam with Continuous Joints in Both Direction

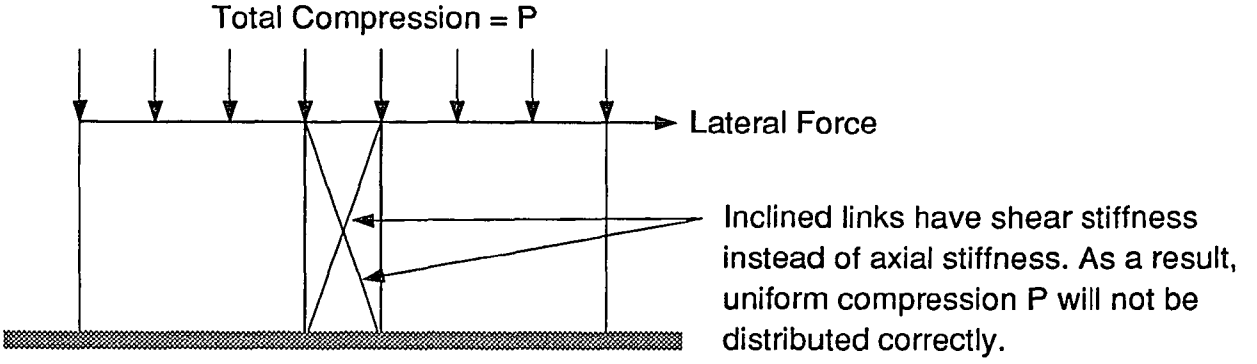

Figure 2.7 Link Model for Joint under Combined Axial and Lateral Loads

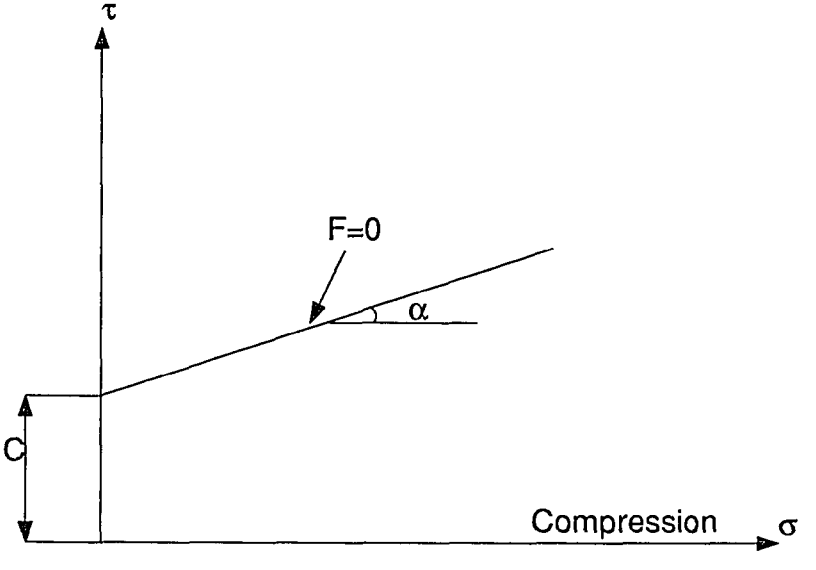

Figure 2.8 Joint Failure Envelope Used by Zienkiewicz and Pande [60]

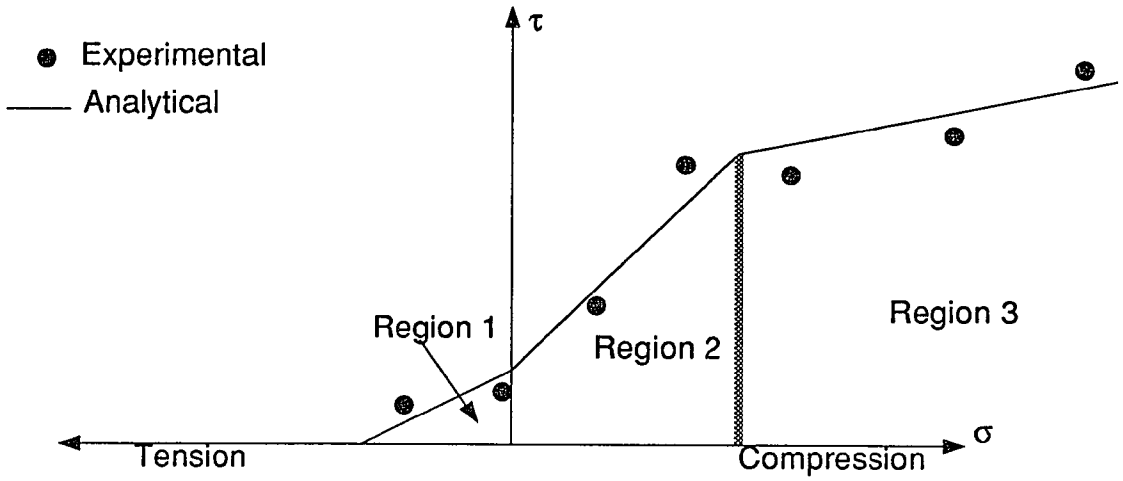

Figure 2.9 Bond Failure Envelope Suggested by Page [43]

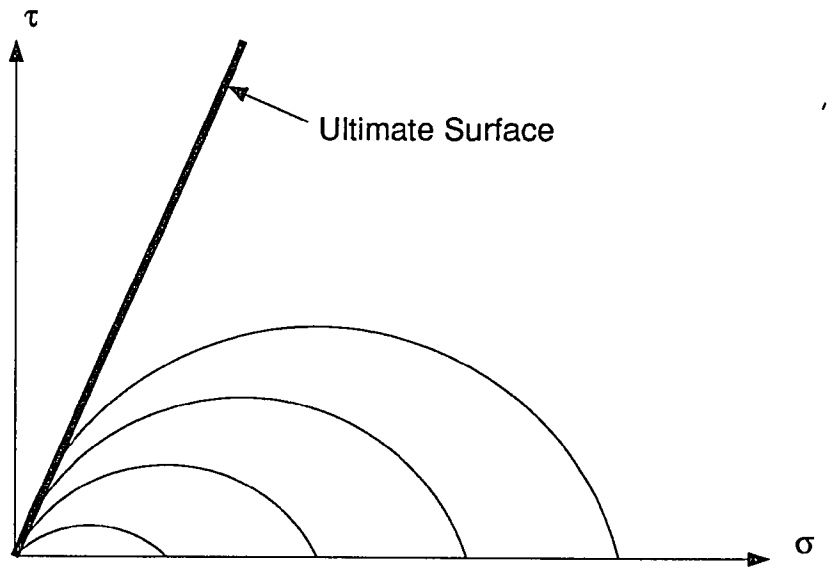

Figure 2.10 Yield Criterion Used by Sharma and Desai [57]

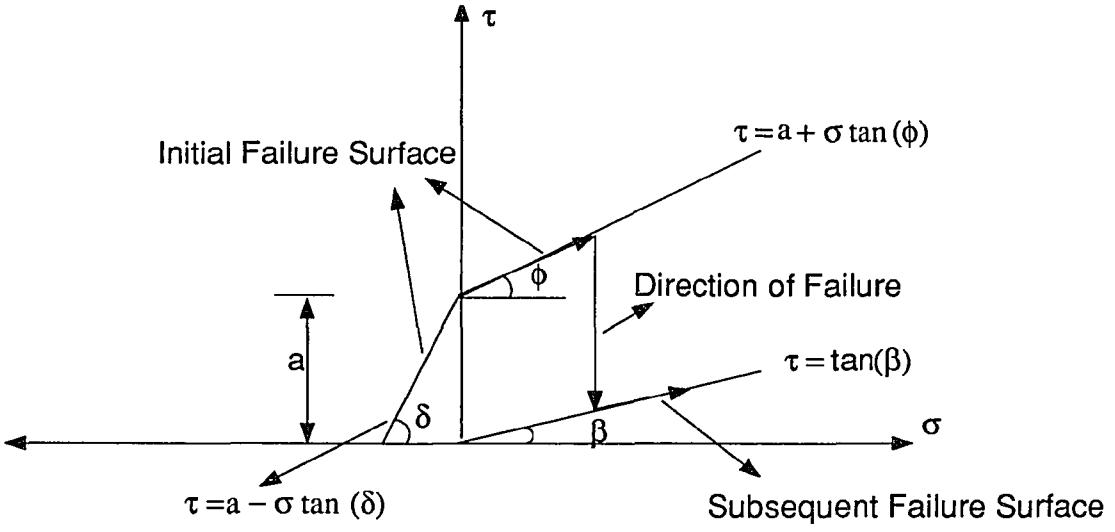

Figure 2.11 Bond Failure Surface for the Present Study

CHAPTER 3

FINITE ELEMENT PROCEDURE

3.1 General

Implementation of the analytical model discussed in section 2.2 is presented in this chapter. There are two possible alternatives for implementation of the analytical model. The first one is to develop a special purpose software. In this case computer programming will be less cumbersome because of the independent functioning of the developed software. Also, the input required for problem definition will be significantly less compared to the second alternative, which is to incorporate the suggested algorithm into a general purpose software. Considerable programming effort is required because of the restrictions imposed by the existing source code of the software consisting of several routines linked together. In addition, programming effort is also required to ensure proper interaction between new developed routines and existing routines. On the other hand, various options of a general purpose software can be effectively utilized for different applications. Such software provide up to date finite element library with different material models. The new element can be combined with other elements and material models to perform linear and nonlinear analysis under static and dynamic loading conditions. Powerful pre- and postprocessor can make data generation and interpretation much easier, justifying greater effort for implementation. Furthermore, this approach would be of more value to many users already familiar with such a general purpose software. It was therefore decided to implement the algorithm in a general purpose software ANSYS.

3.2 Analysis Procedure

ANSYS implementation of bond failure requires that the formulation is based on the theory of plasticity. General numerical procedure for this purpose is described in Appendix 3. Its implementation for modeling bond failure is discussed in this chapter. The solution algorithm for nonlinear equation is discussed briefly and is followed by the description of various routines in the program.

Solution Algorithm: The governing equations in nonlinear finite element procedure is

$$[K_n][\triangle U] = [W] - [R_n]$$

$$and \tag{3.1}$$

$$\{U_{n+1}\} = \{U_n\} + \{\triangle U\}$$

Where R_n is element nodal forces due to internal stresses in the structural system and W is element nodal forces due to applied loading on the system. The term R_n depends on tangent stiffness matrix K_n, displacement vector U_n, and changes with the state of stress in the structural system. Hence, number of iterations are required to arrive at correct solution. Furthermore, most of the nonlinearities such as plasticity, friction etc., are path dependent and require that load (or displacement) be applied in increments describing the loading path. Thus, incremental, iterative solution procedure is required for the solution of equation 3.1. Various algorithms such as Full Newton-Raphson, Modified Newton-Raphson, and Initial Stress Method are available for solution of nonlinear equation depending on the extent of nonlinearity. In Full Newton-Raphson solution tangent stiffness matrix is updated every iteration in all the load steps. If stiffness matrix is updated occasionally, the procedure is called modified Newton-Raphson. If stiffness matrix

is not updated at all, the procedure is known as Initial Stress Method. Full Newton-Raphson algorithm is very effective for problems with sudden nonlinearities such as bond failure, concrete crushing, and hence is used in the present work. Table 3.1 shows the typical phases of an analysis using ANSYS when proposed model is incorporated. Various routines developed for solution of the nonlinear problem are described next.

Subroutine USEREL: This routine is used for preprocessing and element formulation. It defines number of nodes, degrees of freedom per node, type of global transformation and other governing element parameters such as material property number, real constant number, etc. These parameters are used to define the size of variable arrays such as SVR (stored variable) , RVR (real variable), etc.

Subroutine USERPT: This routine defines the shape of the element for plotting. Various shapes such as triangle, tetrahedron, rectangle, and cube can be defined in this routine. For the joint element rectangle shape with 4 nodes is selected. This information is transferred to mesh module via routine USERMH. Mesh module executes actual plotting of the shape.

Subroutine ST100: The information from routine USEREL is used here to formulate the element stiffness matrix in global coordinate system. The information necessary to this routine is transferred through routines GETED, PROPEV, PROPE1, NONTBL. GETED gets data for the element such as element number, integer and real parameters associated with the element, time step, pressure, real constants, stored variables, and displacement vector. Routines PROPEV, PROPE1, and NONTBL are required to transfer linear and nonlinear material properties. Com-

mon storage, STCOM, defines certain global variables for all the routines, and needs to be called in each routine. Stiffness matrix is evaluated as follows.

For the first iteration of the first load step elastic material properties are used for evaluation of stiffness matrix. For subsequent load steps and iterations, routine USERCM is called to decide the status of an element. USERCM returns elasto-plastic material property matrix which is used in the calculation of element stiffness matrix. Various other matrices such as mass matrix, damping matrix, and stress-stiffness matrix can also be formulated if required.

Based on the state of strains in the element, restoring forces are calculated using elastic material properties. The restoring forces will change during the analysis depending on the resistance offered by each element. The resistance of each element depends on linear and nonlinear material properties that are input to the routine. Tension bond failure will release all elastic strains and resistance of element is zero. Compression bond failure will release certain amount of elastic shear strains and shear resistance reduces accordingly. When the element changes status from open to close condition, the resistance remains zero in the first iteration. Such a scheme permits stress release at the location of failure in addition to change in material properties, unlike the procedure discussed in references [21, 23, 43] where redistribution occurs due to change in material properties only.

The element load vector is then completed by adding applied load vector to restoring forces. If the finite element system is in equilibrium for any given loading, the structure load vector, formed using element load vector, will be zero. Otherwise, unbalanced nodal forces will be redistributed based on new structure stiffness matrix and the process continues until structure load vector is zero.

Subroutine USERCM: This routine called from ST100, via CMELPL, does the calculation of elasto-plastic stress-strain matrix. The scalar quantity EPEQ determines the nonlinearity in the element. If EPEQ is zero, no further calculations are done and elastic material properties are used in ST100 for calculation of element stiffness matrix. Nonzero value of EPEQ indicates nonlinearity. Elastic strains, plastic strains and element status code vector, EPSHFT (I), calculated in routine USERPL (called from SR100) are used to decide the status of an element as follows.

If total normal stress is tensile, a check is made to see if the element had failed in previous iteration. The tensile bond strength is zero if failure of the element occurred in previous iteration. Material properties are changed so that both shear and normal stiffness become zero. If the element did not fail in previous iteration, a check is done for bond failure under combined shear stress and tensile stress. Alternate provision for bond failure in terms of principal tension is also made available. If failure has occurred then material properties are changed as discussed earlier. If failure has not occurred, both shear and normal stiffness remain elastic.

Zero normal stress means that element has changed status from tension to compression, i.e. interface is closed from open condition. In this case material properties are changed to elastic material properties.

If normal stress is compressive, bond failure check is done using combined normal compressive and shear stress. Either "initial failure surface" or "subsequent failure surface" is used depending on the status of the element in previous iteration. If compressive bond failure is detected, shear stiffness is reduced to zero. Normal stiffness remains unchanged in this case.

If material failure of joint is desired instead of bond failure, an option is available which will check failure of joint material based on principal stress, determined from normal and shear stress. This option could be of interest if failure of URM wall under vertical compression only is to be simulated. In such cases vertical cracks pass through staggered joints and split the brick elements. Splitting of bricks could be modeled using the pseudo joint element connecting two half bricks. These joint elements will have material failure based on principal tensile stress and direct tensile strength of brick material. Furthermore, simultaneous check for bond as wall as material failure could also be programmed if desired.

Subroutine SR100: In this routine calculations for elastic strains are done. Necessary data is supplied to USERPL by routine GETED. Using nodal displacements strains are calculated. Depending upon the solution algorithm (Newton-Raphson, Initial Stress), strains are either total strains or incremental strains. Incremental strains are added to previously calculated elastic strains to get total elastic strains for the current iteration. The control is then passed to USERPL via PLAST for plasticity calculations. USERPL returns the control to SR100 after modifying elastic and plastic strains. The modified elastic strains are used in calculation of restoring forces in ST100 which determines release of forces due to failure of the joint element. The routine PUTED puts stresses and strains calculated in this routine in **file03.dat** which is used in ST100 and USERCM to retrieve data. The same data is also stored in **file12.dat** for postprocessing. **File12.dat** stores data for specified iterations whereas **file03.dat** stores information for the last iteration only.

Subroutine USERPL: This routine called from SR100 via PLAST updates the existing elastic and plastic strains based on state of stress in an element.

If normal stress is tensile, a check is done to see if the element had failed in previous iteration. If the element did fail in previous iteration, all elastic strains are added to plastic strains and then elastic strains become zero. If the element did not fail in previous iteration then bond failure check is done under tension and shear. Alternative failure criteria based on principal tension is also made available. If tensile bond failure is detected, a flag is set indicating failure and strains are modified as mentioned earlier. Zero elastic strains imply that restoring forces calculated in ST100 will be zero. Consequently, the term R in equation 3.1 will have unbalanced forces resulting from tensile bond failure of the element. These forces will be distributed in subsequent iterations. The normal stress in this iteration is stored for use in the next iteration to check the change of status of the element.

If total normal stress in this iteration is compressive and was tensile in previous iteration then the element has changed the status. This means that the interface has closed from open condition. In such a case no forces will be transferred in the current iteration. Both plastic and elastic strains are zero. The change of status check is necessary to avoid oscillation of the element which may create convergence problems. Normal stress in this iteration is stored for use in the next iteration.

If total normal stress is compressive and was compressive in the last iteration then a check is done for bond failure under compression. If the element had failed previously then "subsequent failure curve" shown in Fig. 2.11 is used for bond strength. If the element did not fail previously then "initial failure envelope" shown in Fig. 2.11 is used for checking bond failure. In either case if bond failure is detected then elastic shear strains are reduced based on frictional resistance

of the element. Normal strains remain unchanged. Total normal stress is stored for use in the next iteration. Once compressive bond failure occurs the shear resistance depends on friction and normal stress.

Convergence check is also done in this routine. Two convergence criteria are used. The first one is based on incremental displacement. If maximum incremental displacement in the current iteration is less than the specified value, the solution satisfies the first convergence criteria. This convergence check is applied to all nodes. The second criterion is based on bond failure of joint elements. Under tensile bond failure condition, convergence occurs if element does not change status in two consecutive iterations. The element does not converge under change of status condition. In case of compressive bond failure, convergence occurs if percentage difference between released shear forces in two consecutive iterations is less than the specified value. The solution is said to have converged if both criteria are satisfied.

Subroutine STCMNT: This routine gives definition of various variables used in the program. The routine does not perform any calculations.

Subroutine UCMNT: This routine explains the status of displacement vector U, i.e. number of iterations for which displacements are stored, depending upon the type of analysis such as linear and nonlinear, static and dynamic.

TABLE 3.1
TYPICAL PHASES OF AN ANALYSIS USING JOINT MODEL

ROUTINE	***EXISTING***	***ADDITION***
PREPROCESSING PHASE		
MESH GENERATION	Aatomatic and Manual	No Addition
GEOMETRY DEFINITION	Truss, Beam.....	Joint Geometry
MATERIAL MODELS	Von Mises, Concrete...	Bond Failure Model
CONSTRAINT DEFFINITION	Coupled DOF.....	No Addition
LOAD DEFINITION	Applied Loads and Displacements	No Addition
MODEL DISPLAYS	Various Shapes	Shape of Joint Element (Rectangular)
SOLUTION PHASE		
ELEMENT MATRIX	Truss, Beam.....	Joint Stiff. Matrix
ELEMENT LOAD	Truss, Beam.....	Joint Load Vector
SOLUTION	Wave Front	No Addition
STRAIN AND STRESS CALCULATION	Truss, Beam.....	Joint Element
POSTPROCESSING PHASE		
DATABASE, PRINTOUTS, SCANNING AND DISPLAYS	Truss, Beam.....	Joint Element

CHAPTER 4

VERIFICATION

Three problems are solved to verify the suggested analytical procedure. The first problem deals with linear analysis of URM wall. Results obtained from a fine mesh model are compared with the suggested model. In the second problem, nonlinear analysis of the same URM wall is performed using the proposed analytical procedure described in the previous chapter. Cracking pattern and load deflection curve obtained from analysis are compared with experimental results. Finally, the third problem presents comparison another analytical model for joints developed recently.

4.1 Comparison with Fine Mesh Model (Example 4.1)

Finite element model using 4 noded isoparametric elements is the most reliable way for plane stress analysis of walls. Because joints are very thin compared to adjacent bricks, large number of elements are necessary to prevent ill conditioning arising due to bad aspect ratio. This results in a very fine mesh model. The wall shown in Fig. 4.1, which is from an experimental test discussed in Section 4.2, was analyzed using such a fine mesh model and the proposed analytical model. Results were compared in linear range for different ratios of E_b /E_m. E_b is modulus of elasticity of bricks and E_m is modulus of elasticity of mortar. The fine mesh model was generated using 4 noded plane stress elements with aspect ratio of 1. For the joint element 10 plane stress isoparametric elements were used. This resulted in 100 such elements for half of a brick. Totally 11397 elements and 11616 nodes were used for the entire wall (Fig. 4.2). Based on

proposed analytical approach 268 elements and 384 nodes were used to model the same wall (Fig. 4.3).

Total lateral load of 132lb was applied at the top edge for both cases. The top edge in this case is allowed to rotate freely and no vertical compression is applied.

From Table 4.1 it can be seen that the maximum deflections based on the suggested model and the fine mesh model are in good agreement. The CPU time using the suggested model is lesser than that for fine mesh model by a factor of 100.

4.2 Comparison with Experimental Results (Example 4.2)

Capability of analytical model to correctly predict progressive bond failure of joints can only be demonstrated by comparison with experimental results. Considerable stress redistribution occurs after beginning of nonlinearity and before final failure. Prediction of correct failure mode is very important before using analytical models in further applications. Nonlinear analysis of the wall shown in Fig. 4.1 was done using the mesh shown in Fig. 4.3. This wall was tested by Woodward and Rankin [28]. Vertical compression of 220 psi (84 kips) was applied through nodal point loads. Plane stress elements with unit thickness were used to model the concrete blocks. Material properties and other input parameters are given in Appendix 2 which lists and explains input required for nonlinear dynamic analysis. Experimental conditions were set so that the wall deflected in double curvature when lateral displacement was applied. This was achieved by not allowing the top edge of the wall to rotate. In analytical modelling this zero rotation condition at the top edge was simulated using coupled degrees of freedom. Coupled degrees of freedom generates a constraint equation assuming that all

nodes in the coupled set will have the same displacement in the given direction. The value of displacement is not known *a priori* and depends on the problem definition. Incremental lateral displacement was applied to all the nodes on the top edge. Incremental displacement analysis is necessary to model the wall behavior after the failure. Incremental load analysis can not be performed because the strength of wall decreases after failure. This creates numerical difficulties as two displacement configurations are possible for the same applied load, destroying uniqueness of the solution. In displacement controlled analysis this problem is averted because there is one and only one load set for the applied displacement.

Cracking pattern predicted from analytical model is shown in Fig. 4.4 (to be compared to experimental cracking pattern shown in Fig. 4.1). Fig. 4.5 shows comparison of load deflection curves. As it can be seen from this figure, the analytical results are in good agreement with the experimental results.

The first crack developed in the staggered joints at the center of the wall when lateral displacement at the top edge was 0.06 in. This crack extended further in stair shaped fashion. Towards corners of the wall the crack extended horizontally. It appears that completed diagonal/horizontal crack served as slip line along which the upper right segment of the wall translated relative to the lower left segment. Similar behavior was observed in the experiment.

From load displacement curve it can be seen that the wall has significant shear strength even after shear crack has fully developed. This shear strength is a function of applied vertical compression and friction between the mortar joints and blocks. In analytical model this is simulated using "subsequent failure surface" and angle β shown in Fig. 2.11

4.3 Comparison with Recent Developments (Example 4.3)

Recently Sharma and Desai [57] used a thin layer model for modeling joint behavior. This model was verified with experimental load deflection curves obtained from shear tests. Six noded joint element with plasticity model described in reference was used for modeling joints. Fig. 4.6a shows the mesh used by Sharma and Desai to simulate the joint behavior. The mesh shown in Fig. 4.6b is based on the proposed model. Fig. 4.7 compares load deflection curve obtained from the models and experiment. Once again good agreement between analytical results and experimental results is evident. It should be noted that the comparison is done at element level. The system shown in Fig. 4.6a does not have any redundancy as far as joint failure is concerned. Thus, the most important aspect of stress redistribution can not be verified using element level tests. Problem discussed in section 4.2 demonstrates this aspect of the element formulation.

Table 4.1
Comparision of Maximum Deflection (Example 4.1)

E_b/E_m	Fine Mesh[1] (in)	Model[2] (in)	Difference
1000	0.01500	0.01480	1.33%
11	0.000343	0.000332	3.20%
1	0.000179	0.000175	2.23%

1) 11616 Nodes, CPU (SPARC 1+) = 1740 Sec
2) 384 Nodes, CPU (SPARC 1+) = 16 Sec

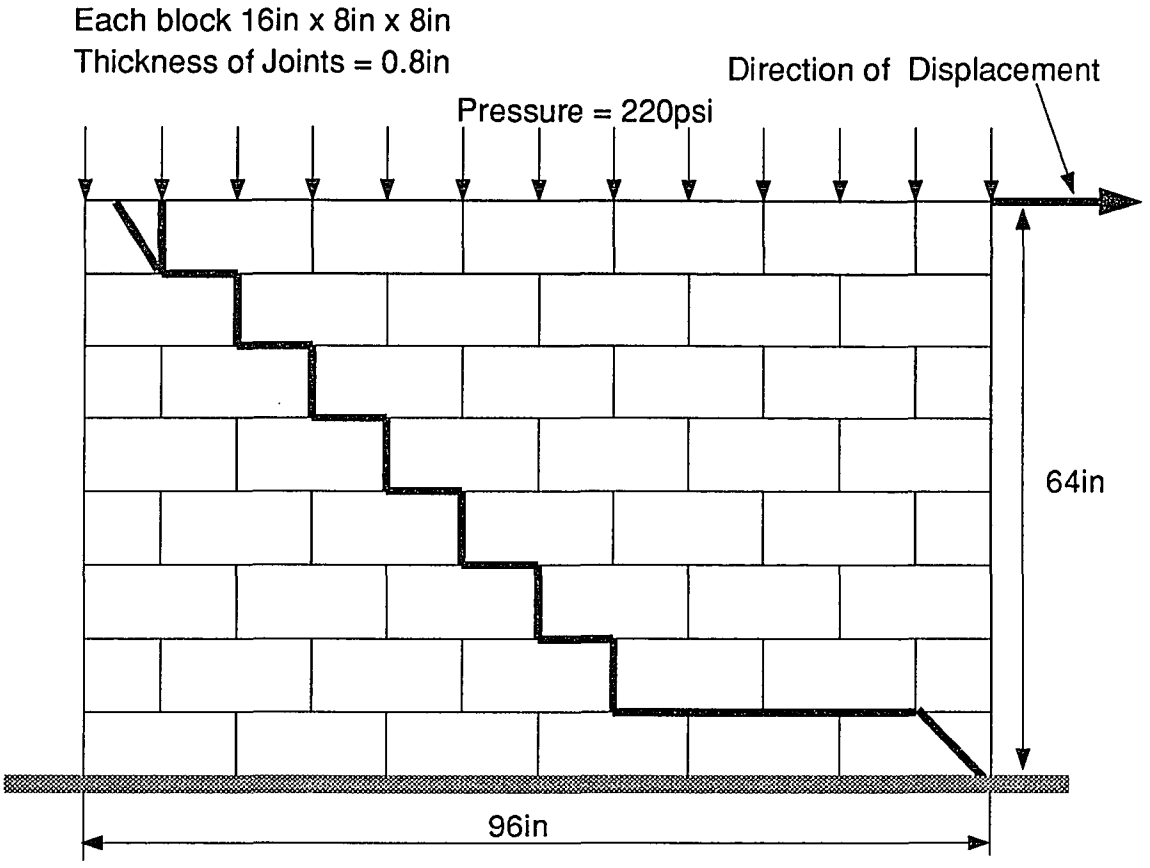

In example 4.1 this wall is used to compare results between fine mesh (Fig. 4.2) and coarse mesh (Fig. 4.3) in linear range.

In example 4.2 this wall is used to compare experimental results with analytical results based on coarse mesh (Fig. 4.3)

Loading conditions shown here are for example 4.2

Figure 4.1 Experimental Cracking Pattern (Woodward & Rankin)

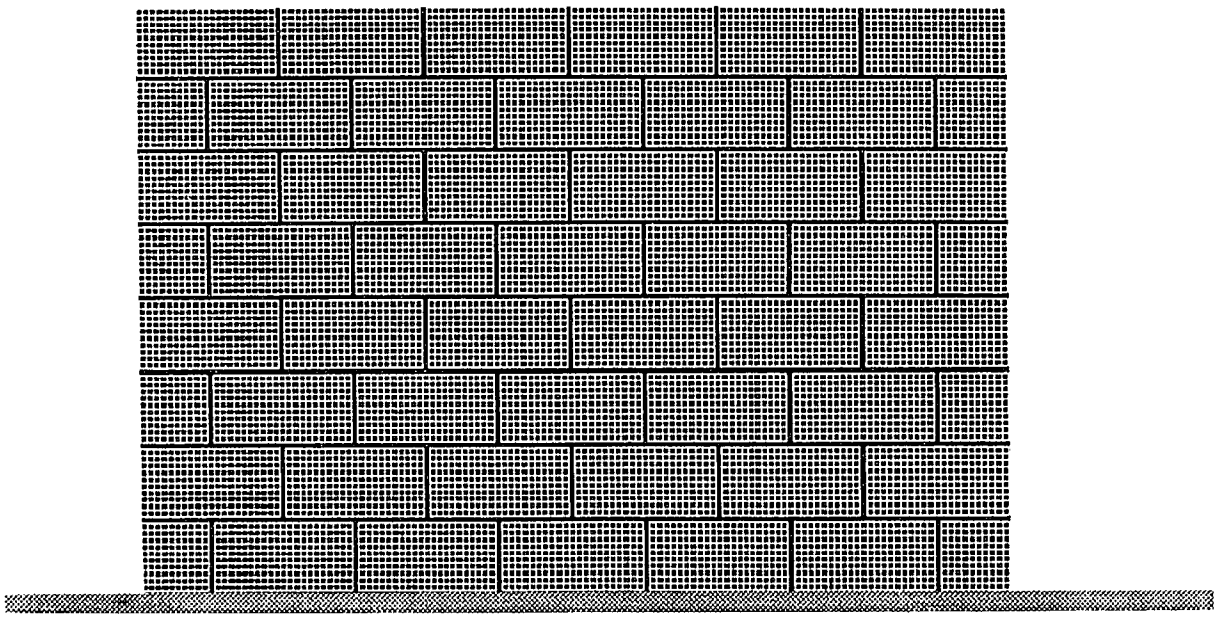

Figure 4.2 Fine Mesh Model for Example 4.1

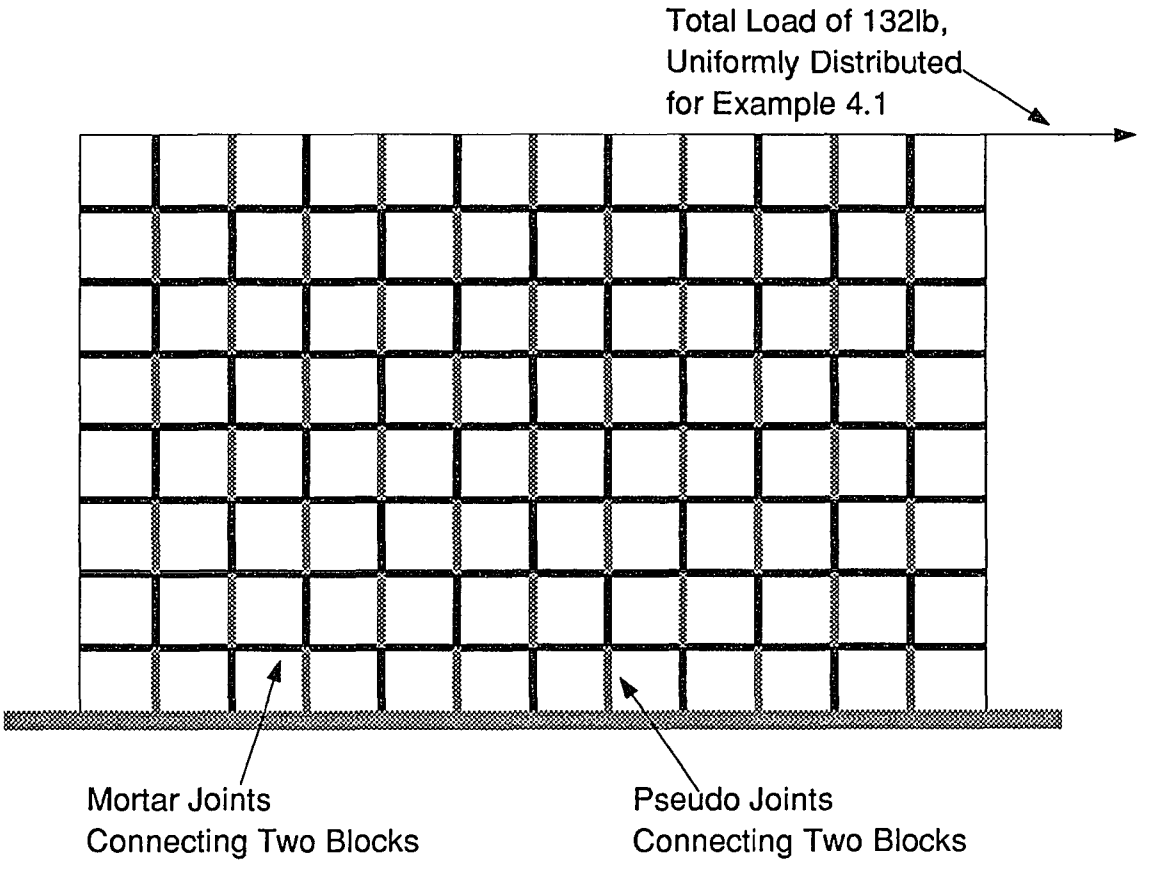

Figure 4.3 Coarse Mesh for Example 4.2

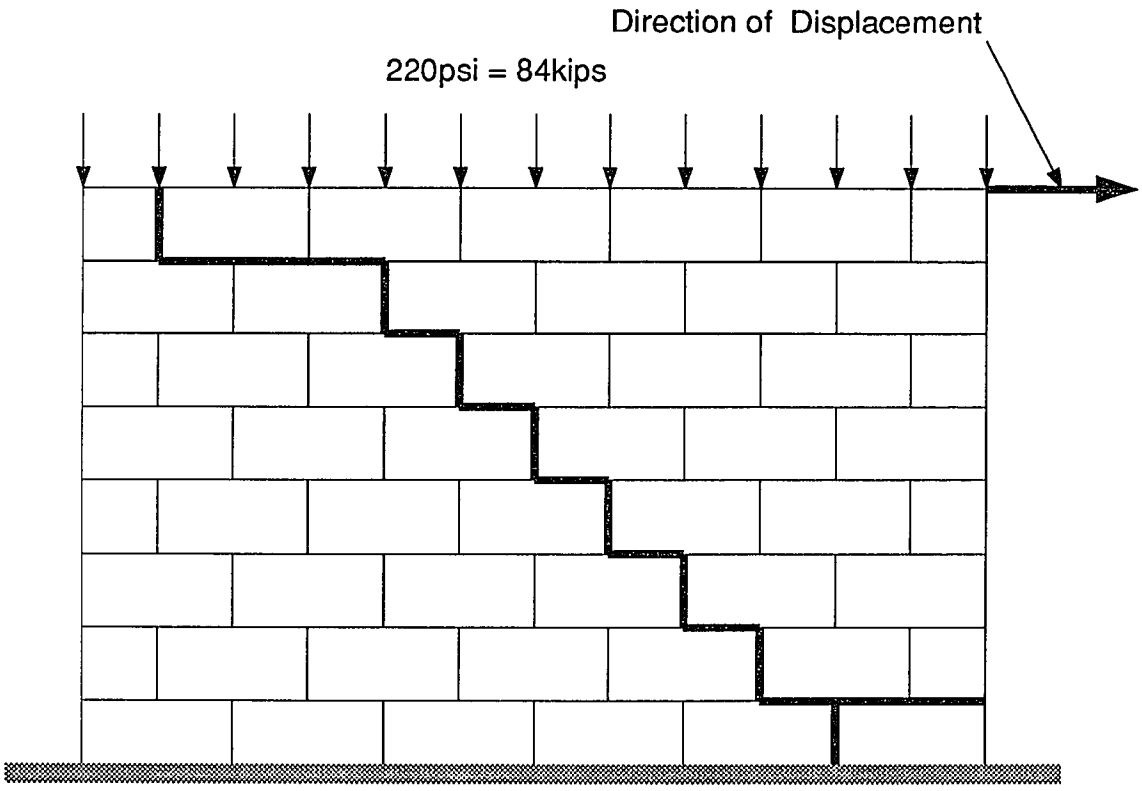

Figure 4.4 Predicted Cracking Pattern

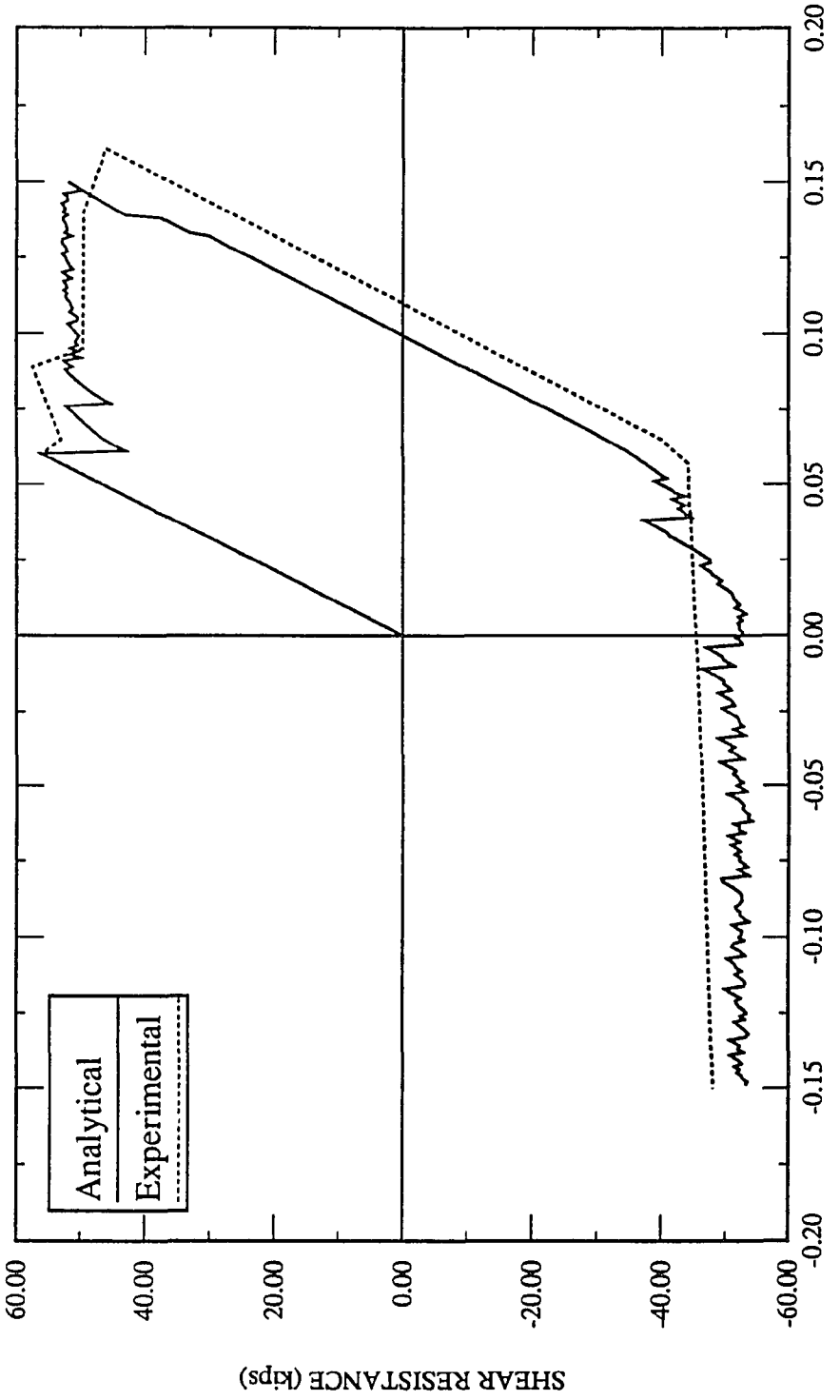

Figure 4.5 Comparison of Load Deflection Curve for Problem 4.2

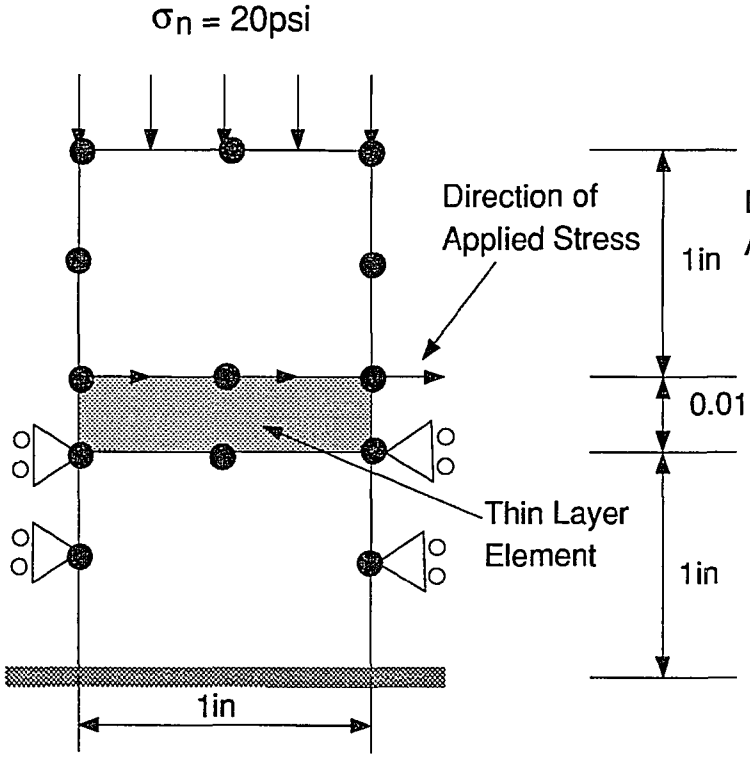

Figure 4.6a Modeling of Direct Shear Test by Sharma and Desai [57]

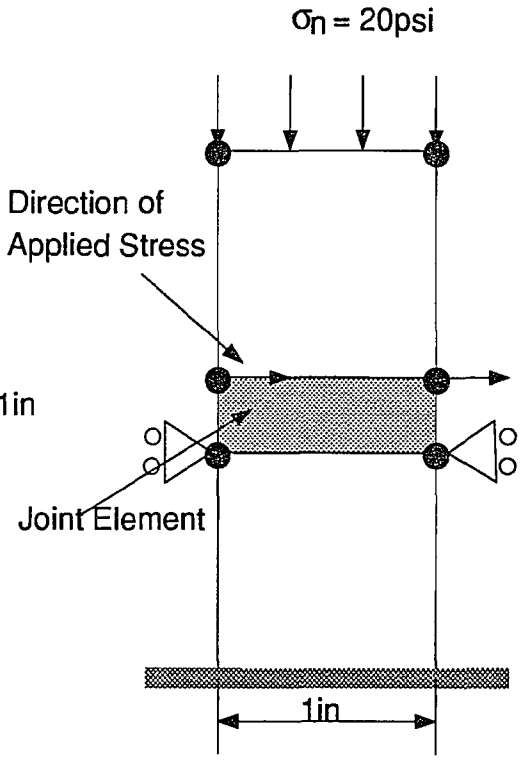

Figure 4.6b Model Developed in this Study

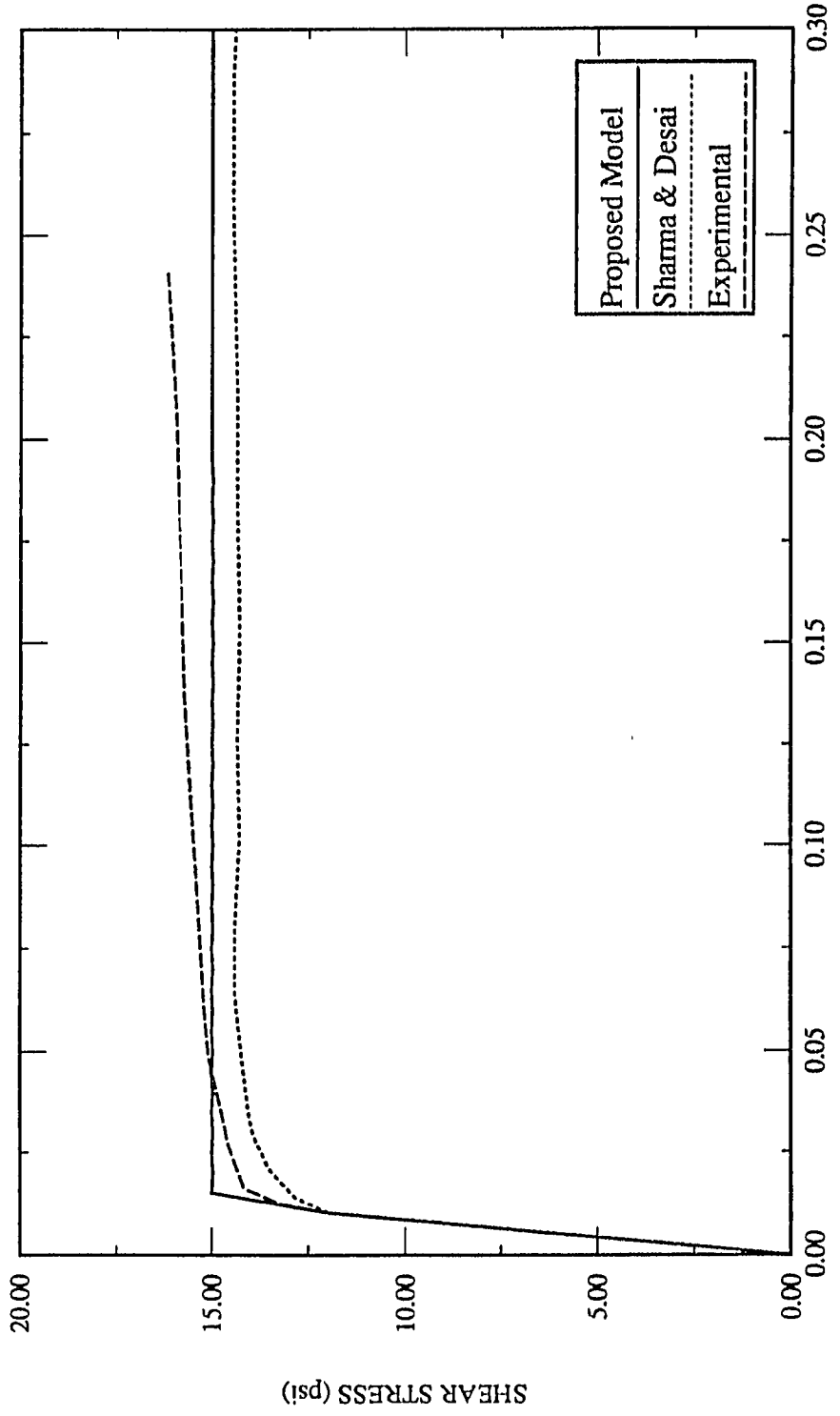

Figure 4.7 Comparison of Load Deflection Curve for Problem 4.3

CHAPTER 5

APPLICATIONS: STATIC ANALYSIS

This chapter is divided into two sections. In the first section, nonlinear analysis of three URM walls is presented followed by the explanation of the observed behavior. In the second section, analysis of two retrofitting schemes commonly used in practice is discussed.

5.1 Nonlinear Analysis of URM Walls

Wall Details: Following nomenclature is used in the discussion of results. The first two numbers represent size of the wall in inches. This is followed by either "W" for wall without opening or "O" for wall with opening. The last number represents total vertical compressive force (kips) applied to the wall. Thus, 96x64W84 represents a wall with length of 96in, height of 64in and vertical compression of 84kips (220psi), which was discussed in the Section 4.2. The total compression was different for different walls so as to simulate the shear failure. In order to make comparison of results, other parameters and boundary conditions for all the URM walls were kept the same as those used in the example 4.2 of the previous chapter.

Analysis of 96X96W96: The behavior of this wall was similar to 96X64W84 wall, i.e. shear failure. If total compression is kept the same as that for 96X64W84 wall (220psi), the wall would exhibit combined shear and bending mode of failure. Little increase in compression would suppress the bending mode of failure and hence total compression of 96kips (300psi) was used. The first two cracks developed in two staggered joints at the center when the lateral displacement was 0.095in.

These cracks propagated towards the corners of the wall. Unlike 96X64W84 wall, no sliding was observed at the corners of the wall. Cracking pattern is shown in Fig. 5.1. Load deflection curve is shown in Fig. 5.2. Maximum shear resistance was 50kips (corresponding to 131psi shear stress).

Analysis of 240x120W210: The aspect ratio (length/height) of this wall is more than that of 96X64W84 wall. If 96X64W84 wall fails in shear for a certain value of compressive force per unit length, then the same force per unit length would ensure shear failure of the wall with larger aspect ratio. Based on this logic total compressive force of 210kips (220psi) was applied. As can be seen from cracking pattern (Fig. 5.3), two cracks run across the wall separating the wall into three parts. These cracks started in staggered joints in the center course when lateral deflection was 0.116in. These joints were at the same distance from the center of the wall. Load displacement curve is shown in Fig. 5.4. Maximum shear resistance was 150kips (157psi).

Analysis of 96X96O96: This wall has an opening of 32x32in^2 at the center. The cracking started at the top left and bottom right corners of the opening when lateral displacement was 0.095in. The crack continued towards the corners of the wall in stair shaped fashion. Figs. 5.5 and 5.6 show cracking pattern and load deflection curve, respectively. Maximum shear resistance was 29kips (114psi).

General Discussion: All walls except the one with opening show drop in strength with the development of crack. The shear resistance drops after failure and increases again. Such a behavior can be explained as follows:

In nonlinear analysis stresses will be redistributed with failure of joint elements. Flow rule decides the redistribution of stresses and direction of failure (yielding).

Flow rule will be associated if failure is perpendicular to failure surface and non-associated otherwise. In the present case flow rule is non-associated as shown in Fig. 2.11. As a result, shear strength drops from "initial failure surface" to "subsequent failure surface" for elements that have failed in compression and shear. This could result in drop in shear strength for the displacement controlled problem as can be seen from load deflection curves (Fig. 5.2 and Fig. 5.4). After the sudden drop, the resistance increases again with increase in the displacement. Under this condition joint elements that have failed in compression and shear will be on "subsequent failure curve" (Fig. 2.11). Shear force in these elements remain constant if vertical compression is constant. All other joint elements will be within "initial failure curve". Stresses in these joint elements will increase with the increase in displacement. Consequently, shear resistance increases after initial failure. The second drop occurs when another transition from "initial failure curve" to "subsequent failure curve" occurs for more elements. The process continues until the crack has fully developed. Similar behavior can also be seen in experimental load-deflection curve shown in Fig. 4.5. In the case of 96X96O96 wall, opening is equivalent to failure of joint elements at zero lateral displacement. This has a considerable effect resulting in lesser strength.

Table 5.1 shows initial stiffness of the walls. This stiffness is shear resistance of walls for unit displacement at the top edge when the wall deflected in double curvature. The stiffness increases with increase in the aspect ratio of the wall. The 96X96O96 wall has its shear area reduced because of opening as compared to 96X96W96 wall, resulting in lower stiffness and strength. The opening reduces shear area by 33% and corresponding reduction in shear strength is 42%.

Considering four equations given in section 6.5.2 of ACI code for URM design

[4], shear strength of all the walls will be governed by the last equation:

$$f_v = 1.5\sqrt{f'_m} \tag{5.1}$$

Where f'_m is compressive strength of masonry (1800psi). Thus, for all walls allowable shear stress will remain the same irrespective of aspect ratio, vertical compressive stress, bond strength, etc. Column 5 in Table 5.1 shows shear resistance of walls using this formula and column 6 gives factor of safety which is the ratio of design shear stress given by ACI to the shear strength obtained from analysis. It can be seen that factor of safety varies from as high as 2.78 for 240X120W210 wall to as low as 1.78 for 96X96O96 wall.

5.2 Evaluation of Some Retrofitting Schemes

According to Federal Emergency Management Agency (FEMA) report for rehabilitating existing buildings [59], inplane shear strength of URM walls can be increased by adding supplemental members. Two possibilities suggested in the report will be discussed. In the first scheme, hereafter referred to as Rehab1 (extension .R1 for Tables and Graphs), a steel frame around the wall is used to strengthen the wall. As pointed out by task group for masonry structures (in a workshop sponsored by NSF on repair and retrofit of existing structures) [50], this is a frequently used method to provide strength and ductility to existing URM structures and research efforts are especially needed for steel frame with masonry infill. In the second scheme, denoted by Rehab2 (extension .R2 for Tables and Graphs), bracing along the diagonals of the walls are used to strengthen the wall.

5.2.1 Design of Rehab1

For design of the frame surrounding the wall (Fig. 5.7), concept of relative stiffness

is used. Relative stiffness parameter, introduced by Safford & Smith [40] for the design of infilled frames, is the ratio of wall stiffness to frame stiffness. This parameter is derived based on the assumption that the infill acts as equivalent strut along the diagonals of the frame. Values ranging from 4 to 12 have been reported in literature [44]. From the load deflection curves of URM walls, initial stiffness of the wall can be determined. Relative stiffness parameter between 3 to 4 was selected to determine moment of inertia of columns in the steel frame. From AISC, a steel section was selected and equivalent plane stress element was designed so as to have the same area and moment of inertia as the original section. Four noded isoparametric plane stress elements with unit thickness were used to model steel frame. Two possibilities were considered. In the first case analysis was done such that total compression in the Rehab schemes would be same as that on URM walls discussed in previous section (see Table 5.1). This total compression would be distributed between frame and wall according to their axial stiffness. In the second case total compressive force was increased so that the portion going to the wall would be same as the vertical force given in Table 5.1.

Boundary Conditions: The top edge of the beam remained horizontal throughout the analysis. Base of the frame and wall was fixed. Lateral incremental displacement was applied to the top edge of the beam. For linear analysis, two cases for interface conditions were considered. The first case assumed no bond between frame and wall. In the second case full interaction between frame and wall was assumed. For nonlinear analysis, only the second case (i.e. perfect interaction between wall and frame) was assumed. Kinematic bilinear hardening rule was used to model yielding of steel frame. Bond failure surface, as discussed

before, was used to model failure of joints. Brick elements were assumed to be linear.

General Discussion: Table 5.2 shows shear stiffness of frame and wall for two possibilities, no interaction and full interaction. No interaction between frame and wall implies that each one is free to deform so as to have the minimum strain energy in each component. The relative stiffness based on no interaction was used to design the frame. If perfect bond is assumed between frame and wall the stiffness of both wall and frame increases. Full interaction can be viewed as a constraint so that deflection at the interface is same for both frame and wall. Consequently deflected shape of each component no longer correspond to minimum strain energy, increasing stiffness of each component. It can be seen that the increase in stiffness of frame is much more than the increase in stiffness of walls (149% for frame as against 1% for wall, in the case of 96X64W.R1). Consequently, relative stiffness decreases and contribution of frame in resisting lateral forces increases significantly. Steel frame is a structural system used to strengthen the existing URM wall, and is more ductile than the wall. Hence increased contribution of steel frame would be good for efficiency and overall performance of the system.

In the first case of nonlinear analysis, assuming full interaction, total compression on the system was the same as compressive force on the corresponding URM wall discussed in section 5.1 and given in Table 5.1. Two walls were analysed for this case. Figs. 5.8 and 5.9 show load-displacement curves for 96X64W.R1 and 96X96W.R1. From Table 5.3, it can be seen that the axial stiffness of the frame is four to five times that of the URM wall. The total compressive force

was distributed according to these stiffnesses, resulting in significant reduction in compressive force on the wall. Therefore, the shear resistance at the beginning of cracking is significantly smaller as compared to the corresponding value for URM wall alone. From load deflection curves it can be seen that the failure of the system is sudden. Such a behavior can again be attributed to the significant reduction in compression on the wall and can be explained as follows. Shear resistance of joints after the first failure (Fig. 2.11) is proportional to the compressive force and would be close to zero if compressive force is very small. Consequently, large amount of shear force will be released due to failure of joints, causing crack to develop fully in single load step which results in sudden failure. Steel frame remained within elastic limit. The reduction in the shear strength of URM offsets the increase in capacity due to addition of steel frame. As a result, the increase in strength of combined system over corresponding URM wall is 20 % for 96X64W.R1 and 33% for 96X96W.R1. It can be concluded that interaction of both axial and flexural/shear stiffness needs to be considered while designing the strengthening scheme.

In the second case, total compressive force on the system was increased so that the portion going to wall would be equal to the total vertical force on the corresponding URM wall alone as discussed in section 5.1 (Table 5.1). Walls would exhibit shear mode of failure in this case. See Figs. 5.10 to 5.12 for load displacement curves. Table 5.4 shows the total compression and shear strength of each component in the system. From load displacement curves it can be seen that the stiffness of frame is perturbed by the stiffness change in wall. Interaction between wall and frame is the cause for such a perturbation. With the failure of elements in the wall, its deflected shape changes. This influences the deflected

shape of the frame due to perfect bond conditions at the interface, resulting in disturbance in the frame stiffness. When the failure of combined system occurred, the steel frame had yielded. The increase in shear capacity over the original URM wall is 159% for 96X64W.R1, 176% for 96X96W.R1, and 303% for 96X96O.R1.

5.2.2 Design of Rehab2

As mentioned before, this scheme uses diagonal bracing for strengthening URM walls. In order to compare relative merits of the two retrofitting schemes, total volume of steel used in strengthening two solid walls was approximately kept equal. Cross sectional area of tie-down members and bracing members was kept same. Beam element with zero inertia was used to simulate effect of bracing. For the case of wall with opening, steel frame was placed around the opening. The depth of this frame was equal to the thickness of the blocks (Fig. 5.14). It is found that construction of bracing system is quite sensitive to actual dimension of existing structure. Ensuring proper joint matchup and correct length for members requires larger degree of fabrication in the field than that would be expected in new steel construction. All members of the bracing system should be selected based on considerations of fabrication, facilitation of connections between masonry and steel, and aesthetics. Some of the important construction aspects of the bracing system for strengthening existing structures are discussed in reference [13].

Boundary Conditions: All walls were fixed at the base. No rotation condition at the top edge was maintained throughout the analysis. This was done using coupled degrees of freedom discussed in section 4.3. Perfect bond was assumed between ends of the bracing bars and corresponding corners of the wall. Lateral incremental displacement was applied at the top edge of the wall. Kinematic

bilinear hardening rule was used to model yielding of bracing bars. Bond failure surface was used to model failure of joints. Brick elements were assumed to be linear.

General Discussion: As done in case 2 of Rehab1, total compression was increased so that the part going to the wall would be same as compression on corresponding URM wall discussed in the first section of this chapter (see Table 5.1). Load deflection curves for three examples are shown in Figs. 5.15 to 5.17. The walls exhibited shear mode of failure in all the cases. Diagonal bracing member started yielding at the point of maximum shear resistance. From load deflection curves for solid walls it can be seen that the cracking in masonry developed when displacement was 0.06 in for 96X64W.R2 and 0.1 in for 96X96W.R2. The shear resistance of solid walls remained almost constant thereafter until the failure displacement (0.19 in for 96X64W.R2 and 0.245 in for 96X96W.R2). As already mentioned, after the first failure of joints in URM walls, shear resistance is proportional to friction and compressive load. Thus, if enough compressive load is applied on URM walls, the resistance of combined system (i.e. both wall and bracing) will be the summation of the shear resistance of individual component.

One of the important points regarding the performance of bracing system is buckling of compression members. Normally cross members are connected at the point of intersection. This would reduce the effective length of members by 50%. Shear strength based on the buckling of diagonal bracing members was found to be more than the shear resistance of bracing system given in Table 5.5. Shear resistance based on buckling strength can be increased by providing more connections between wall and the diagonal members, if necessary.

5.3 Comparison of Rehab Schemes

Table 5.6 shows effectiveness of the two Rehab schemes in increasing the shear capacity of URM walls. For solid walls, the increase in capacity of the combined system is significantly higher for Rehab2 as compared to Rehab1. Rehab1 increases capacity of URM walls by the factor of two to three, where as Rehab2 increases the capacity of URM walls by the factor of nine to eleven. In bracing system axial stiffness of steel members is used to resist the shear force. In the frame system load transfer is through bending/shear stiffness of columns. For the given cross section and length axial stiffness is significantly higher than the bending/shear stiffness. Consequently, Rehab2 offers higher resistance as compared to Rehab1. Ductility requirement is inversely proportional to strength of the system. Thus, larger increase in strength of the retrofitted scheme using bracing system would require lesser ductility demand as compared to frame-wall system.

In the case of the wall with opening, Rehab2 does not show any advantage over Rehab1. The presence of opening does not provide a continuous path across the diagonals for transfer of shear force based only on axial deformation. As a result, both Rehab2 and Rehab3 function in somewhat similar way as far as lateral resistance is concerned.

In both Rehab schemes final failure of the system occurred with yielding of steel members although cracking of walls started much earlier. Normally steel members show significant ductility after yielding. However, as can be seen from the load deflection curves, combined wall-frame system does not show much ductility. This is because full cracking of URM wall occurs much

before steel members start yielding. The shear resistance of combined system increases because of the stiffness provided by the rehabilitation schemes. Once steel members start yielding, numerical procedure does not converge because extensive cracking of walls has already occurred. If improved ductility is desired after the yielding of steel then it is necessary to design Rehab scheme in which full cracking of masonry wall can be delayed after the first failure. External addition of structural system can significantly increase the strength and stiffness but may not be very useful if improved ductility performance is desired.

Table 5.1
Initial Stiffness and Shear Strength of URM Walls

Wall Name	Pressure (Kips)	Initial Stiffness (Kips/in)	Shear Strength (Kips)	Shear Strength (ACI) (Kips)	Factor of Safety
240x120W210	210.00	1310.00	150.00	61.09	2.45
96x64W84	84.00	982.00	58.00*	24.24	2.39
96x96W96	96.00	523.00	50.00	24.24	2.06
96x96O96	96.00	238.00	29.00	16.29	1.78

* Verified Using Experimental Results

Table 5.2
Comparision of Initial Shear Stiffness of Wall and Frame

		No Interaction between Frame & Wall			Perfect Bond between Frame & Wall		
Wall Name	Column Depth (in)	K_w[1] (kips/in)	K_f[2] (kips/in)	K_w/K_f	K_w (kips/in)	K_f (kips/in)	K_w/K_f
96x64W.R1	12.20	982.00	284.50	3.45	992.00	708.00	1.40
96x96W.R1	15.00	523.00	135.60	3.86	610.00	505.00	1.21
96X96O.R1[3]	12.00	238.00	73.00	3.26	454.00	235.00	1.93
96x96O.R1	15.00	238.00	135.60	1.76	438.00	305.00	1.44

1. K_w is Shear Stiffness of Wall
2. K_f is Shear Stiffness of Frame
3. Linear Analysis Only.

Table 5.3
Rehab1, Case I Total Compression is Same as Given in Table 5.1

Wall Name	$R^1=K_{fa}/K_{wa}$	S_w^2(kips)	S_f^3(kips)	S_t (kips)	Increase in Strength[4]
96X64W.R1	4.71	40.00	29.00	69.00	1.20
96X96W.R1	4.49	36.50	30.00	66.50	1.33

1. R=Ratio of Axial Stiffness of Frame to Axial Stiffness of Wall
2. S_w is Maximum Shear Resistance of Wall
3. S_f is Maximum Shear Resistance of Frame
4. Increase in Strength is Based on Shear Strength of URM Walls in Table 5.1

Table 5.4
Rehab2, Case 2 Total Compression Increased so that Compression on URM Wall is Same as Given in Table 5.1

Wall Name	Compression (kips)	S_w (kips)	S_f (kips)	S_t (kips)	Increase Over URM
96x64W.R2	396.00	75.00	75.00	150.00	2.59
96x96W.R2	523.00	60.00	78.00	138.00	2.76
96x96O.R2	738.00	51.00	66.00	117.00	4.03

Table 5.5
Rehab2, Total Compression Increased so that the Wall has Same Precompression as Shown in Table 5.1

Wall Name	Compression (kips)	S_w (kips)	S_b (kips)	S_t (kips)	Increase Over URM
96x64W.R2	325.00	53.00	512.00	565.00	9.74
96x96W.R2	457.00	49.00	484.00	533.00	11.06
96x96O.R2	638.00	27.00	77.00	104.00	3.58

Table 5.6
Effectiveness of Rehab Schemes in Increasing Strength of URM

Wall Name	Rehab 1, Case 2	Rehab2
96x64W	2.59	9.74
96x96W	2.76	11.06
96x96O	3.34	3.58

E_b= 2,410,000psi
E_m= 1,210,000psi
Thickness of Joint = 0.8in

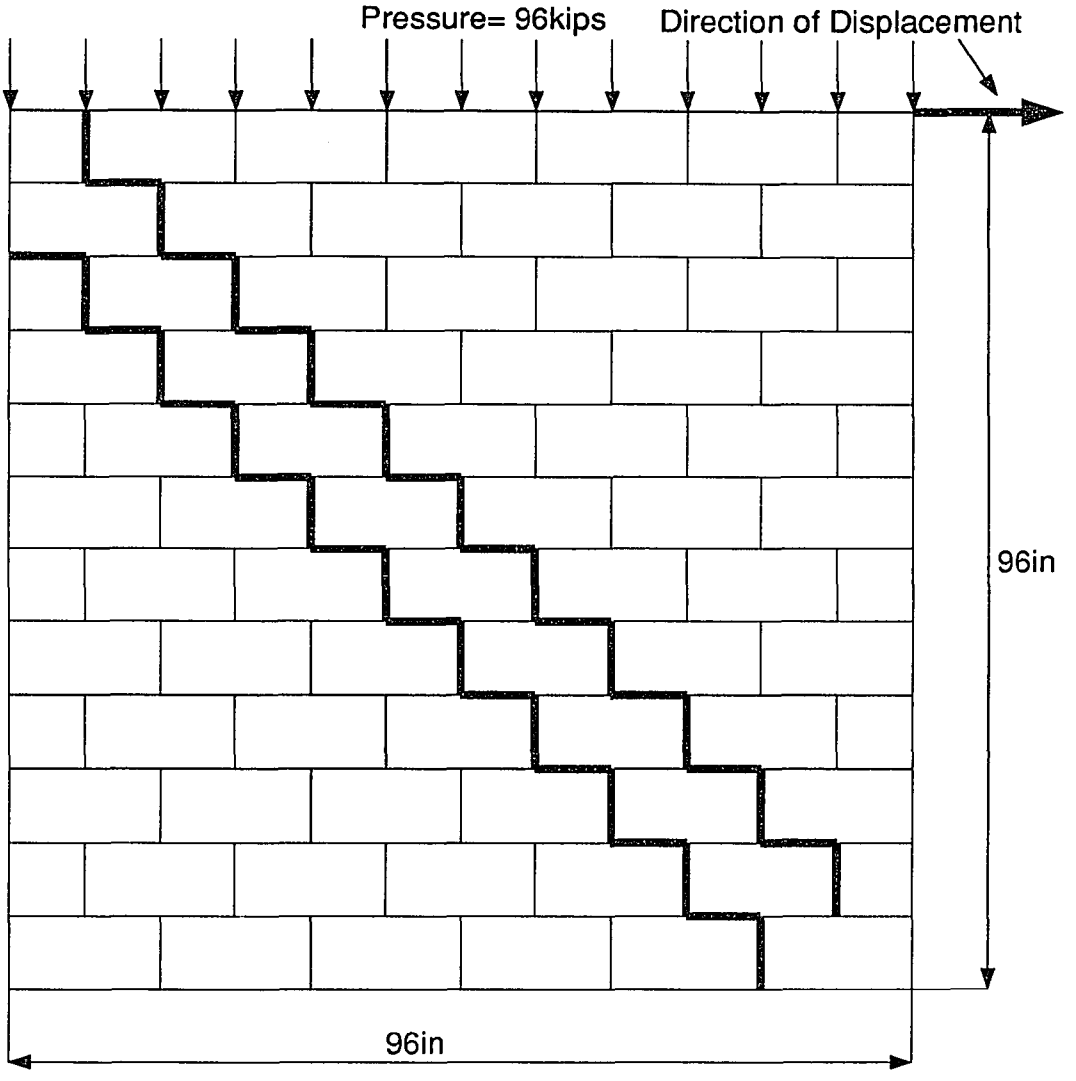

Figure 5.1 96X96W96: Cracking Pattern

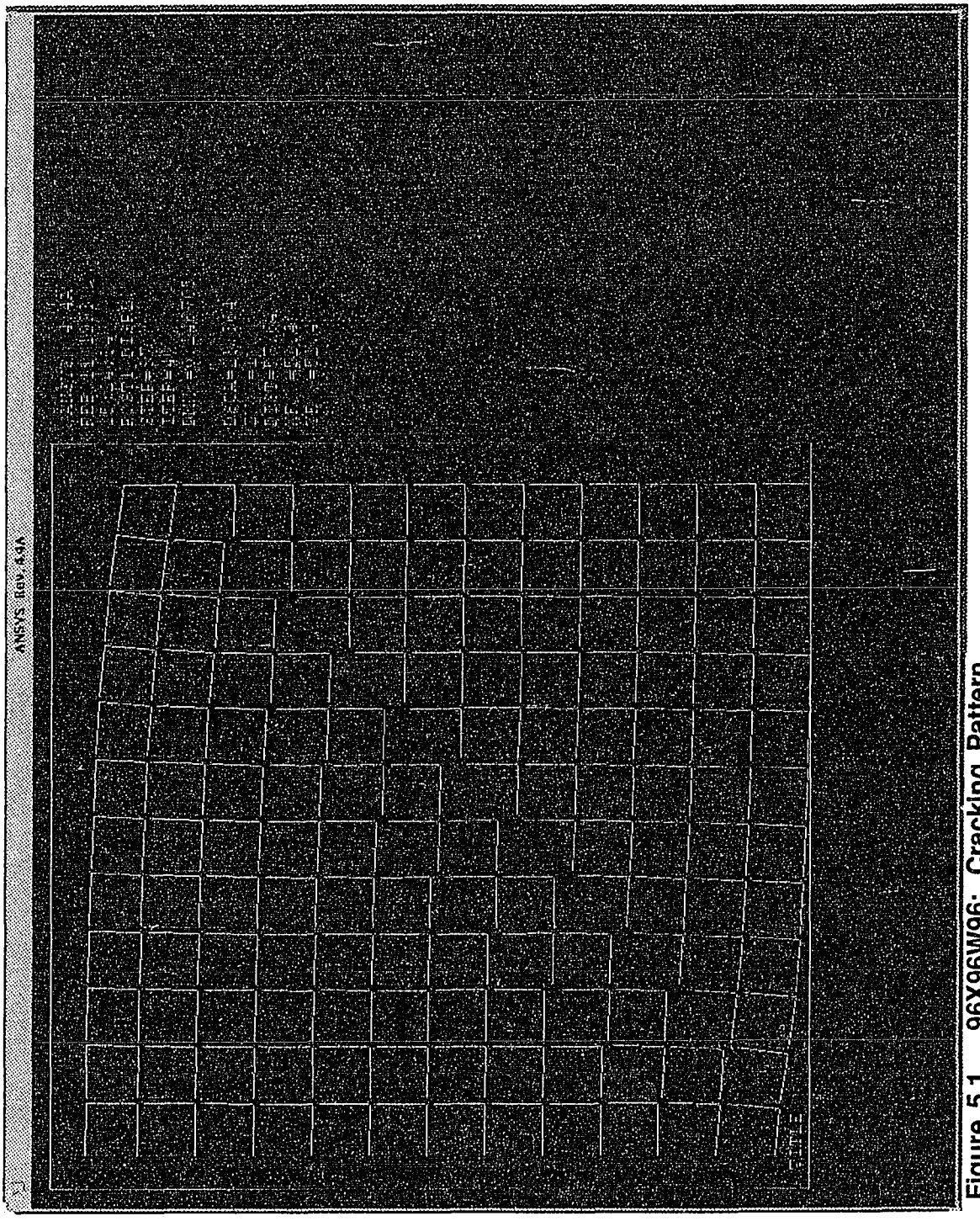

Figure 5.1 96X96W96: Cracking Pattern

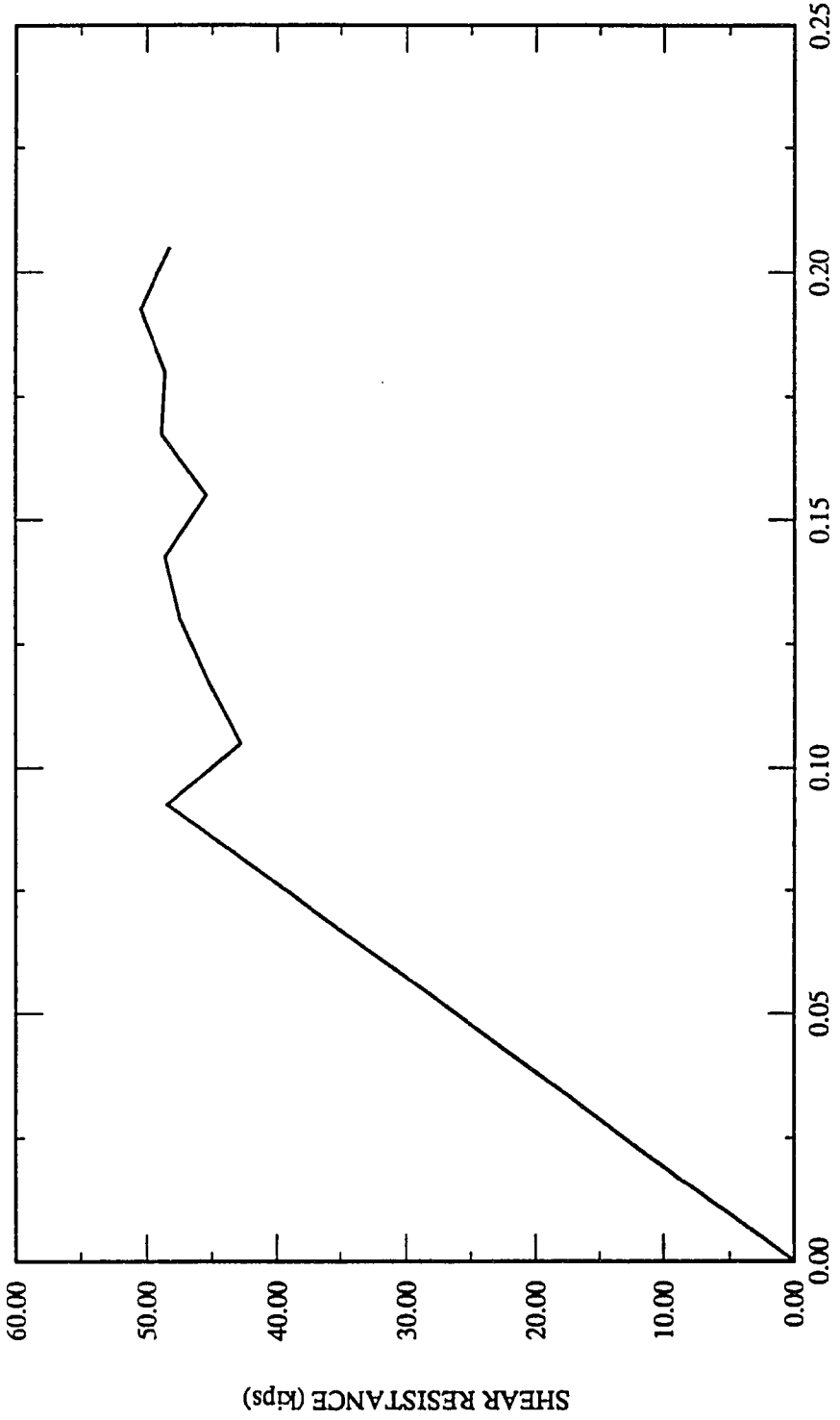

Figure 5.2 Load Deflection Curve for 96X96W96

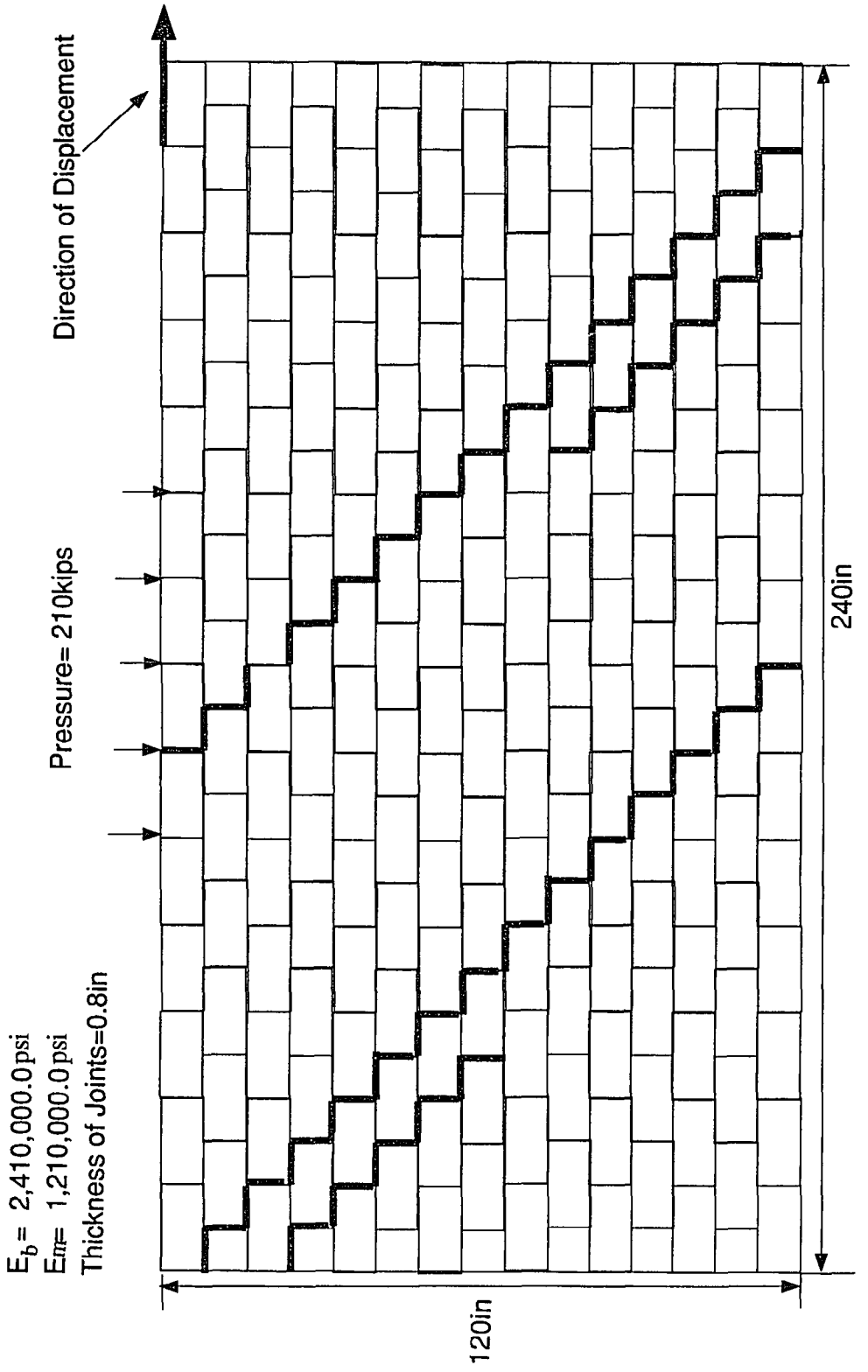

Figure 5.3 120X240W210: Cracking Pattern

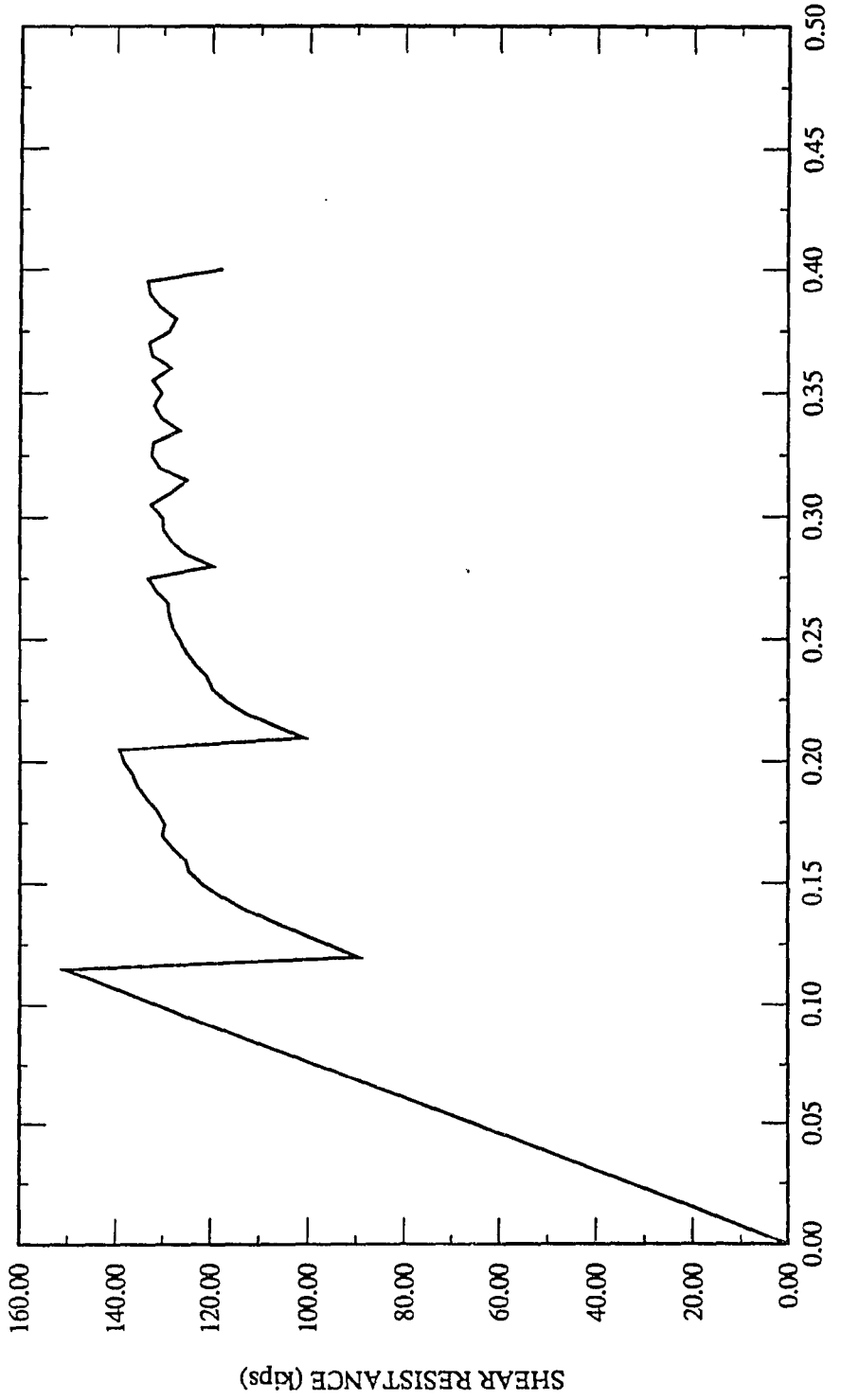

Figure 5.4 Load Deflection Curve for 120X240W210

E_b = 2,410,000 psi
E_m = 1,210,000 psi
Thickness of joints = 0.8in
Opening Size 32 in x 32in

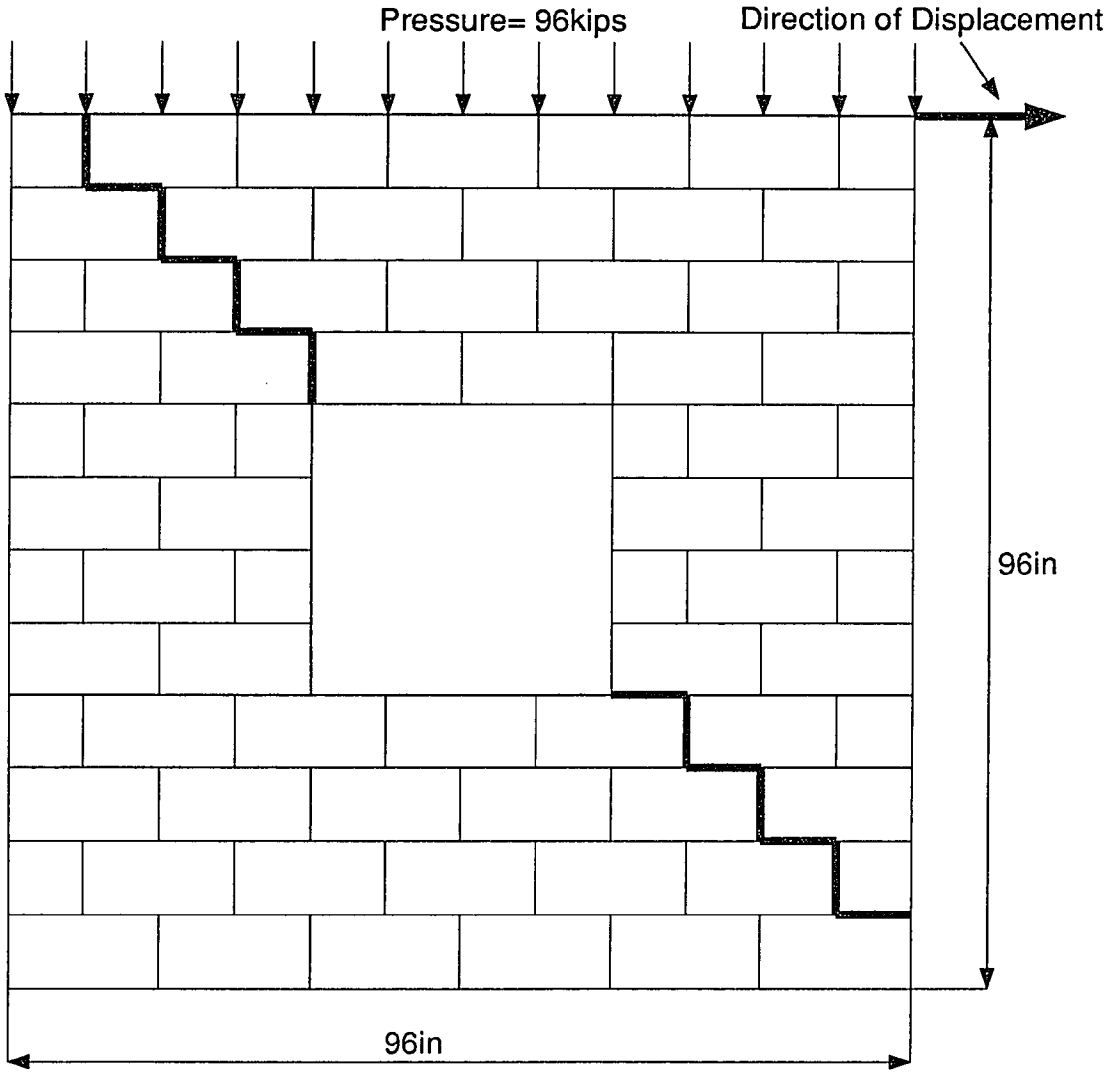

Figure 5.5 96X96O96: Cracking Pattern

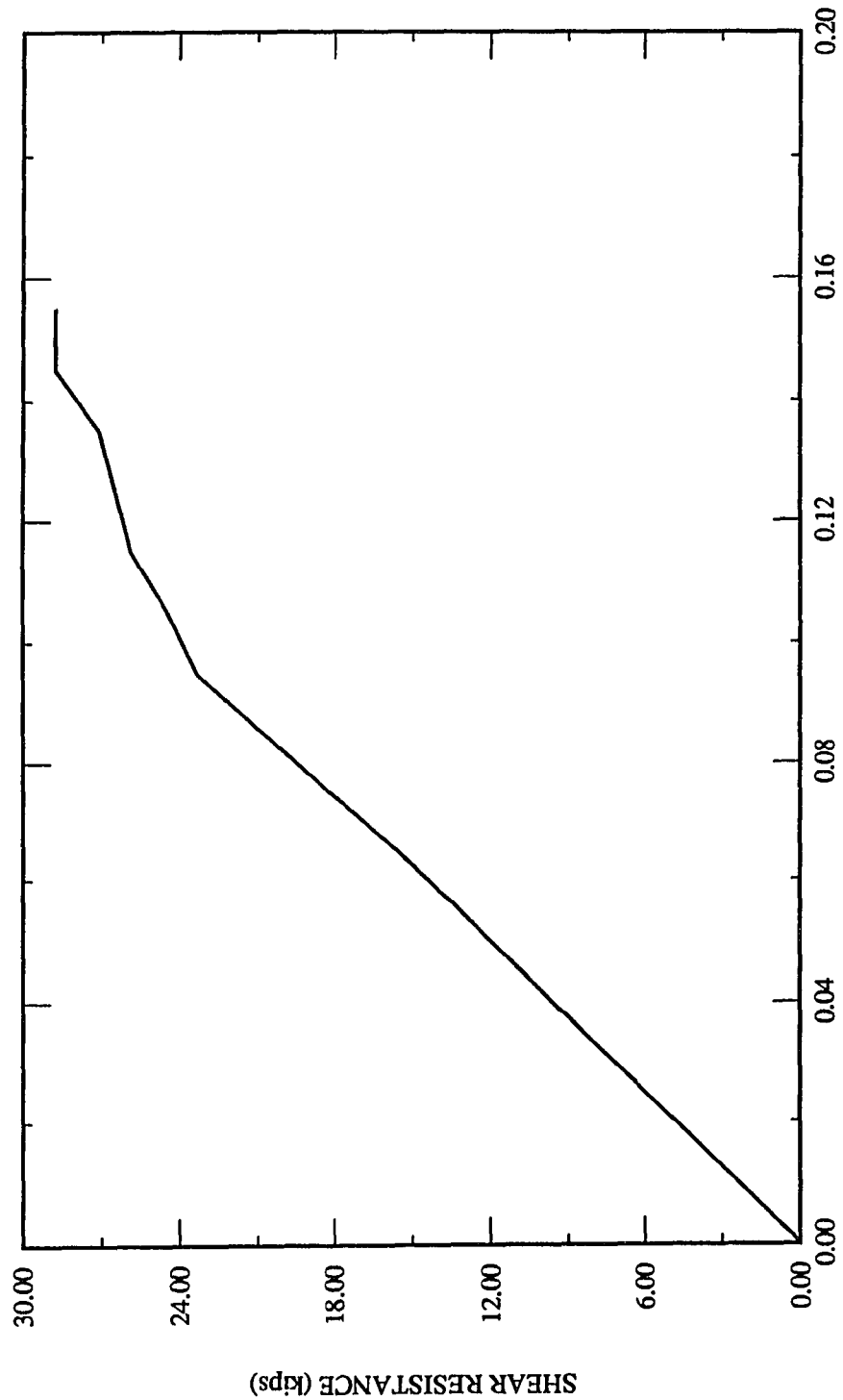

Figure 5.6 Load Deflection Curve for 96X96O96

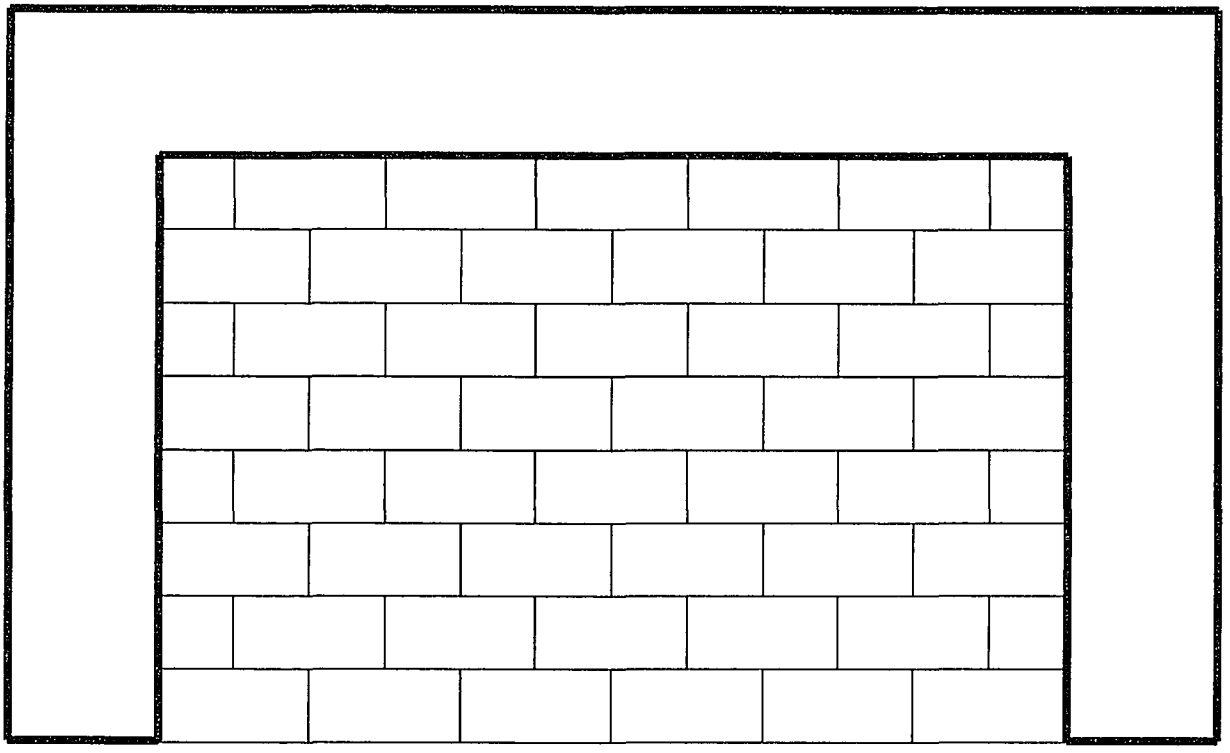

Figure 5.7 Rehab1, Frame Surrounding the Wall

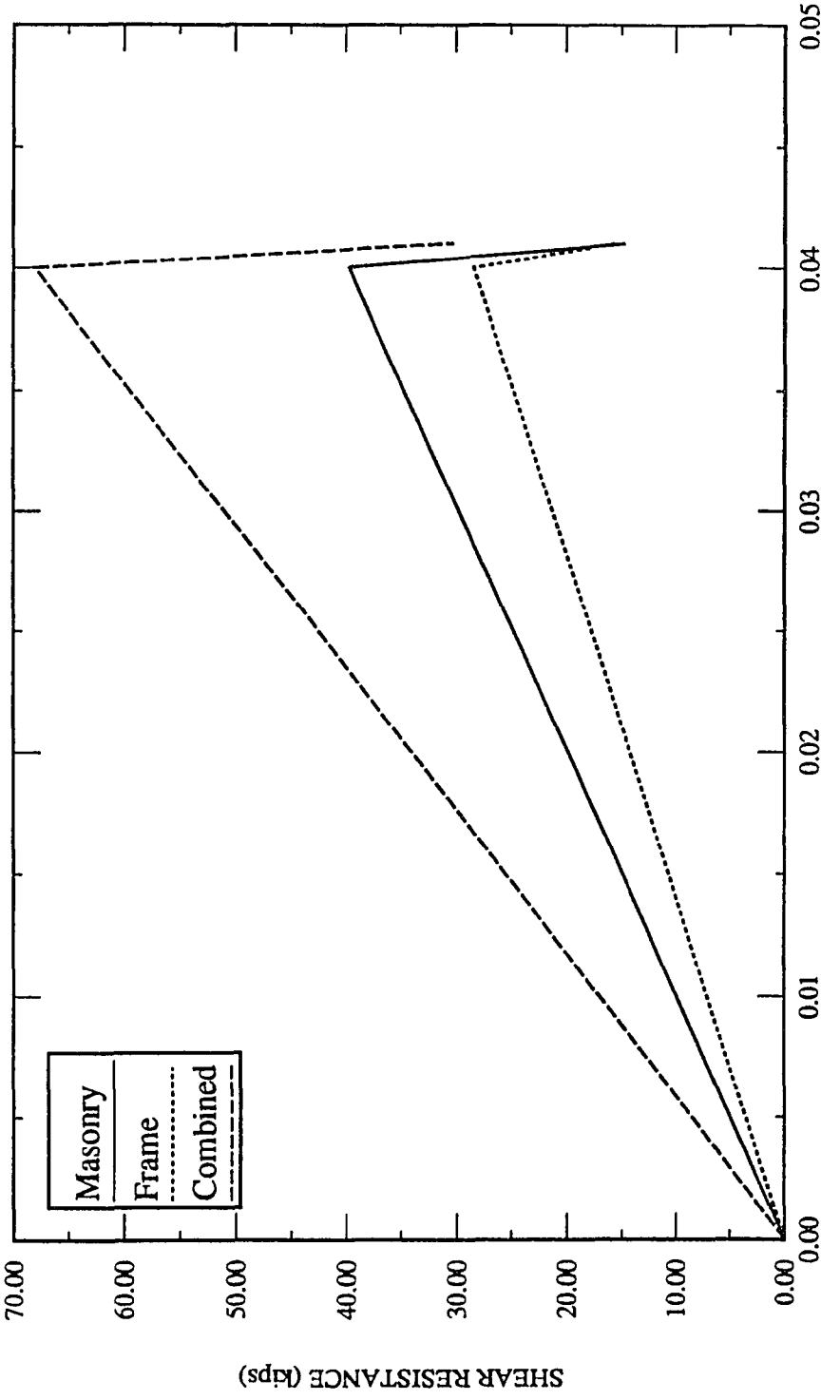

Figure 5.8 Load Deflection Curve for 96X64W.R1, Case1

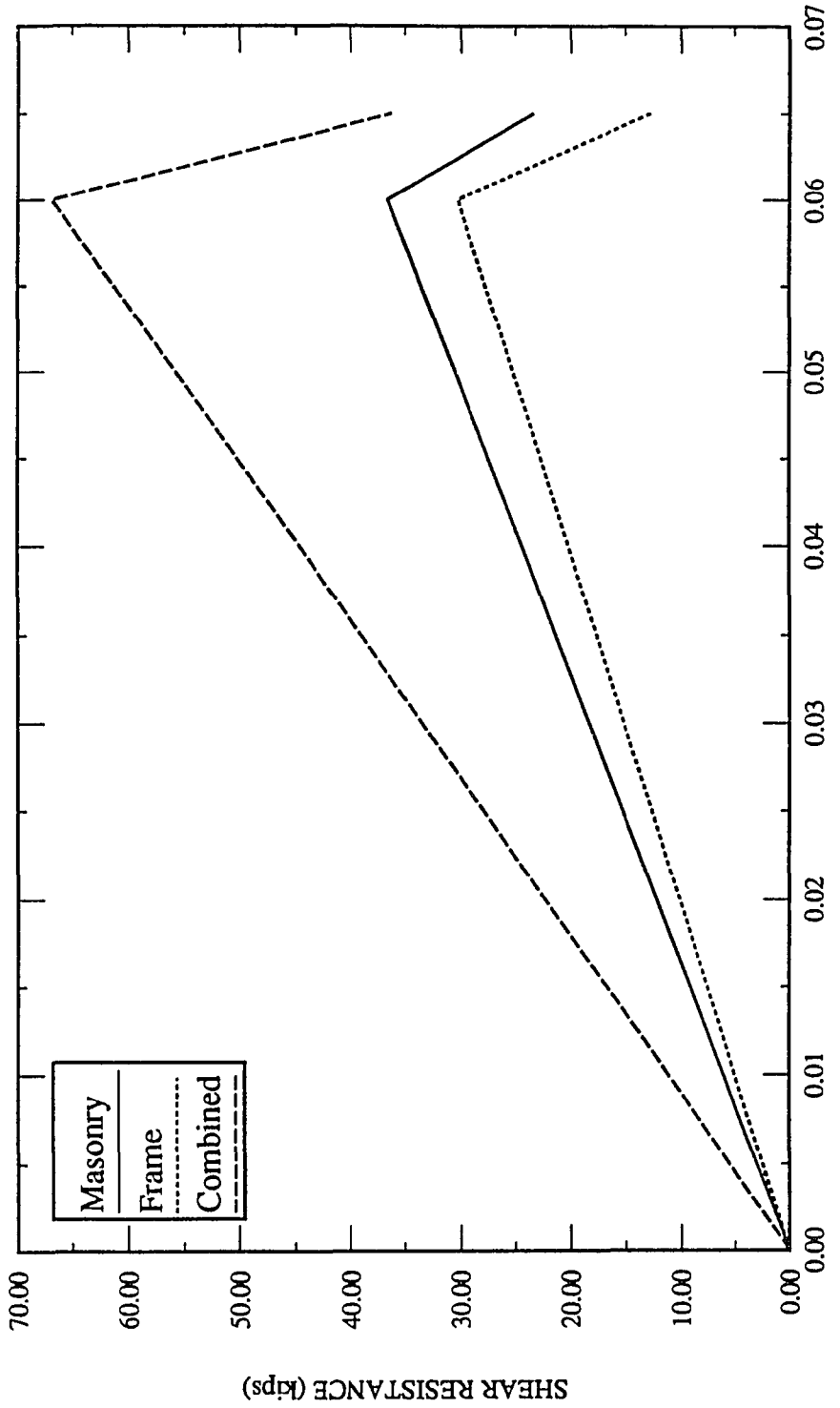

Figure 5.9 Load Deflection Curve for 96X96W.R1, Case1

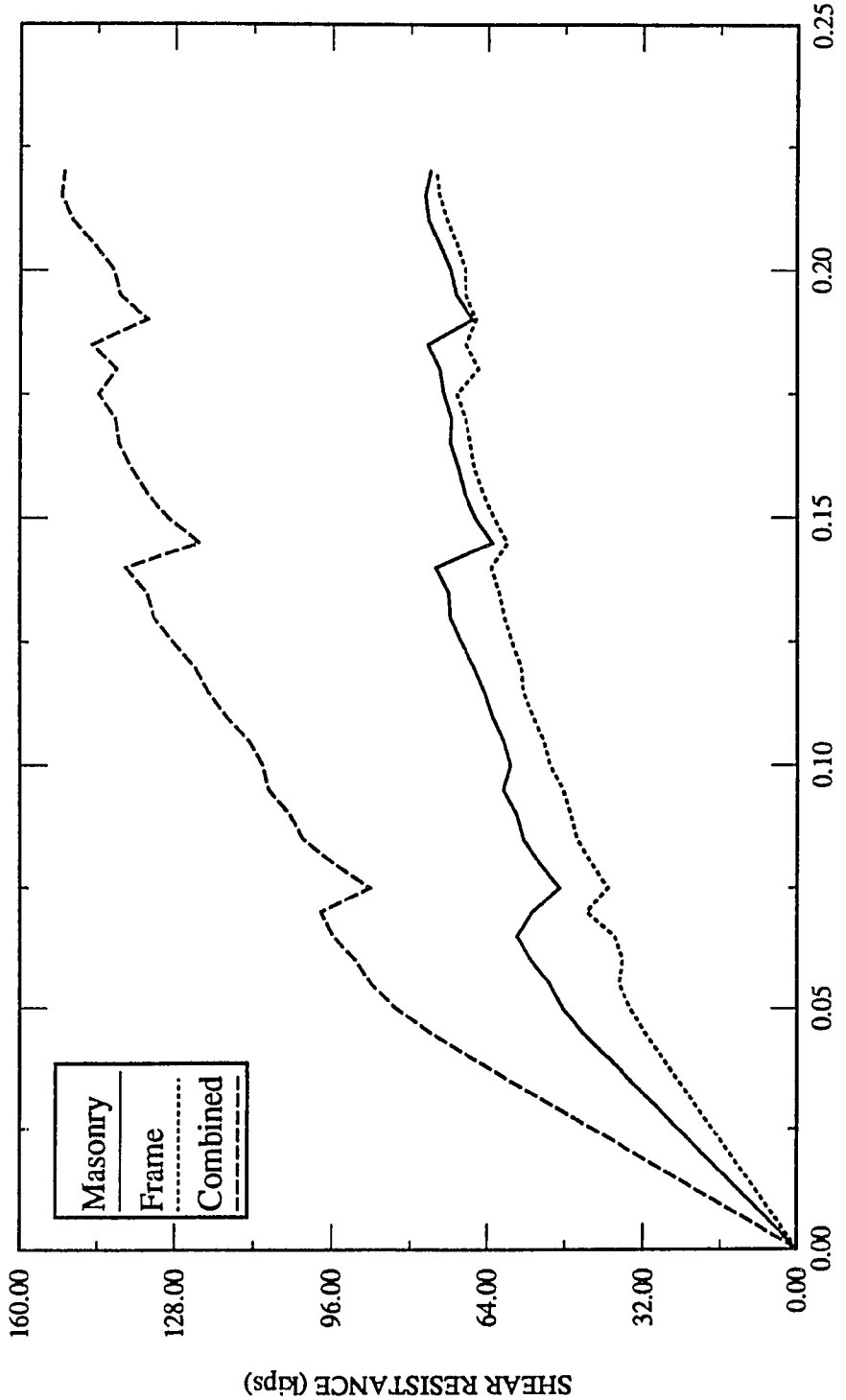

Figure 5.10 Load Deflection Curve for 96X64W.R1, Case2

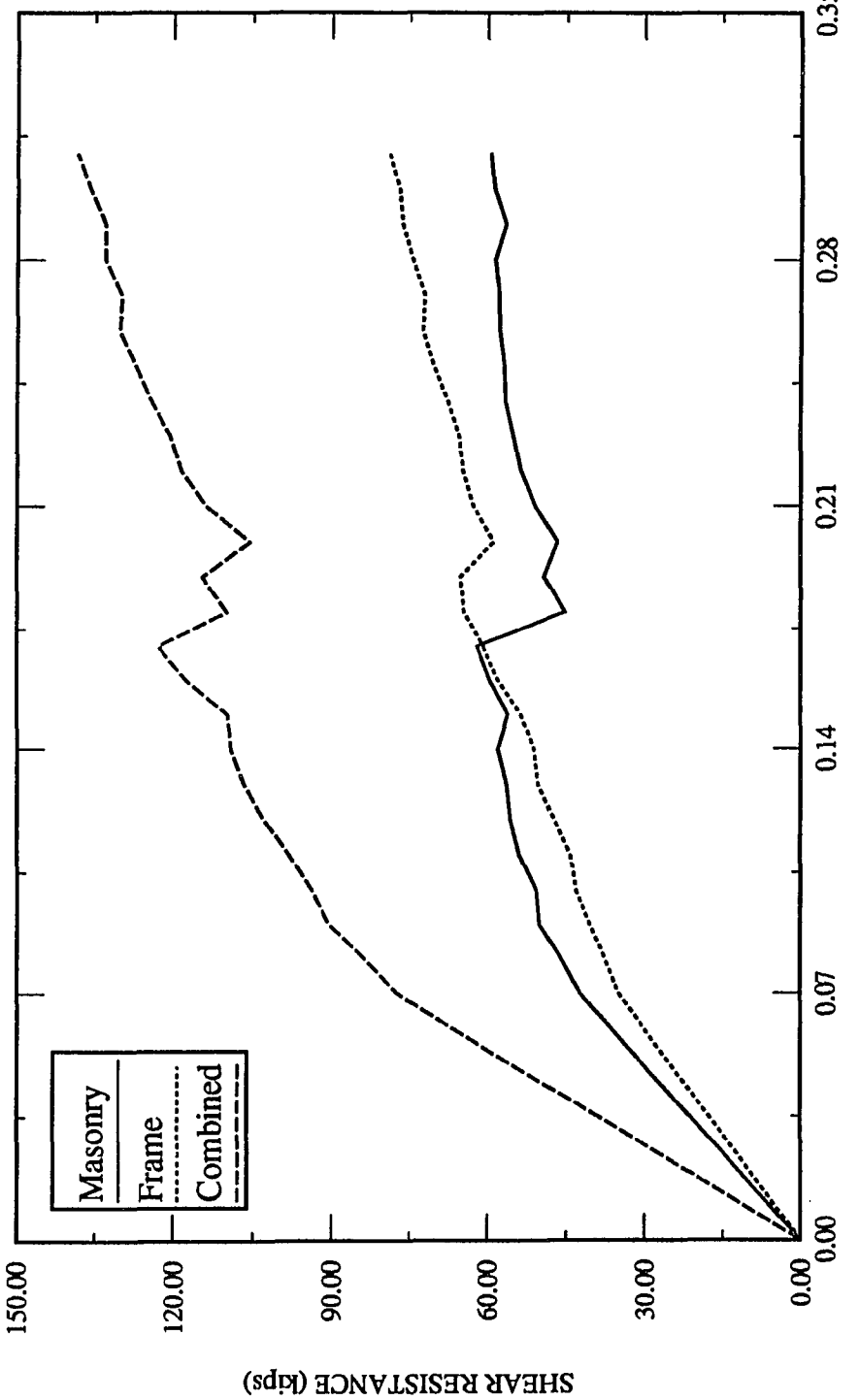

Figure 5.11 Load Deflection Curve for 96X96W.R1, Case2

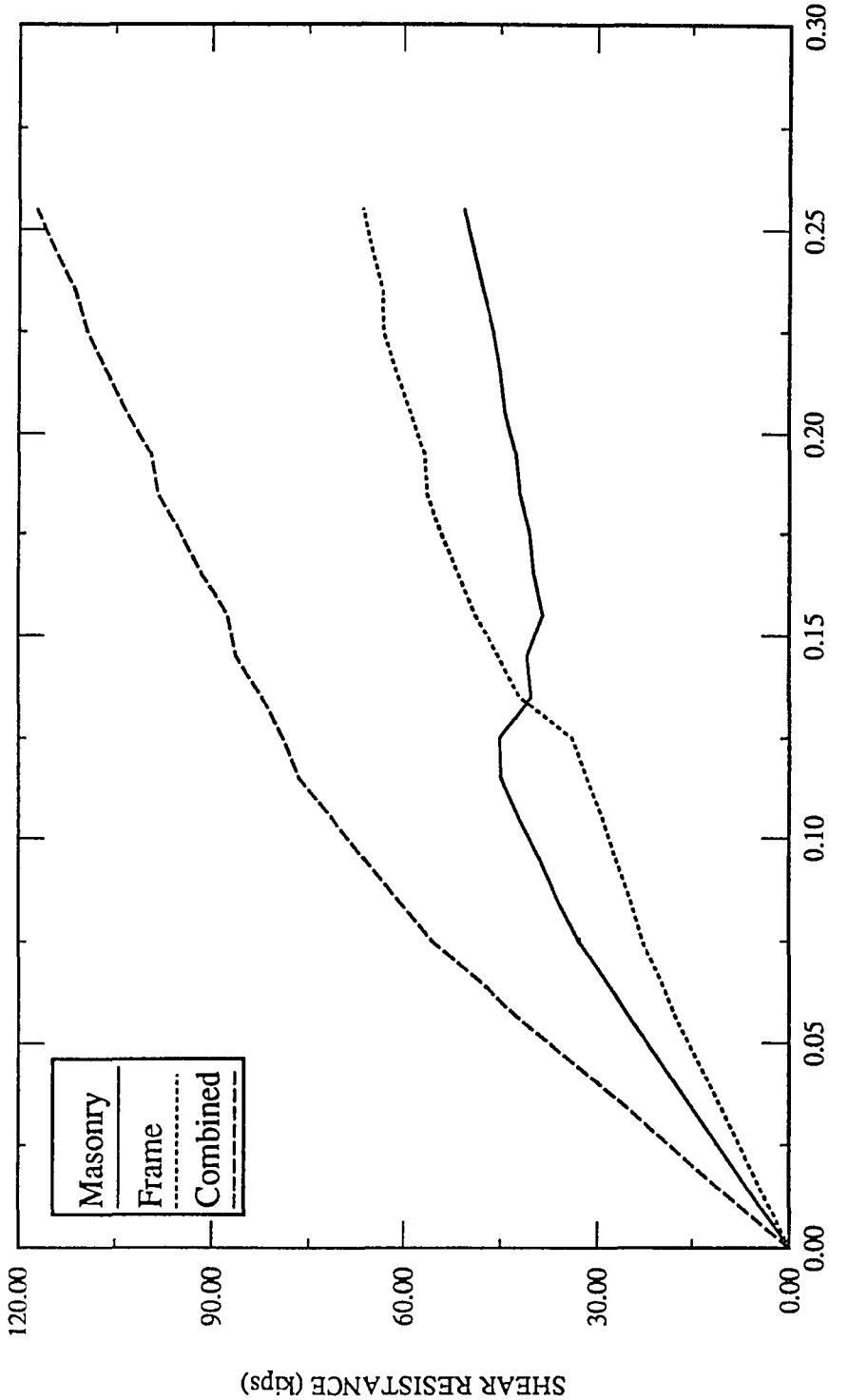

Figure 5.12 Load Deflection Curve for 96X96O.R1, Case2

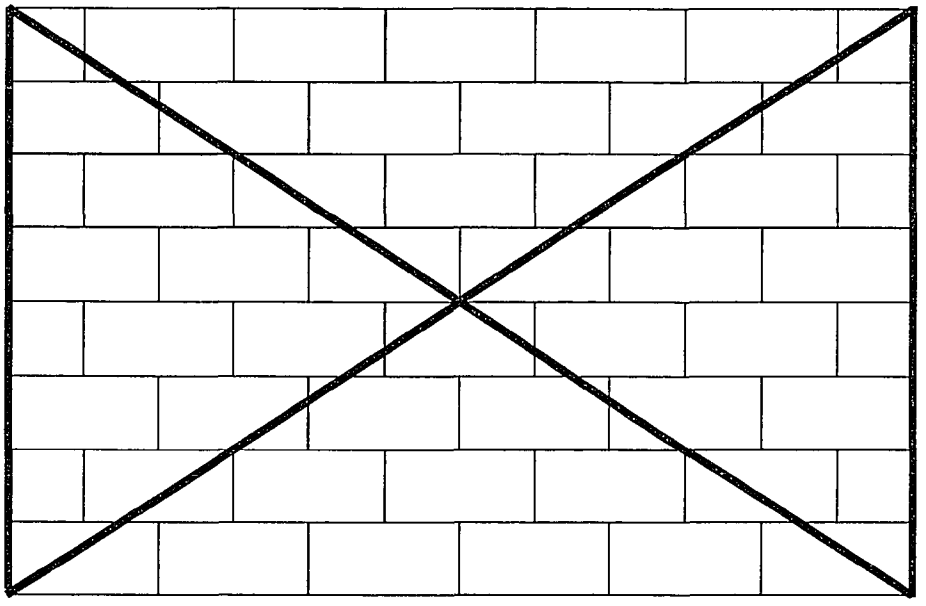

Figure 5.13 Rehab2, Bracing System to Strengthen Wall

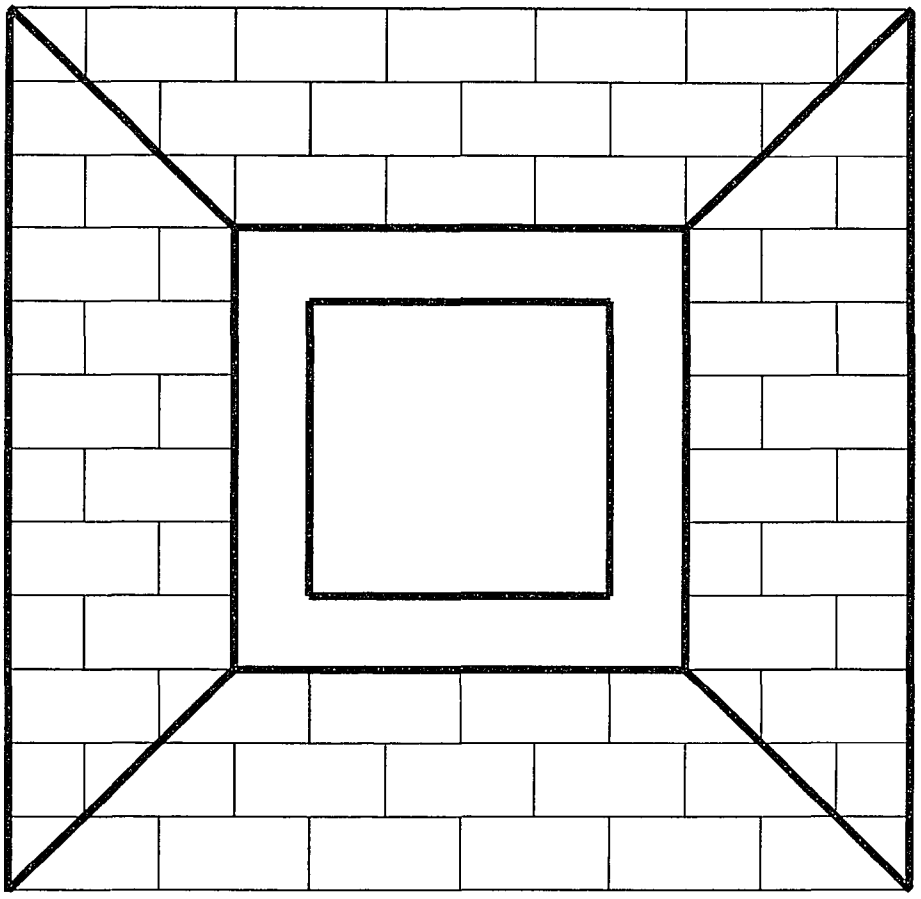

Figure 5.14 Rehab2 for Wall with Opening

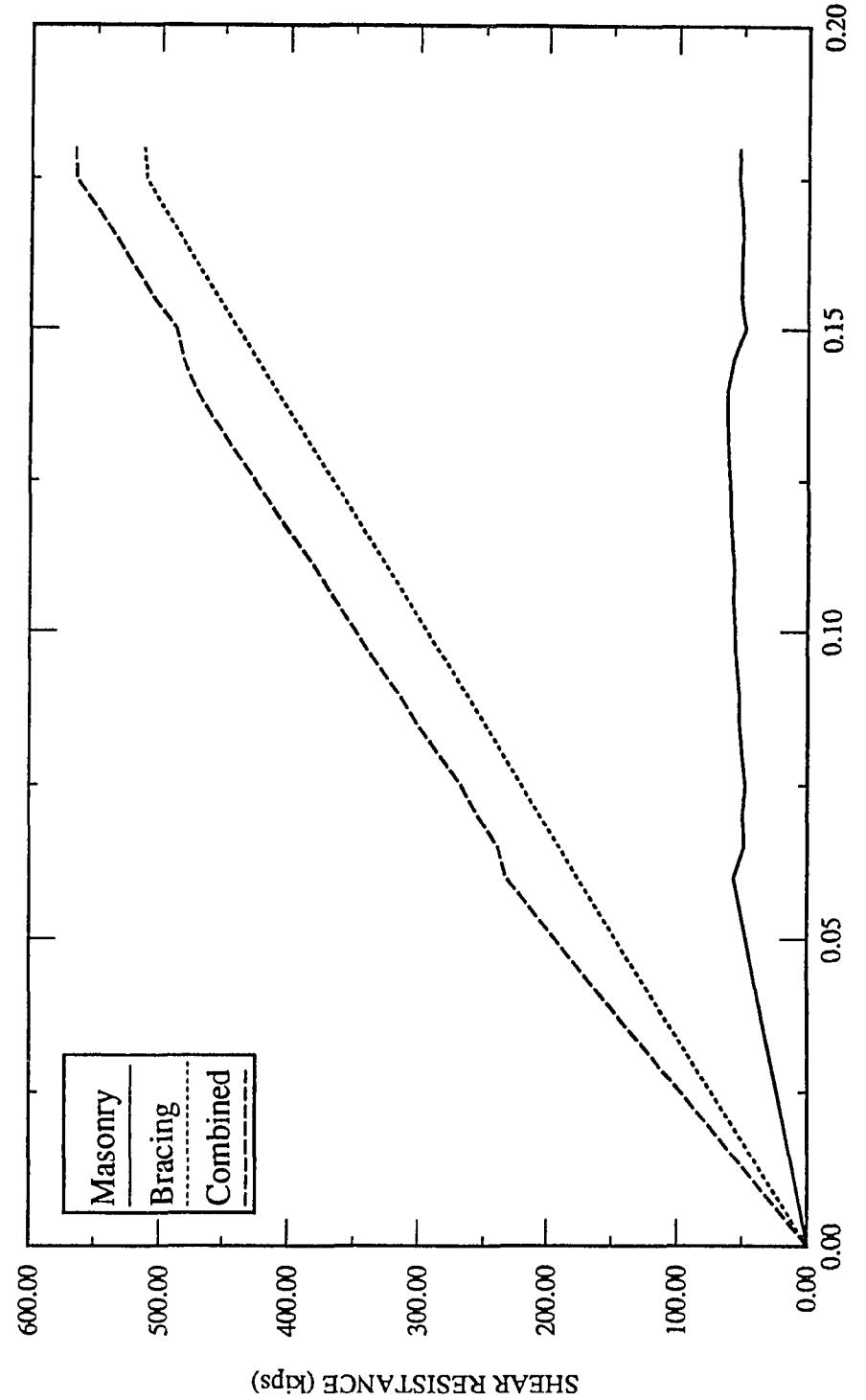

Figure 5.15 Load Deflection Curve for 96X64W.R2

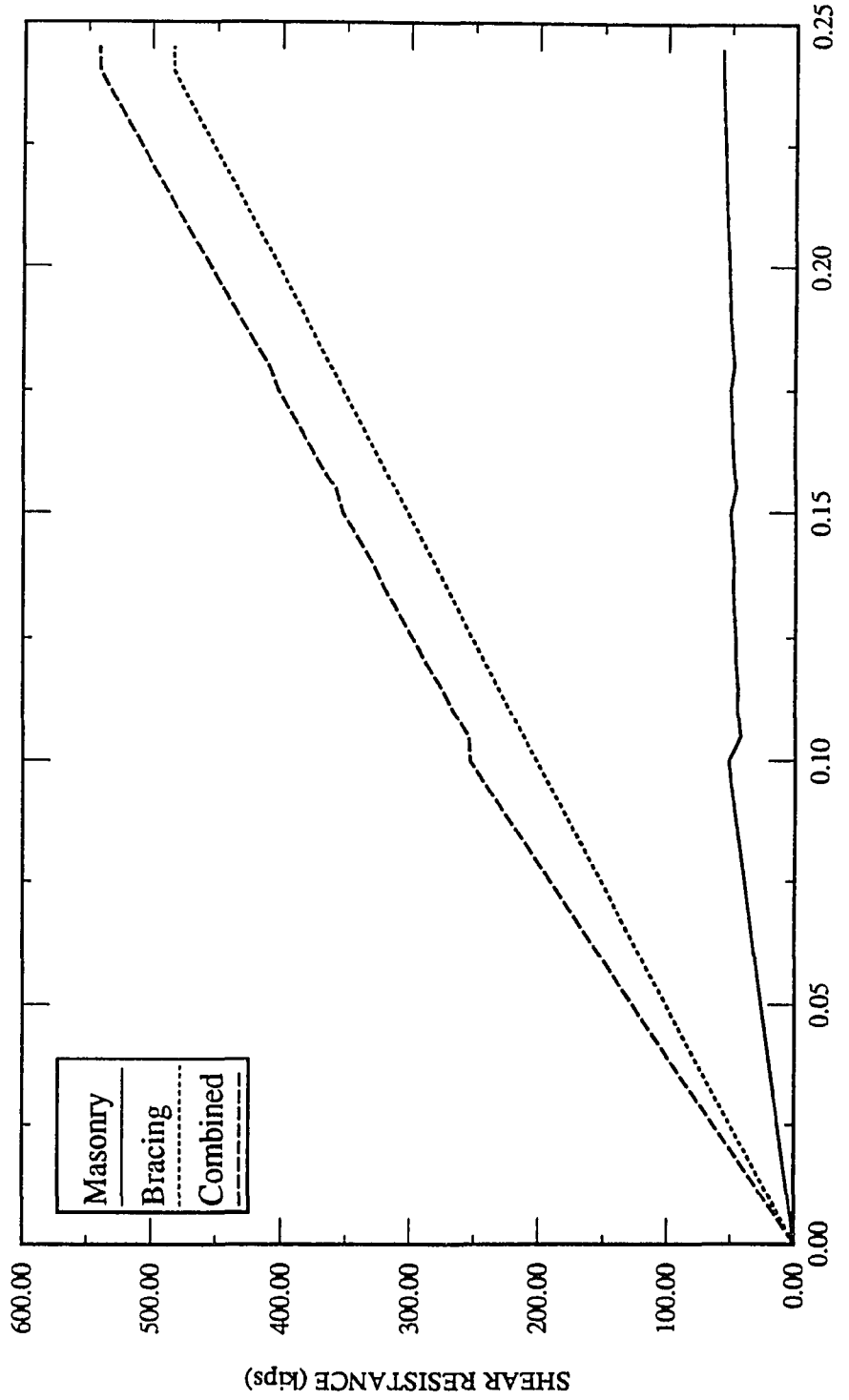

Figure 5.16 Load Deflection Curve for 96X96W.R2

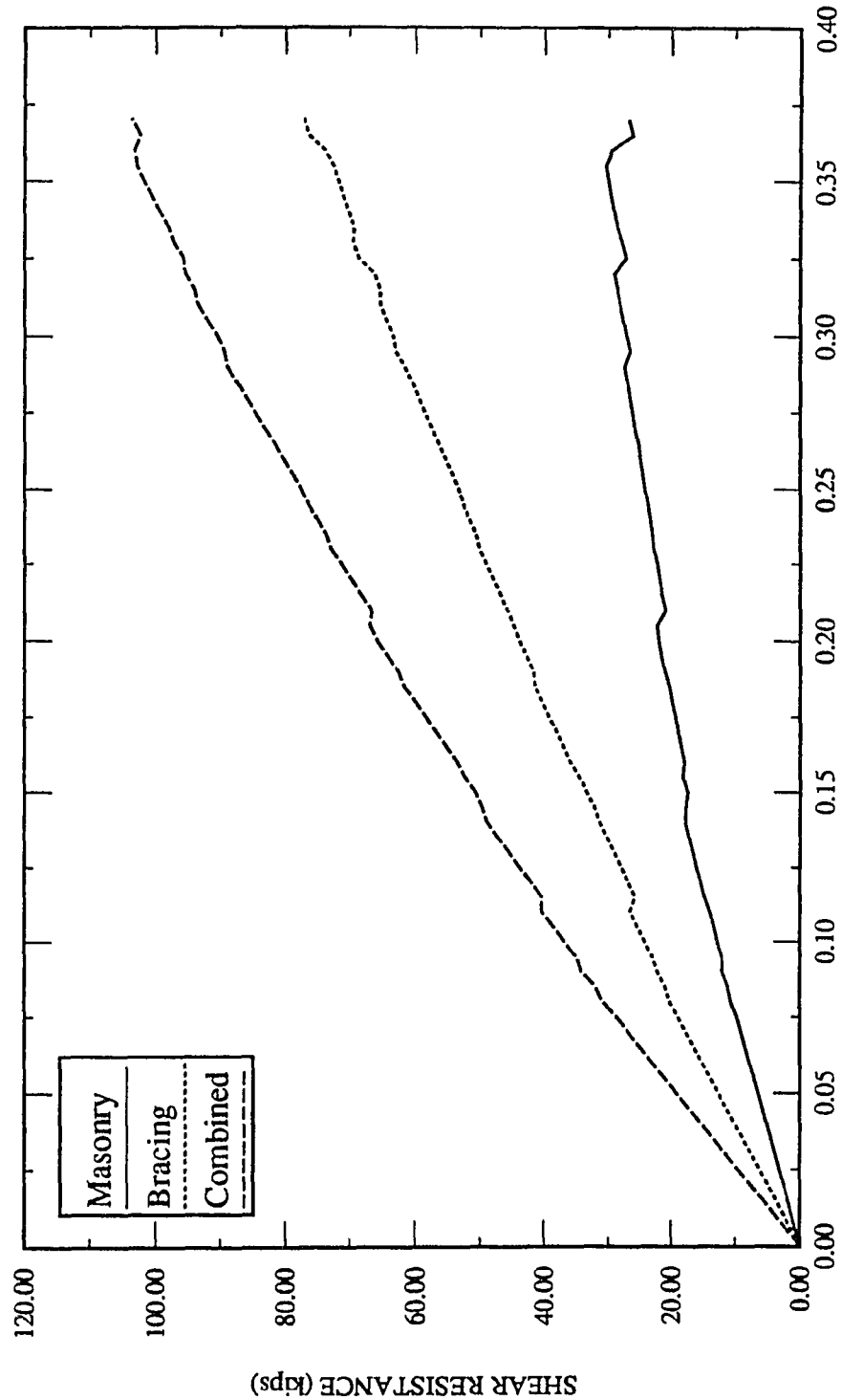

Figure 5.17 Load Deflection Curve for 96X96O.R2

CHAPTER 6

APPLICATIONS: DYNAMIC ANALYSIS

The first section of this chapter describes the basic procedure for dynamic analysis. Nonlinear dynamic analysis of one of the solid walls and corresponding Rehab schemes are discussed in the second section. Finally, use of response spectra in predicting structural behavior is presented.

Nonlinear dynamic analysis of URM structures requires model with cyclic loading capability. Furthermore, random variation of input acceleration in earthquake analysis may cause numerical problems because of sudden change in incremental loads. On the other hand, mass effect tends to make dynamic problems more stable. One of the most critical variables governing the effect of these two parameters is integration time step (ITS). It is the intent of this chapter to demonstrate the cyclic loading capability of the analytical model and perform time history analysis on some structural systems discussed in the previous chapter.

6.1 Procedure for Dynamic Analysis

The dynamic equilibrium equation is:

$$[M]\left\{\ddot{U}\right\} + [C]\left\{\dot{U}\right\} + [K]\{U\} = \{F\} \tag{6.1}$$

where:

[M] = structural mass matrix

[C] = structural damping matrix

[K] = structural stiffness matrix

$\left\{\ddot{U}\right\}$ = nodal acceleration vector

$\left\{\dot{U}\right\}$ = nodal velocity vector

$\{U\}$ = nodal displacement vector

{ F } = force vector.

Equation 6.1 may be nonlinear in that the coefficients [K], [C] and [M] can vary during the analysis. In the present study nonlinearity will only be due to changes in structural stiffness matrix [K]. The procedure employed for the solution of the nonlinear equation 6.1 is Newmark integration method in conjunction with the Newton-Raphson iterations. The Newton-Raphson procedure is discussed in Appendix 3 and the Newmark method is presented in this section.

The Newmark method uses finite difference expansions in the time interval Δt, in which it is assumed that [10]:

$$\left\{\dot{U}_{n+1,i}\right\} = \left\{\dot{U}_n\right\} + \left[(1-\delta)\left\{\ddot{U}_n\right\} + \delta\left\{\ddot{U}_{n+1,i}\right\}\right]\Delta t \tag{6.2}$$

$$\{U_{n+1,i}\} = \{U_n\} + \left\{\dot{U}_n\right\}\Delta t + \left[\left(\frac{1}{2}-\alpha\right)\left\{\ddot{U}_n\right\} + \alpha\left\{\ddot{U}_{n+1,i}\right\}\right]\Delta t^2 \tag{6.3}$$

where:

α and δ are Newmark integration parameters, written as

$\alpha = \frac{1}{4}(1+\gamma)^2$, $\delta = \frac{1}{2} + \gamma$, γ is amplitude decay factor.

$\{U_n\}$ = nodal displacement vector at time t_n

$\left\{\dot{U}_n\right\}$ = nodal velocity vector at time t_n

$\left\{\ddot{U}_n\right\}$ = nodal acceleration vector at time t_n

and so on.

For unconditional stability of Newmark integration scheme, $\gamma > 0$ [8]. If $\gamma = 0$, the Newmark method becomes constant average acceleration method, and does

not show any amplitude decay. If other sources of damping are not represented, the lack of numerical damping can be undesirable in that the higher modes of the structure can produce unacceptable levels of numerical noise. In the present study γ = 0.05 is used, permitting damping of higher modes.

To solve the nonlinear dynamic equations, concept of equilibrium iteration is introduced in equations 6.2 and 6.3. Equilibrium iterations are used to establish convergence at time step t_n, t_{n+1}, etc. The number of equilibrium iterations required is proportional to the extent of nonlinearity. Since the primary aim is to compute displacement at time t_{n+1}, the governing equation 6.1 can be written as:

$$\begin{aligned}&(a_0[M] + a_1[C] + [K])\{U_{n+1,i}\} = \{F\} + \\ &[M]\left(a_0\{U_n\} + a_2\left\{\dot{U}_n\right\} + a_3\left\{\ddot{U}_n\right\}\right) + \\ &[C]\left(a_1\{U_n\} + a_4\left\{\dot{U}_n\right\} + a_5\left\{\ddot{U}_n\right\}\right)\end{aligned} \tag{6.4}$$

values of a_i are given in Appendix 3.

Equation 6.4 is solved for $U_{n+1,i}$. Stresses corresponding to this displacement configuration are calculated and status of elements is evaluated. The structure stiffness matrix [K] is formed and equation 6.4 is solved again to get $U_{n+1,i+1}$. The iterative procedure continues until convergence is achieved for $(n+1)^{th}$ step. The time marching scheme continues for $(n+2)^{th}$, $(n+3)^{th}$, ... load steps.

Damping Matrix: Normally, damping matrix [C] is expressed in terms of stiffness matrix [K] and mass matrix [M] (Rayleigh damping). That is:

$$[C] = \theta[M] + \psi[K] \tag{6.5}$$

In practice it is easier to express damping in terms of damping ratios, ξ_i, of actual damping to critical damping of a particular mode of vibration, i. For natural frequency ω_i and modal damping ratio ξ_i, θ and Ψ should satisfy the following relation:

$$\xi_i = \frac{\theta}{2\omega_i} + \frac{\psi\omega_i}{2} \tag{6.6}$$

Both damping terms depend strongly on frequencies of structure. It can be seen from equation 6.6 that damping of higher modes depend on Ψ where as damping of lower modes depend on θ. However, for two different frequencies, total damping due to both θ and Ψ will nearly remain constant [8]. Thus, for a particular value of damping ratio ξ, equation 6.6 can be solved simultaneously for two frequencies defining the frequency range over which constant damping is desired.

In nonlinear analysis structure stiffness matrix [K] keeps changing with time. Numerical problems will arise if ψ keeps changing with [K]. Hence ψ=0 is used in this analysis. θ is selected so as to have 5% damping corresponding to the first lateral mode of vibration. Prior to nonlinear time history analysis, frequency analysis is performed in order to determine mode shapes and frequencies of the system.

Integration Time Step: Selection of correct time step is very critical in nonlinear dynamic analysis. Large time steps tend to introduce numerical error which affects the dynamic response of the higher modes. In the limit as integration time step Δt tends to infinity, the dynamic analysis becomes static analysis. Time step should be selected considering following factors [8]:

1) Resolve the Input Curve: The integration time step (ITS) should be small enough to characterize the input force or displacement curve. The smaller the integration time step, more closely the input curve will be followed. For good

representation of input curve, seven integration points should occur within the load time step. Acceleration curves of discontinuous slope cannot be followed exactly with the integration procedure but "rounded" corners are produced.

2). Resolve the Response Frequency: The integration time step should be small enough to resolve the motion of the structure. The motion may be characterized as being composed of natural modes of increasing frequency. Numerical error for single degree of freedom system can be expressed in terms of integration points per cycle. Generally, 20 integration points per cycle will result in negligible numerical error. Thus, time step can be calculated from ITS=1/(20f), where f is the highest frequency of interest.

3). Resolve Contact Frequency: Dynamic analysis with joint elements create additional problem. Rate of joint opening and closing will significantly affect the dynamic analysis. They may even cause convergence problem. ITS should be small enough to resolve the contact frequency. Generally contact frequency depends on the stiffness of springs. However, with the present algorithm closing of joints from open status is achieved in two stages. This procedure prevents "bouncing" and "rebounding" of joint elements and helps to reduce numerical vibrations.

4). Resolve Load Increment: Lastly, in nonlinear dynamic analysis, ITS determines incremental load applied on the structure. As mentioned in Chapter 3, bond failure is a path-dependent nonlinear phenomenon. It is therefore necessary that load increment be small. In earthquake analysis input motion is generally in the form of ground acceleration. If single load step is used in the time interval, load increment will be proportional to the difference in acceleration at the corresponding time points. For instance, maximum difference between

two time points for El-Centro earthquake is 352cm/s^2. This value multiplied by the total mass will be the maximum input force increment for single load step. Erroneous results will be obtained if load increment is disproportionately large. Static nonlinear analysis provides some guidelines regarding the load increment. Using this information, ITS can be computed for the given mass.

After several trials, it was found that the fourth criteria governs the selection of integration time step. It was decided to use ITS= 0.0005sec.

Loading Function for Earthquake Analysis: In earthquake analysis, loading function can either be input ground displacement versus time or input ground acceleration versus time. In the first case equation of motion becomes:

$$[M]\left\{\ddot{U}_t\right\} + [C]\left\{\dot{U}_t - \dot{U}_g\right\} + [K]\{U_t - U_g\} = [0]$$

$$hence \tag{6.7}$$

$$[M]\left\{\ddot{U}_t\right\} + [C]\left\{\dot{U}_t\right\} + [K]\{U_t\} = [K]\{U_g\} + [C]\left\{\dot{U}_g\right\}$$

where U_g is ground displacement vector and total displacement will be calculated. The relative displacement of interest will be total displacement minus ground displacement.

In the second case equation of motion in terms of relative displacement becomes:

$$[M]\left\{\ddot{U} + \ddot{U}_g\right\} + [C]\left\{\dot{U}\right\} + [K]\{U\} = [0]$$

$$hence \tag{6.8}$$

$$[M]\left\{\ddot{U}\right\} + [C]\left\{\dot{U}\right\} + [K]\{U\} = -[M]\left\{\ddot{U}_g\right\}$$

Where $\left\{\ddot{U}_g\right\}$ is ground acceleration vector. Relative displacement will be calculated directly in this case. In most problems relative displacement is of interest and hence input motion in the form of ground acceleration is used.

6.2 Analysis of URM Walls

One of the URM walls discussed in the Chapter 4 (96X64W84) was analyzed. First, cyclic displacement in form of sine wave of increasing amplitude was applied to the top edge of the wall. The response of the wall in terms of loading, unloading and reloading is shown in Fig. 6.1. It can be seen that unloading curves are almost parallel to the load-displacement curve within the elastic range. Similar behavior can also be seen in unloading portion of experimental load-deflection curve shown in Fig. 4.5. The maximum shear resistance during cyclic loading occurs at the time of the first cracking which is consistent with monotonic load-displacement curve (Fig. 4.5). In fact, monotonic curve serves as an envelope for the cyclic response of the wall. To study the response of this wall (96X64W84) to earthquake loading, time history analysis was performed next. FEMA (ATC-22) [9] has developed design charts for input acceleration to be used in evaluation of dynamic characteristics of existing structures. The recommended value in the region of high seismicity is around 0.4g. Hence, El-Centro (S00E component, Fig. 6.2) record was used as input acceleration for the purpose of analysis (maximum ground acceleration =0.35g). Total mass was applied at the top of

the wall. Total mass was compressive force at the top of the wall divided by acceleration due to gravity. Incremental force would be mass matrix multiplied by the applied ground acceleration. Compressive stress should be applied before the beginning of transient analysis and hence static analysis is done in the first load step. Time history analysis would start from the second load step. Table 6.1 gives frequency of the wall in vertical and horizontal directions and total mass on the wall. The dynamic analysis failed to converge at 5.02sec for 96X64W84. This can be explained based on the static load deflection curve. From the static

load displacement curve (Fig. 4.5) it can be seen that the peak shear strength under increasing lateral displacement corresponds to the shear resistance at the first failure point. In such cases if "load control" analysis is performed, the solution will not converge after reaching the first peak. This is because the structural equilibrium can not be satisfied for the given load. The displacement, therefore, increases indefinitely and solution does not converge. Time history for displacement and load is shown in Figs. 6.3 and 6.4. Hysteresis loops for the wall do not show any nonlinear deformation (Fig. 6.5). This brittle behavior makes URM structures one of the most hazardous construction.

Generally maximum damage to the structure occurs if the frequency is in the range of 1–5Hz. As can be seen from Table 6.1, frequencies of the wall are relatively high. The frequency of vibration decreases after the damage to the structure because stiffness decreases. This would bring URM walls in the frequency range where input energy into the structure would be maximum. For other structures when frequency is in the range of 1–5Hz, reduction in frequency will tend to dampen the vibration because the system will move out of phase with input motion. In the case of URM walls, reduction in frequency will bring the wall in the range of maximum damage. This is another reason for hazardous nature of URM buildings.

6.3 Analysis of Rehab Schemes

Two retrofitting schemes Rehab1 and Rehab2 were analysed for the 96X64W84. Table 6.2 shows frequencies and total mass used in the analysis. Total mass was calculated by dividing compressive force on 96W64.R1 (Table 5.4) by acceleration due to gravity. Retrofitting scheme with frame (Rehab1) failed to converge at 1.88sec. It was found that total load on the system at failure was more than

150kips, that is more than the maximum strength of the system obtained from monotonic load deflection curve. Hysteresis loops (Figs. 6.6 to 6.8) do not show much energy dissipation before failure. Time histories for masonry shear, frame shear, total shear and displacement are shown in Figs. 6.9 to 6.12, respectively. Retrofitting scheme with bracing survived the entire duration of El-Centro earthquake. From hysteresis loops (Figs. 6.13 to 6.15) it can be seen that nonlinearity in the system is only because of the damage to the URM walls. Resistance of bracing remains linear and elastic. Time histories for masonry shear, bracing shear, total shear and displacement are shown in Figs. 6.16 to 6.19.

6.4 Use of Response Spectra in Dynamic Analysis

Response spectrum is a plot of maximum value of response (acceleration, velocity and displacement) to an earthquake, based on the analysis of single degree of freedom (SDOF) system with different frequencies. Many times, during preliminary evaluation of the structural system, an engineer needs to know the maximum intensity of earthquake (in terms of g) that a system would survive. Response spectra can be of great use in such a case, especially when the response of the structure is dominated by single mode.

In linear dynamic analysis response spectra can accurately predict the maximum stresses that would be developed in structures that can be idealized as SDOF system. In nonlinear analysis, the response of system changes with progressive failure of elements. Thus, maximum values based on linear analysis may not be valid. However, if static nonlinear analysis is available and if the system does not have much ductility, the response can still be predicted from the linear response spectra. That is, it is possible to find out that the structure would survive

an earthquake or not. To verify this method, problems discussed in sections 6.2 and 6.3 were solved as follows:

For the given frequency of the system maximum acceleration is found from the response spectra. If response spectra is not available, linear dynamic analysis on SDOF system can be performed to obtain the maximum values of acceleration, velocity and displacement that would be developed in the system. Maximum acceleration multiplied by the total mass would give the maximum force that would be developed in the system. If this force exceeds the capacity of the system as obtained from nonlinear static analysis then the structure would not survive an earthquake and vice versa. These calculations are shown in Table 6.2. Nonlinear dynamic analysis discussed in previous sections confirms the results predicted using response spectra. For instance, 96X64W84 has the maximum shear capacity of 58kips. Based on response spectrum analysis, demand on the wall would be 101.92kips which is significantly more than the capacity. Also, nonlinear static analysis shows that the wall does not have much ductility (Fig. 4.5). As a result, this wall would not survive the earthquake under consideration. Similarly, 96X64W.R1 would not survive the earthquake and 96X64W.R2 would withstand the earthquake.

Table 6.1
Dynamic Properties of URM Wall

Name	Frequency (Hz)	Mass (kips-s^2/in)
96X64W84	10.41	217.00

Table 6.2
Dynamic Properties of Retrofitting Schemes

Name	Frequency (Hz)	Mass (kips-s^2/in)
96X64W.R1	6.58	1026.00
96X96W.R2	9.76	1026.00

Table 6.3
Use of Response Spectra in Predicting Nonlinear Dynamic Response

Name	Frequency (Hz)	Total Mass (kips-sec^2/in)	Spectal Accl.[1] (in/sec^2)	Spectral Force[2] (kips)	Capacity[3] (kips)	Prediction[4]	Conclusion[5]
96X64W84	10.41	217.00	466.32 (1.21g)	101.92	58.00	Fails	Failed
96X64W.R1	6.58	1026.00	683.70 (1.77g)	701.00	150.00 (0.38g)	Fails	Failed
96X64W.R2	9.76	1026.00	448.84 (1.43g)	460.50	565.00 (1.43g)	Survives	Survived

1. See Response Spectra for ElCentro Earthquake, Quantity in Paranthesis is in Terms of g
2. Mass in Column 2 Multiplied by Spectral Acceleration in Column 3 Gives Spectral Force
3. Obtained from Nonlinear Static Analysis, Quantity in Paranthesis Gives Capacity in Terms of g.
4. This is the Prediction Using Response Spectrum.
5. This is Conclusion of Nonlinear Tranisent Dynamic Analysis.

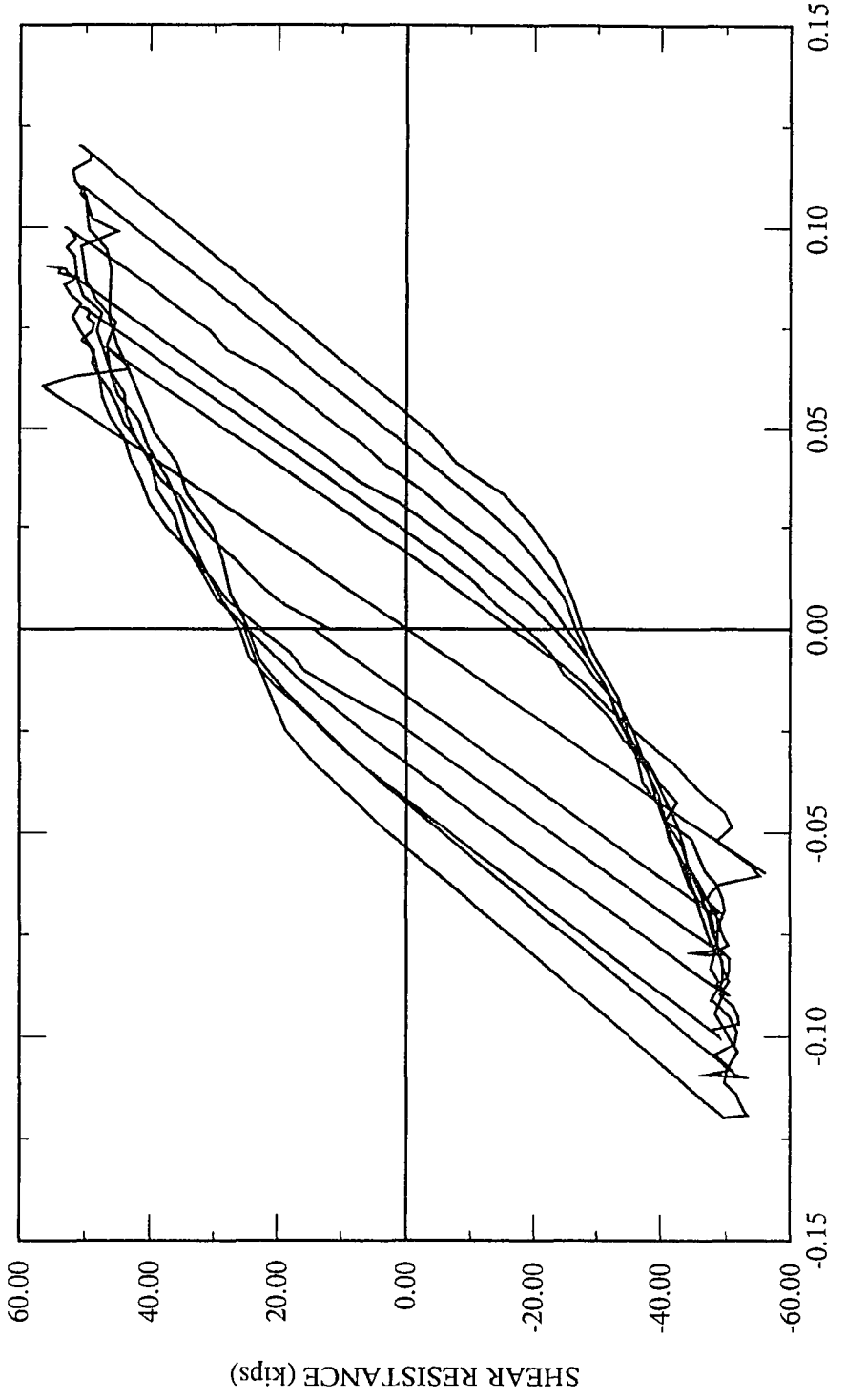

Figure 6.1 Response of 96X64W84 to Cyclic Displacement

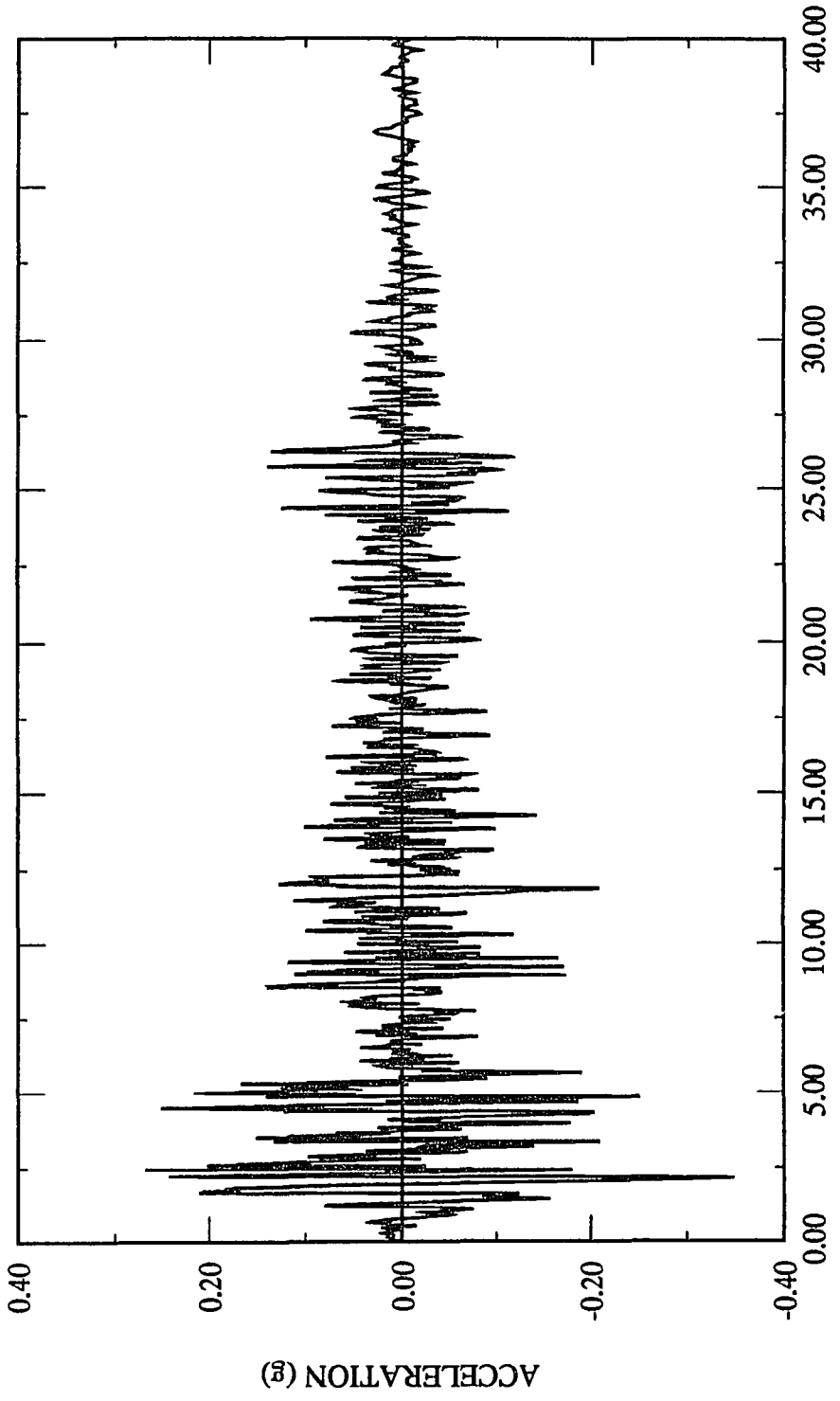

Figure 6.2 Ground Acceleration for El-Centro S-E Component

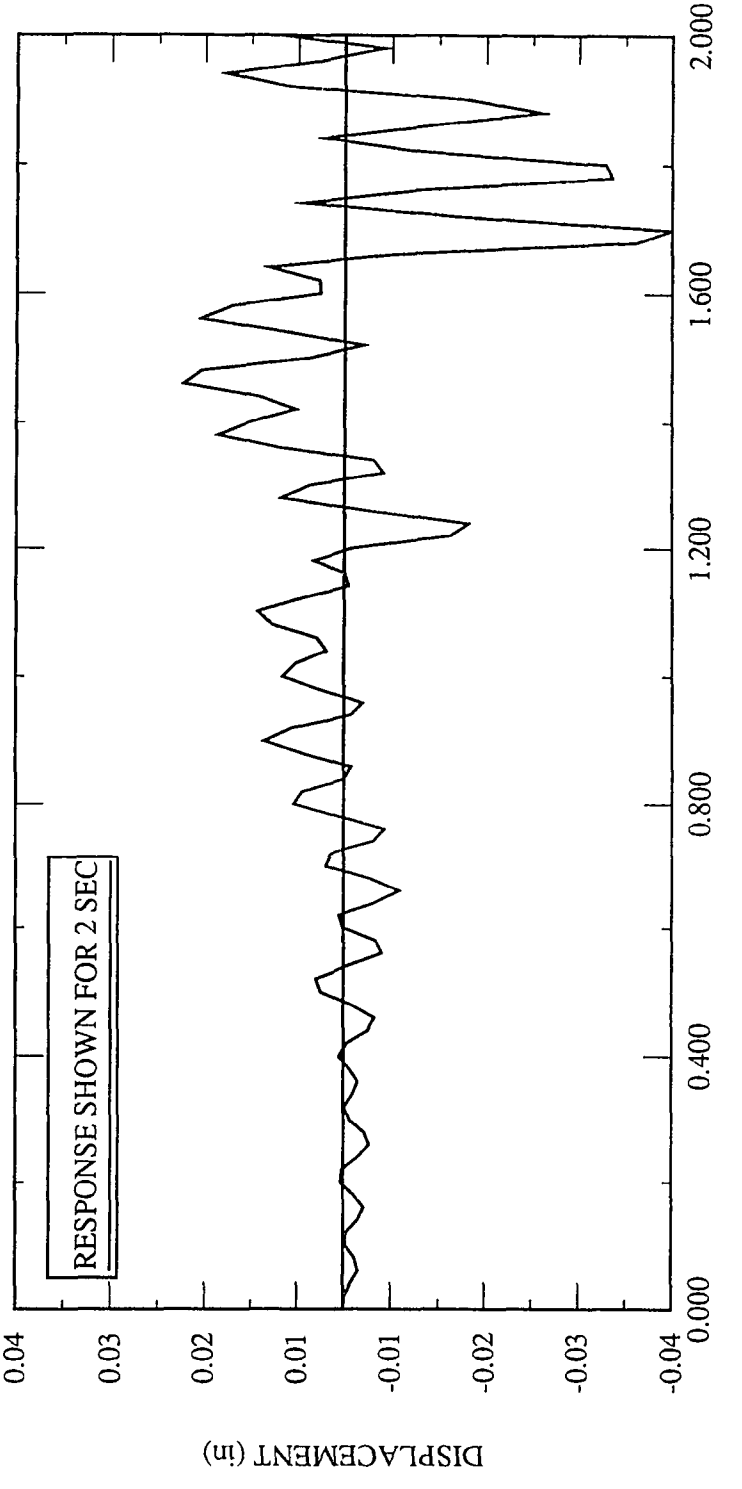

Figure 6.3 Displacement Time History for 96X64W84

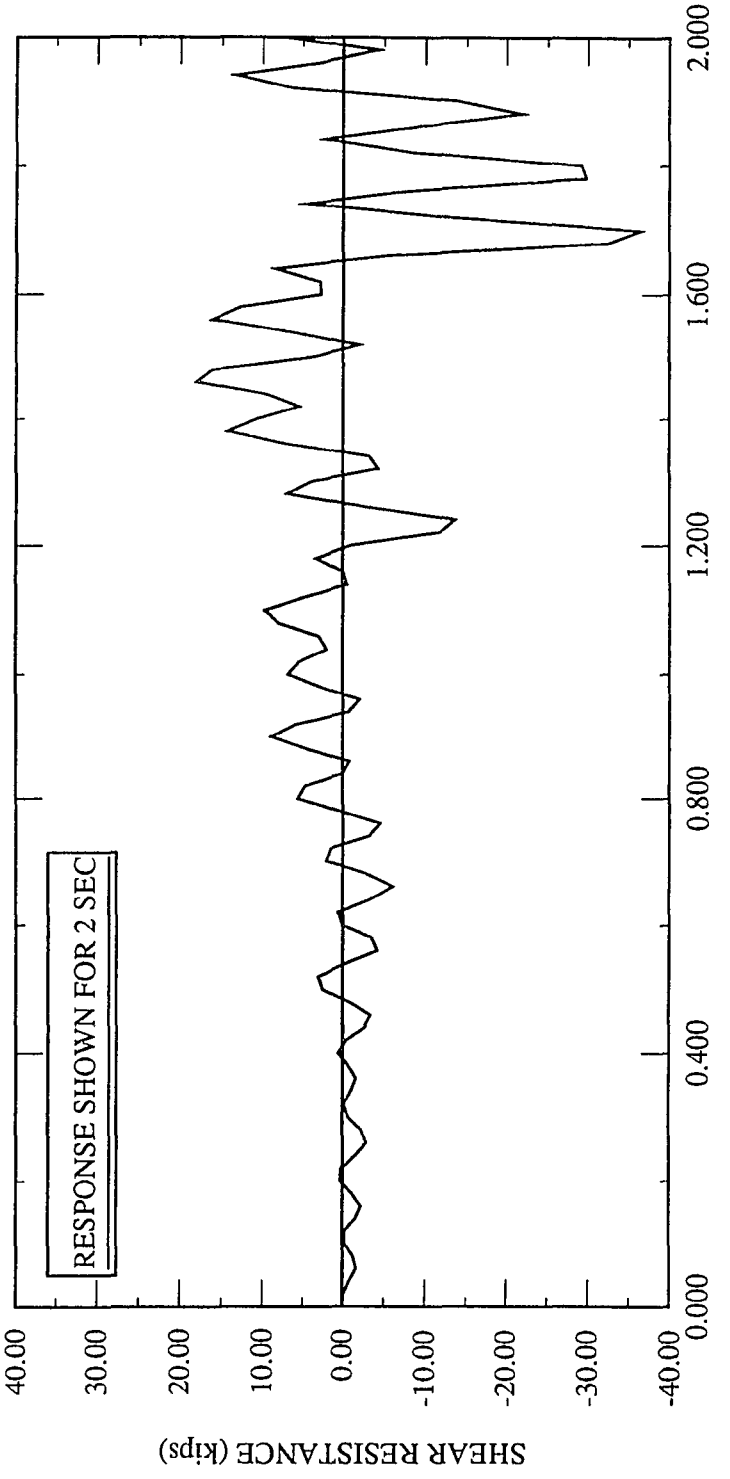

Figure 6.4 Load Time History for 96X64W84

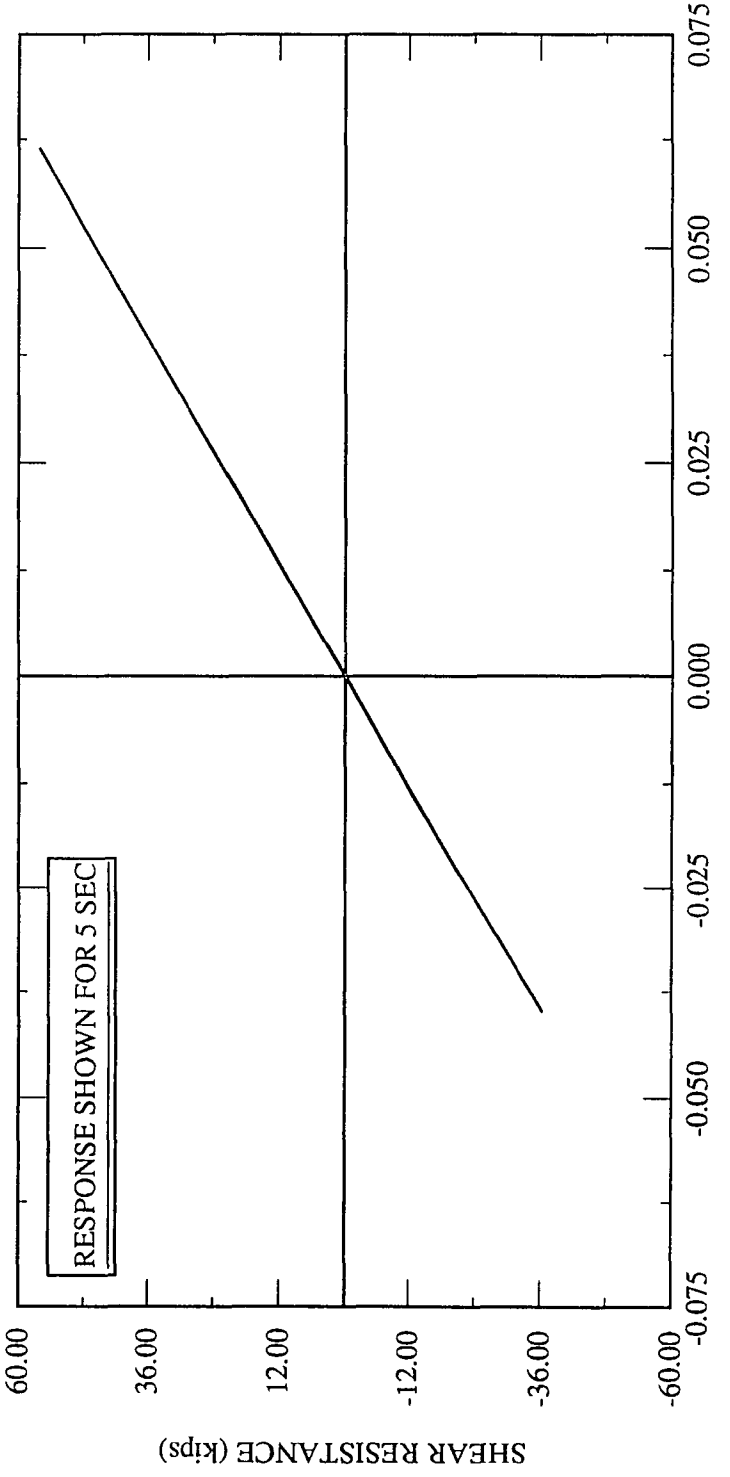

Figure 6.5 Load Displacement Hysteresis Loops for 96X64W84

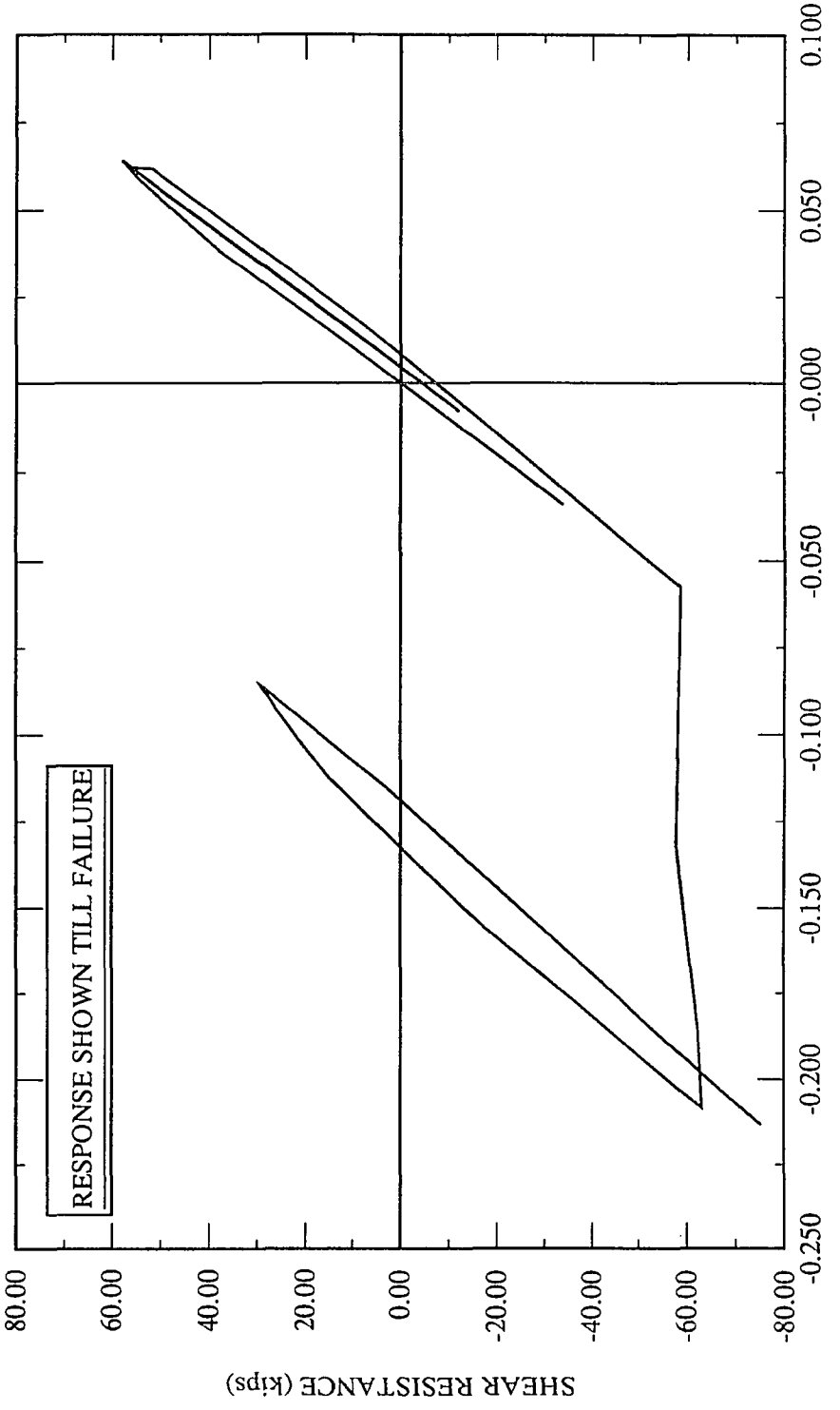

Figure 6.6 Load Displacement Hysteresis Loops for 96X64W.R1, Masonry Wall

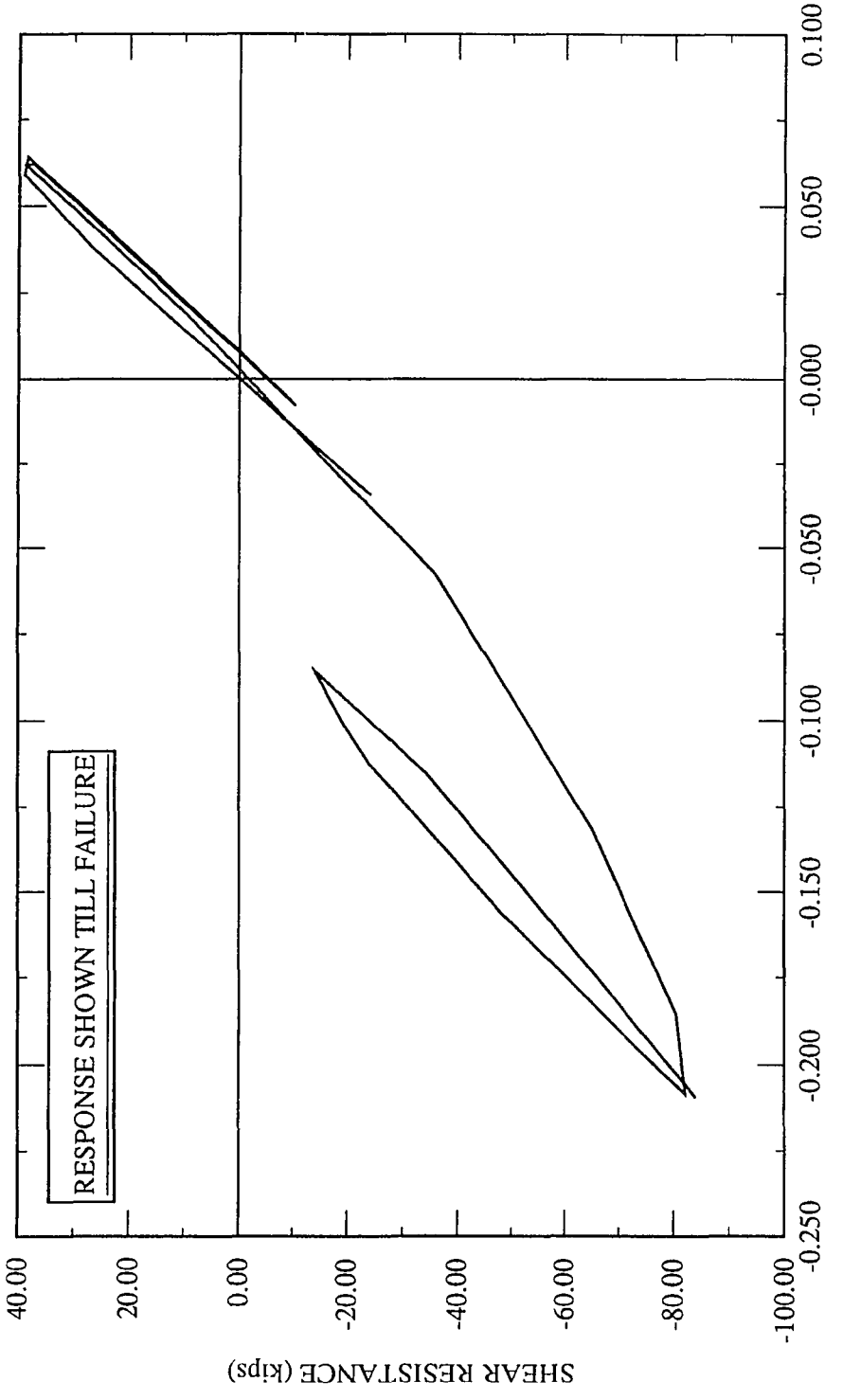

Figure 6.7 Load Displacement Hysteresis Loops for 96X64W.R1, Frame

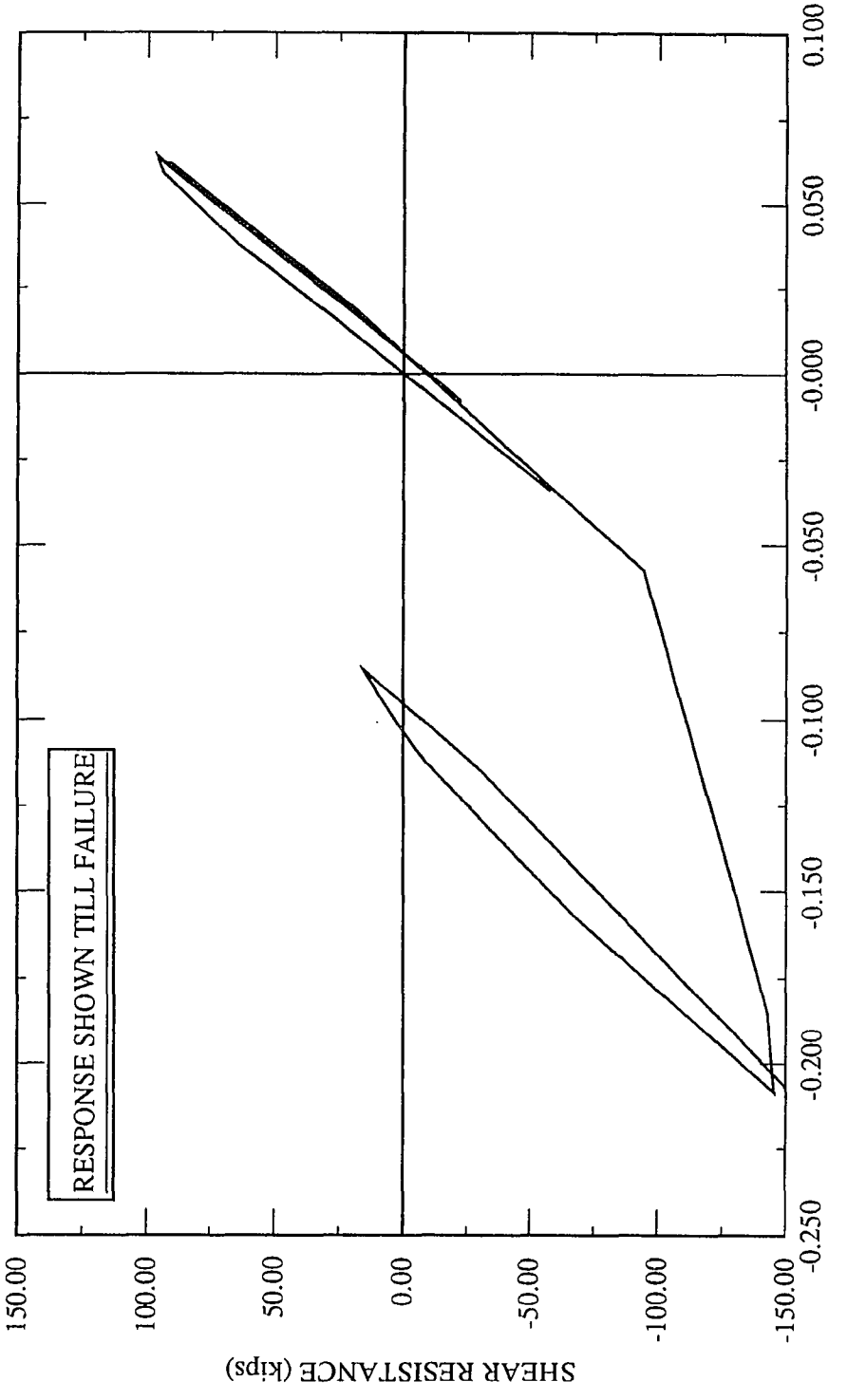

Figure 6.8 Load Displacement Hysteresis Loops for 96X64W.R1, Total

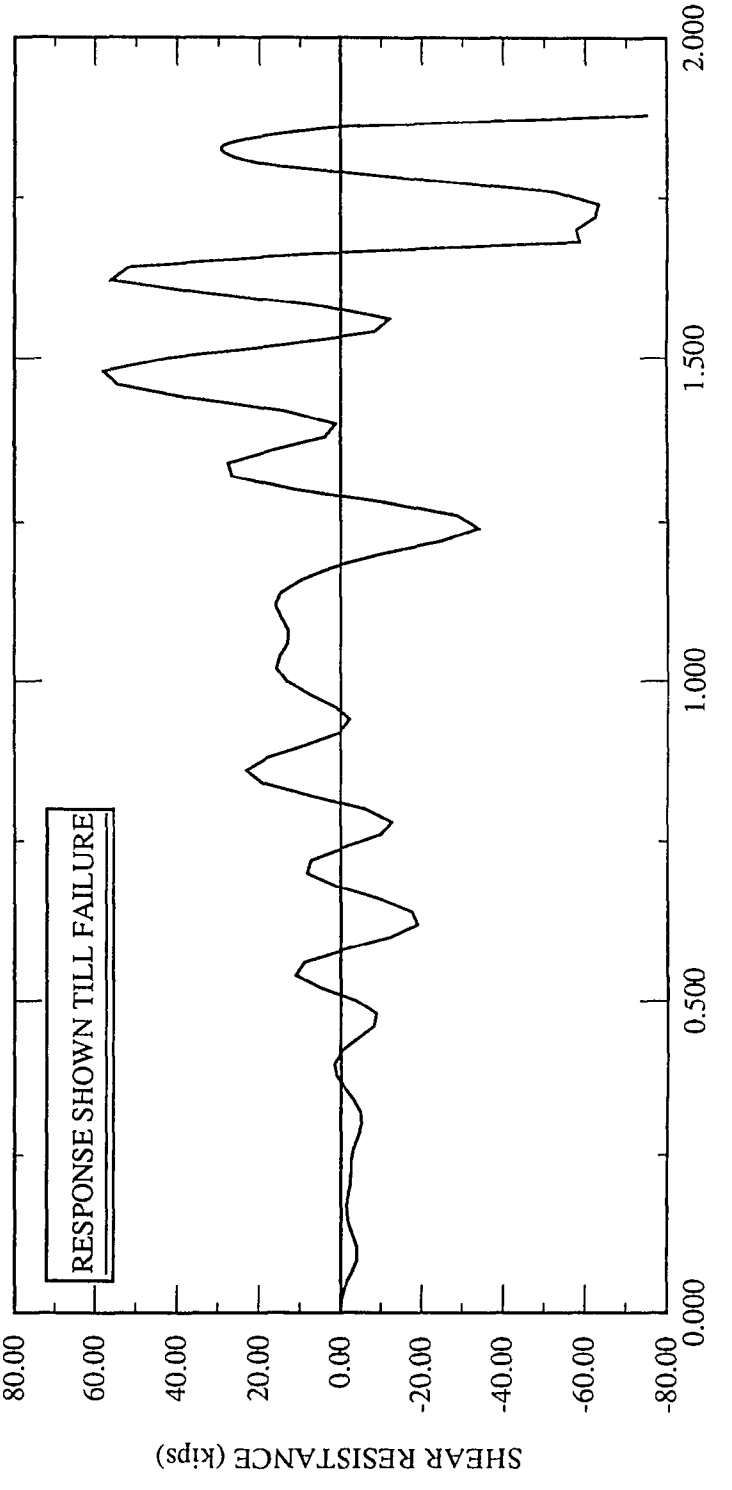

Figure 6.9 Load Time History for 96X64W.R1, Masonry Wall

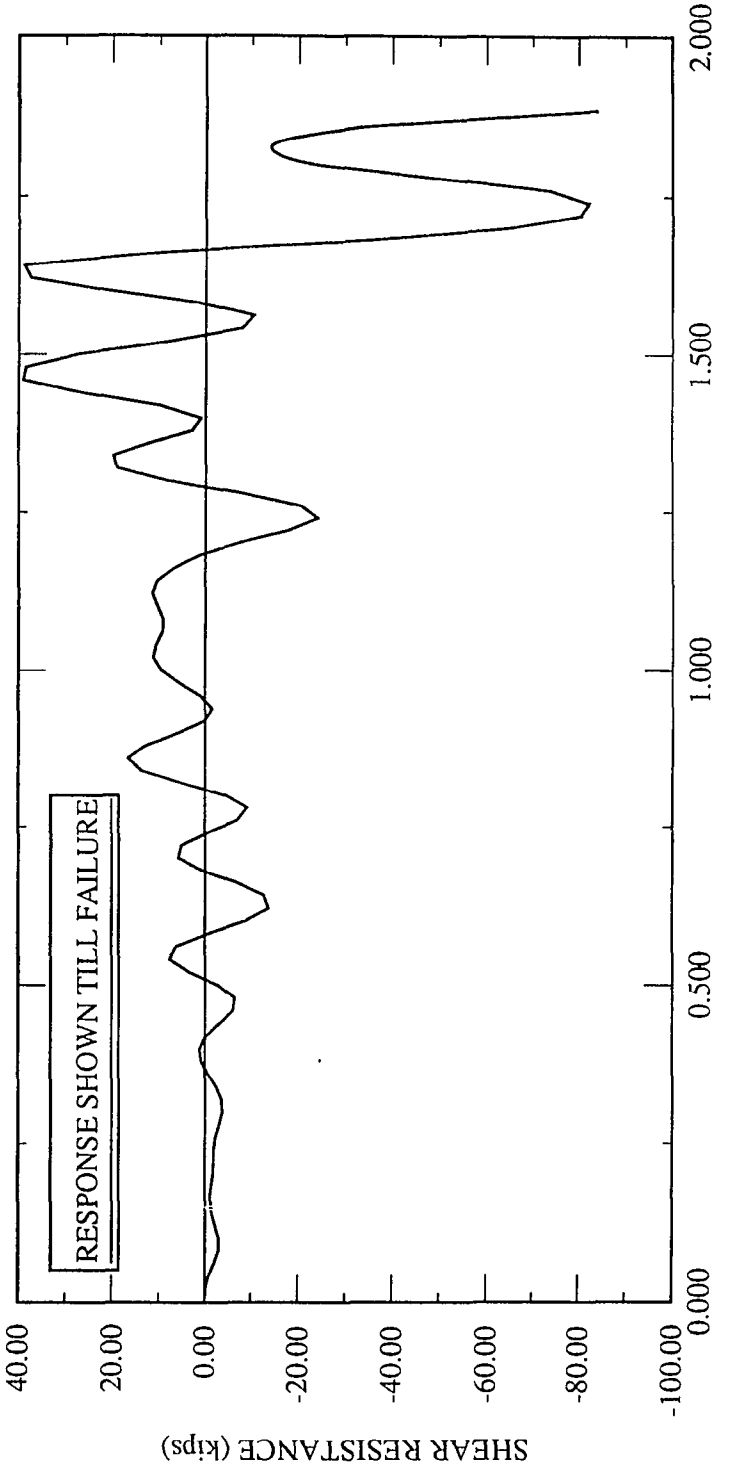

Figure 6.10 Load Time History for 96X64W.R1, Frame

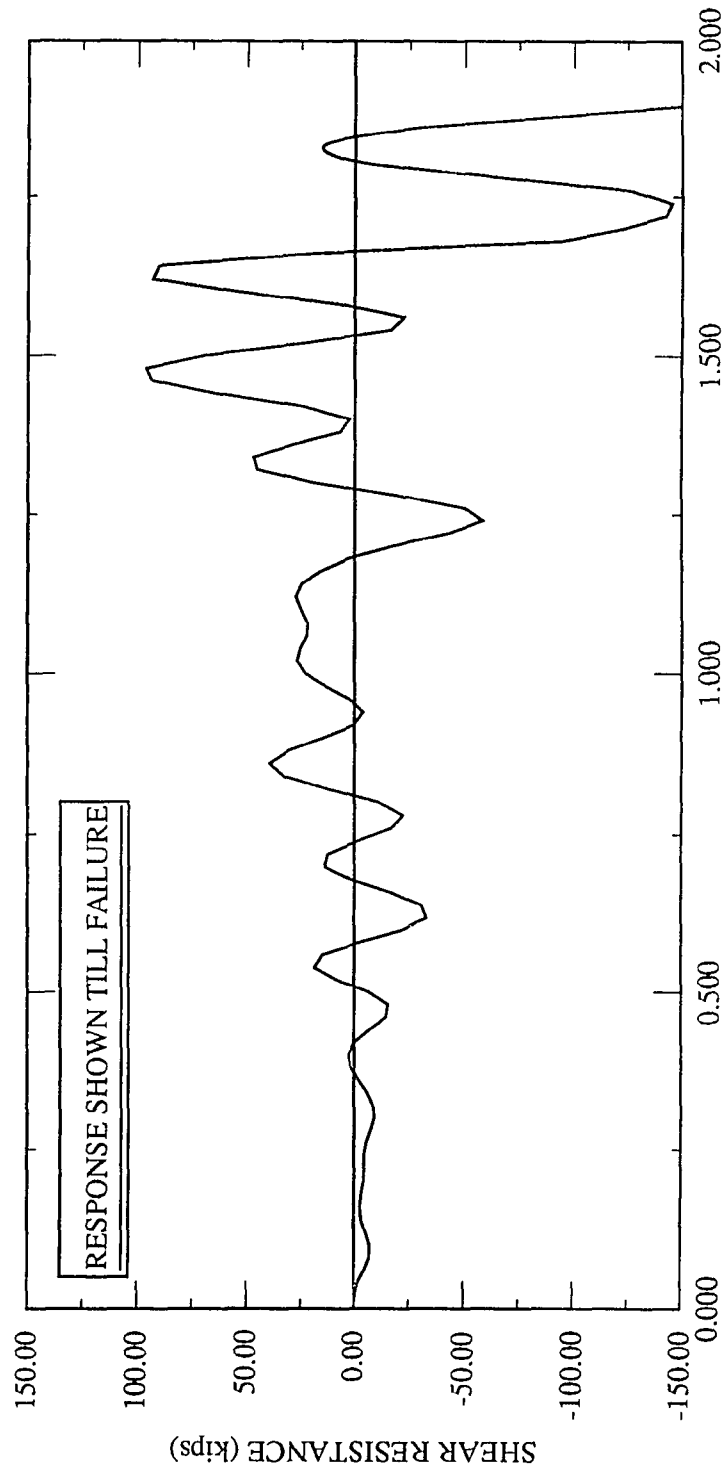

Figure 6.11 Load Time History for 96X64W.R1, Total

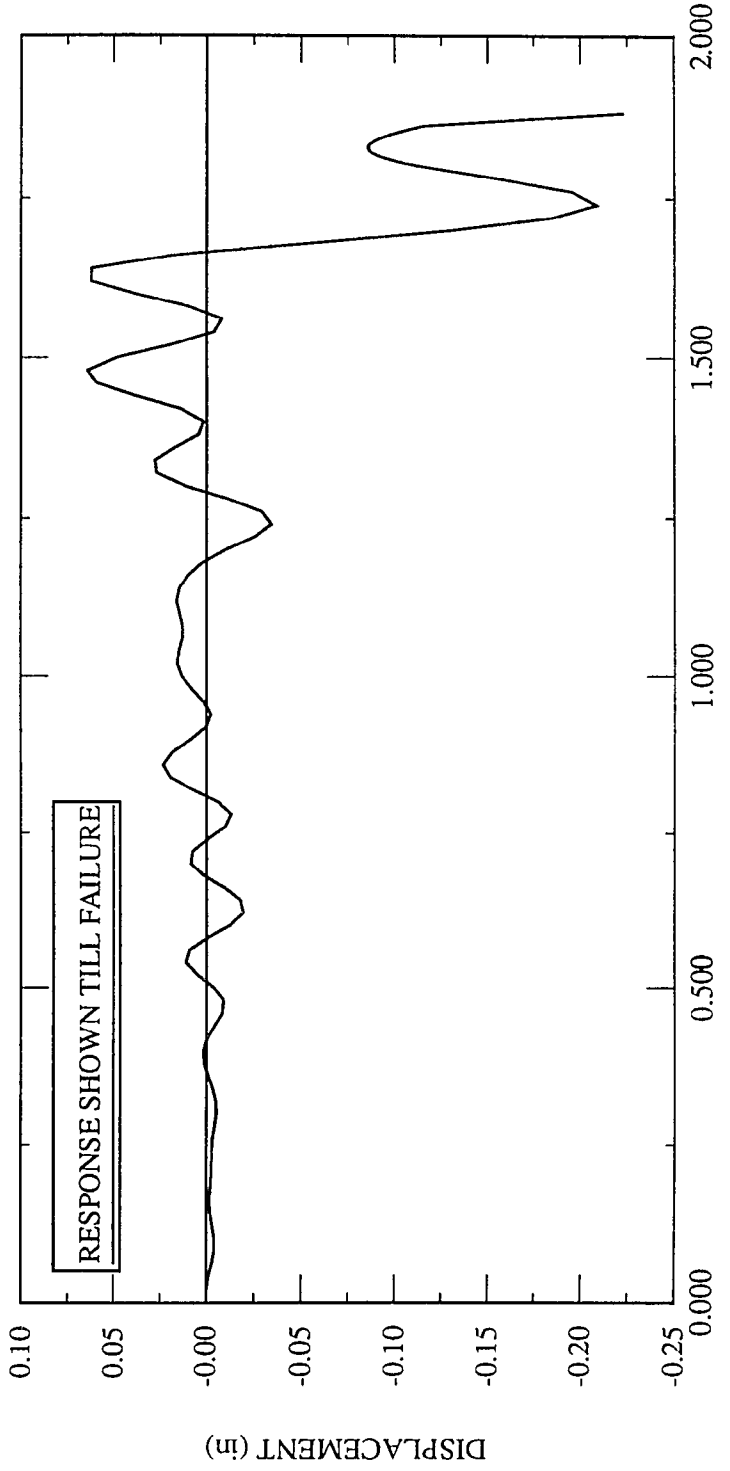

Figure 6.12 Displacement Time History for 96X64W.R1

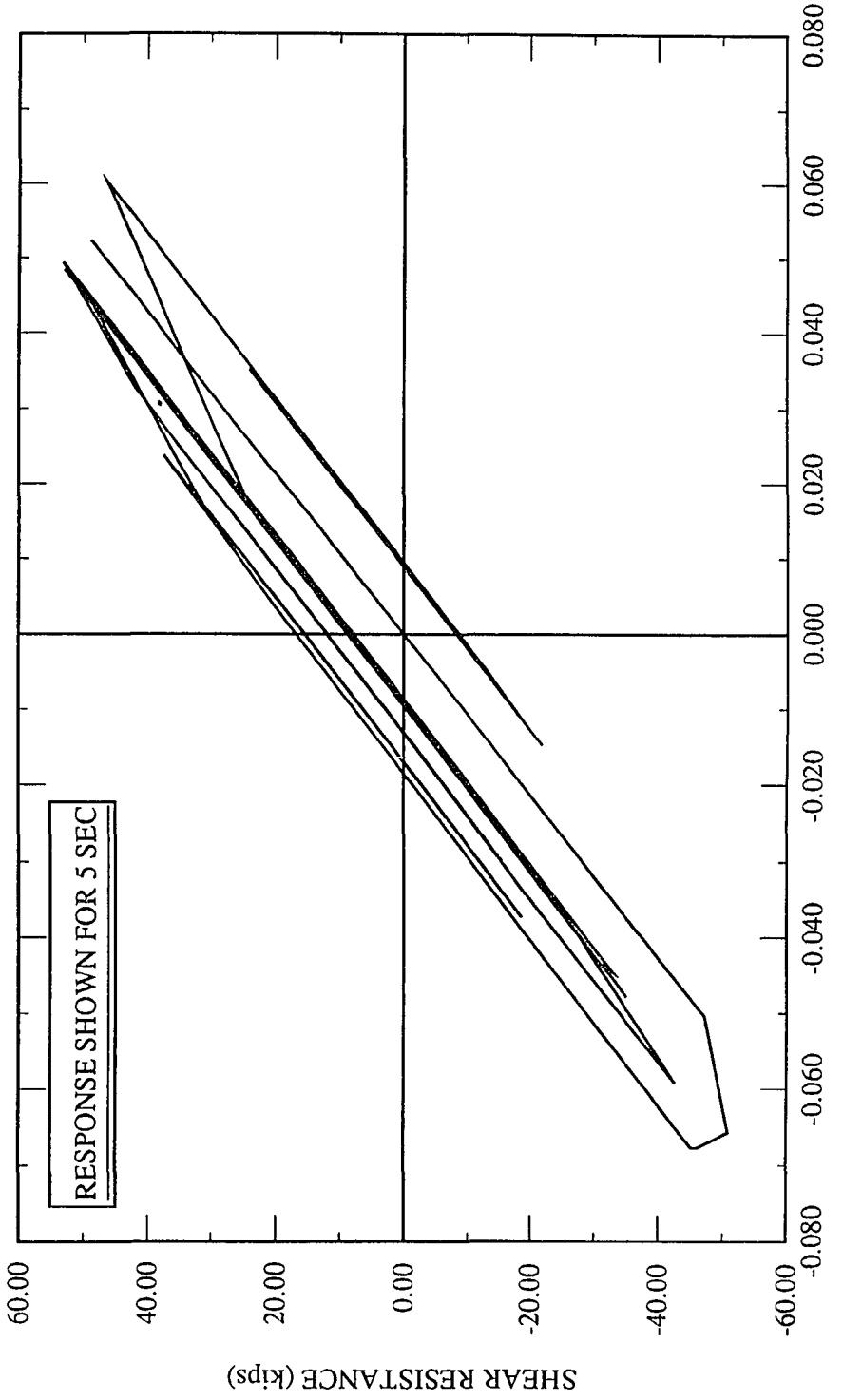

Figure 6.13 Load Displacement Hysteresis Loops for 96X64W.R2, Masonry Wall

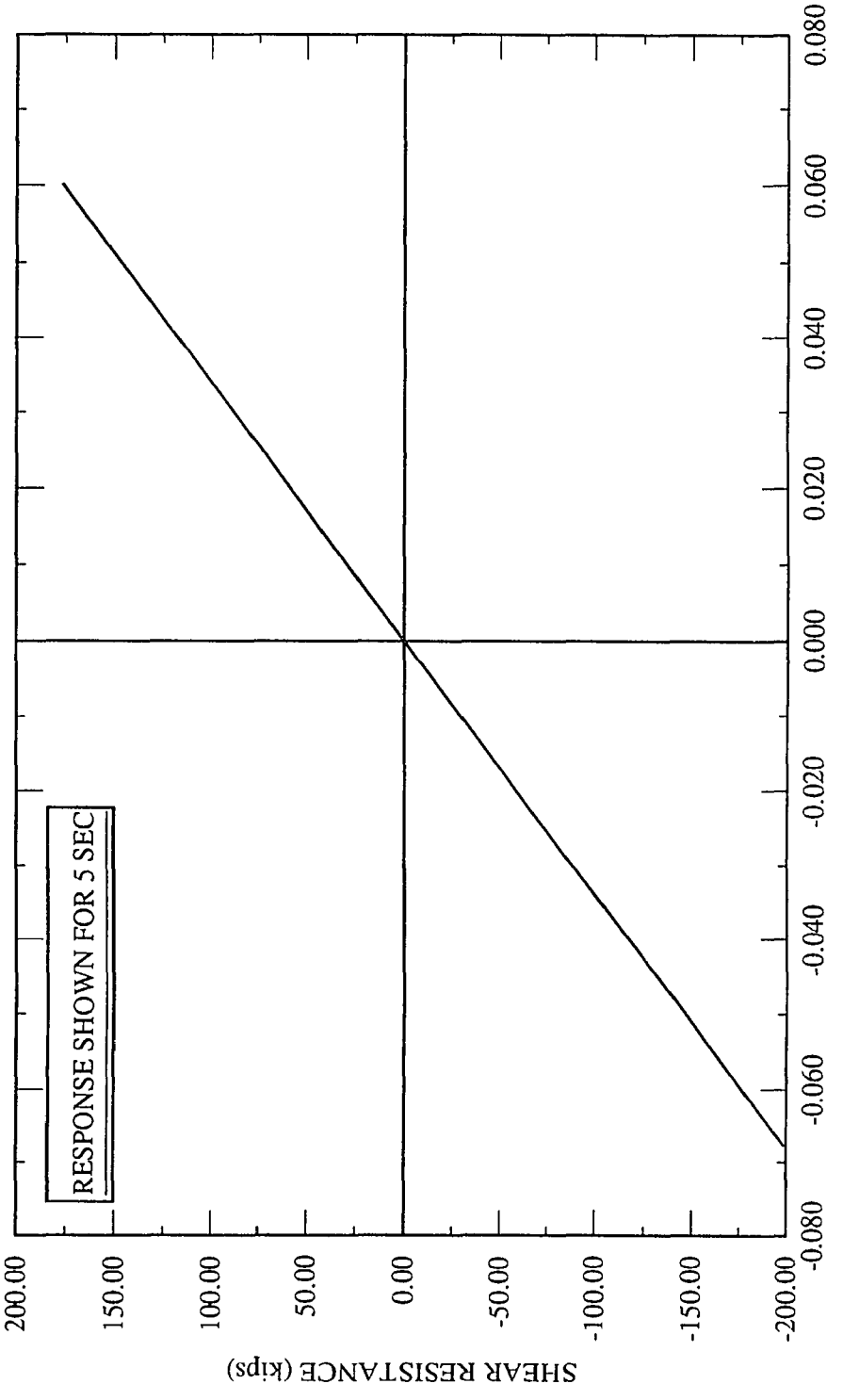

Figure 6.14 Load Displacement Hysteresis Loops for 96X64W.R2, Bracing

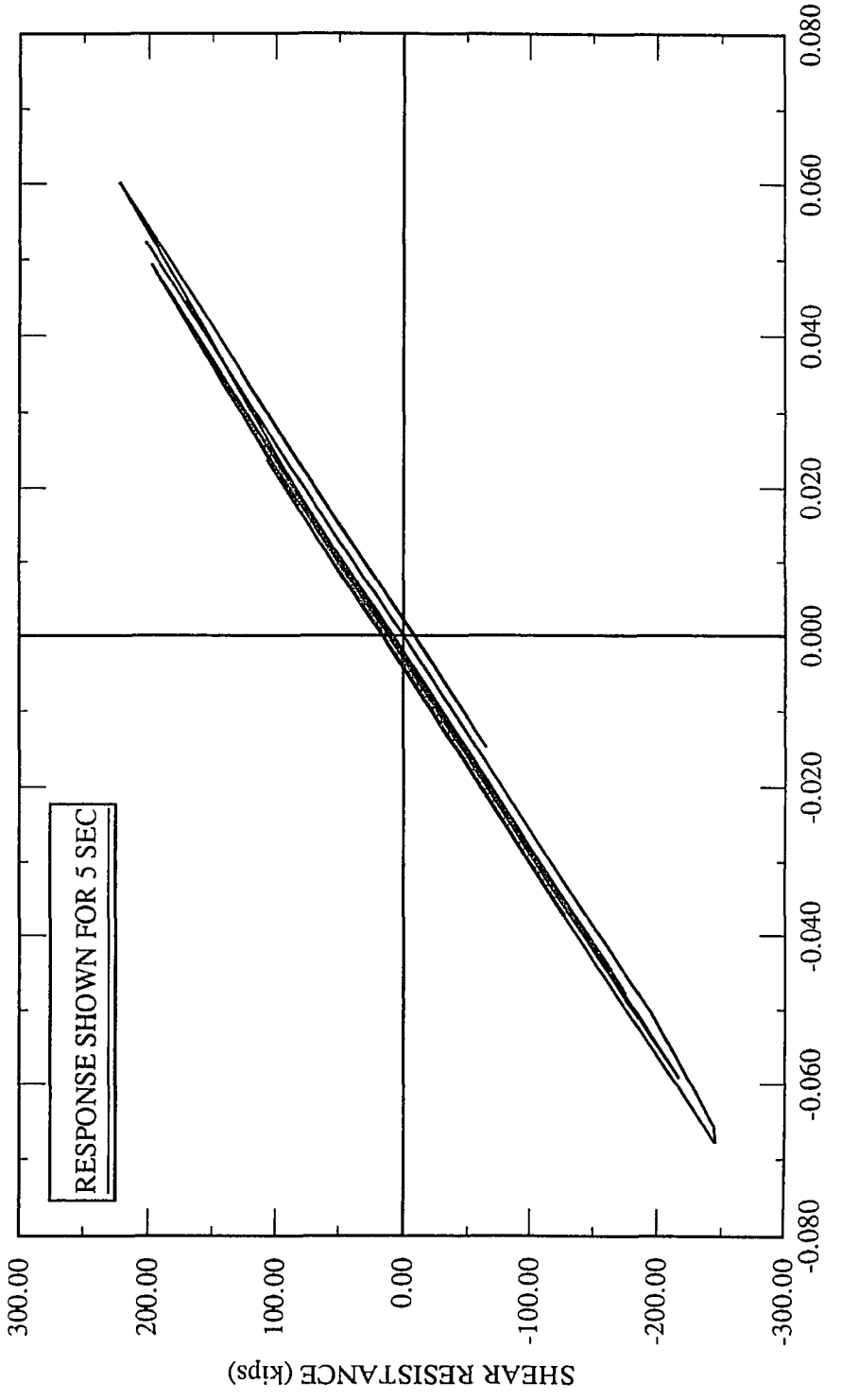

Figure 6.15 Load Displacement Hysteresis Loops for 96X64W.R2, Total

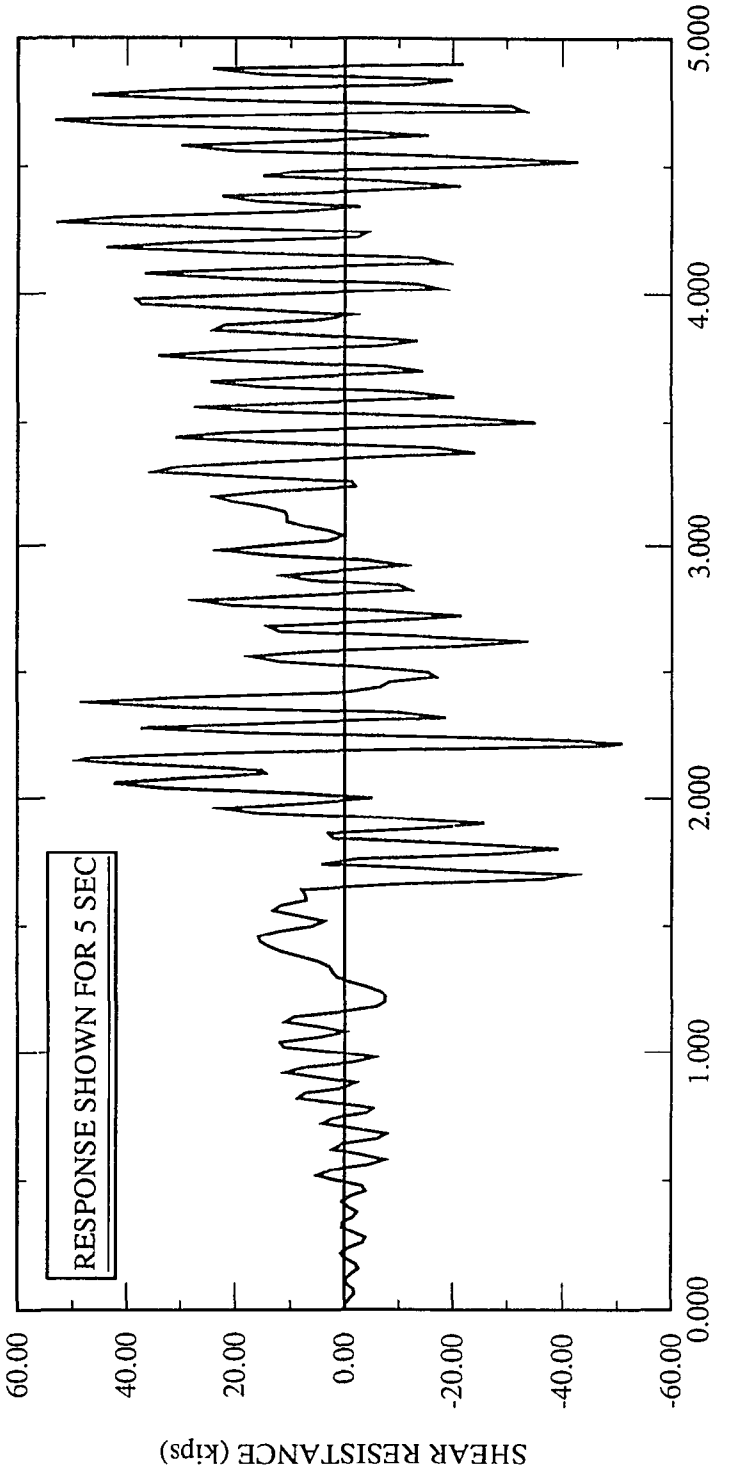

Figure 6.16 Load Time History for 96X64W.R3, Masonry Wall

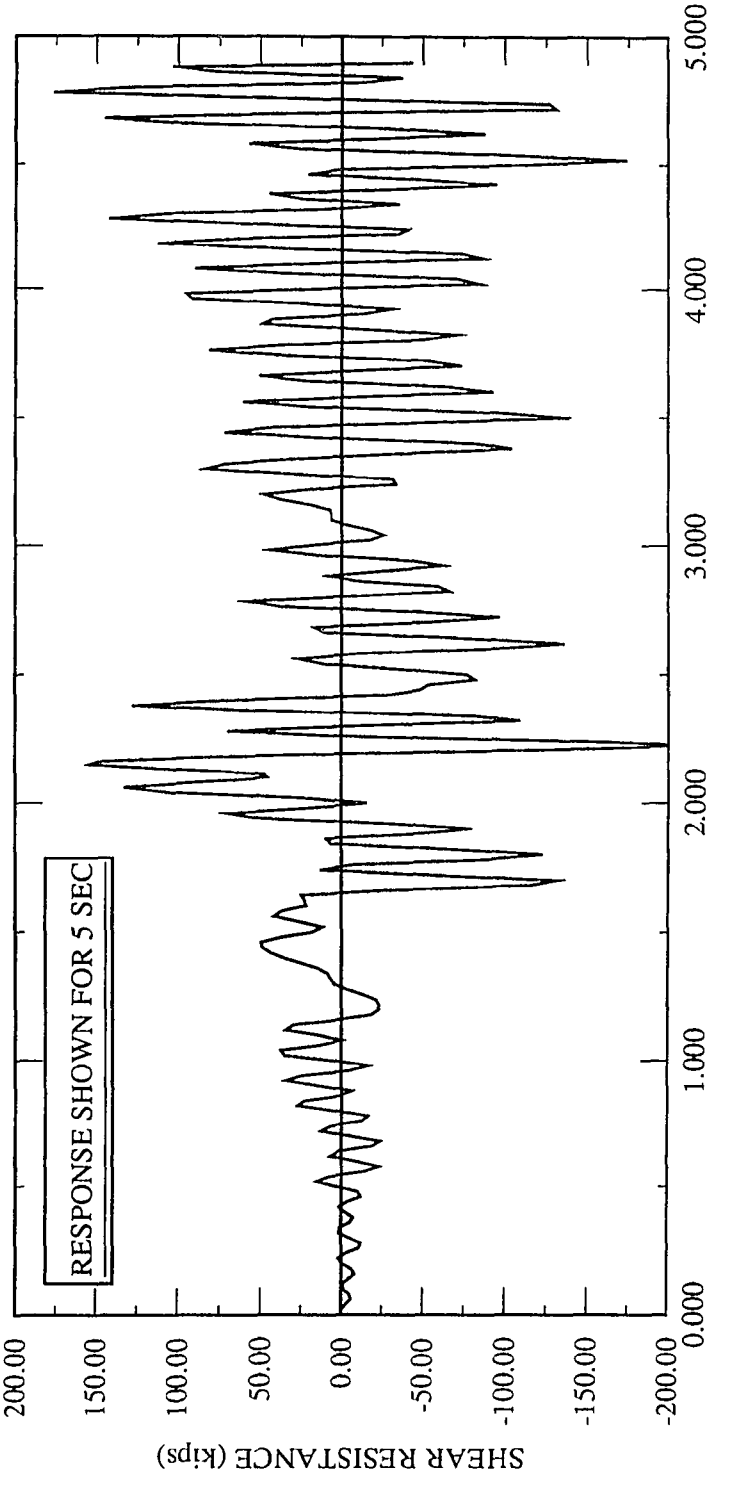

Figure 6.17 Load Time History for 96X64W.R2, Bracing

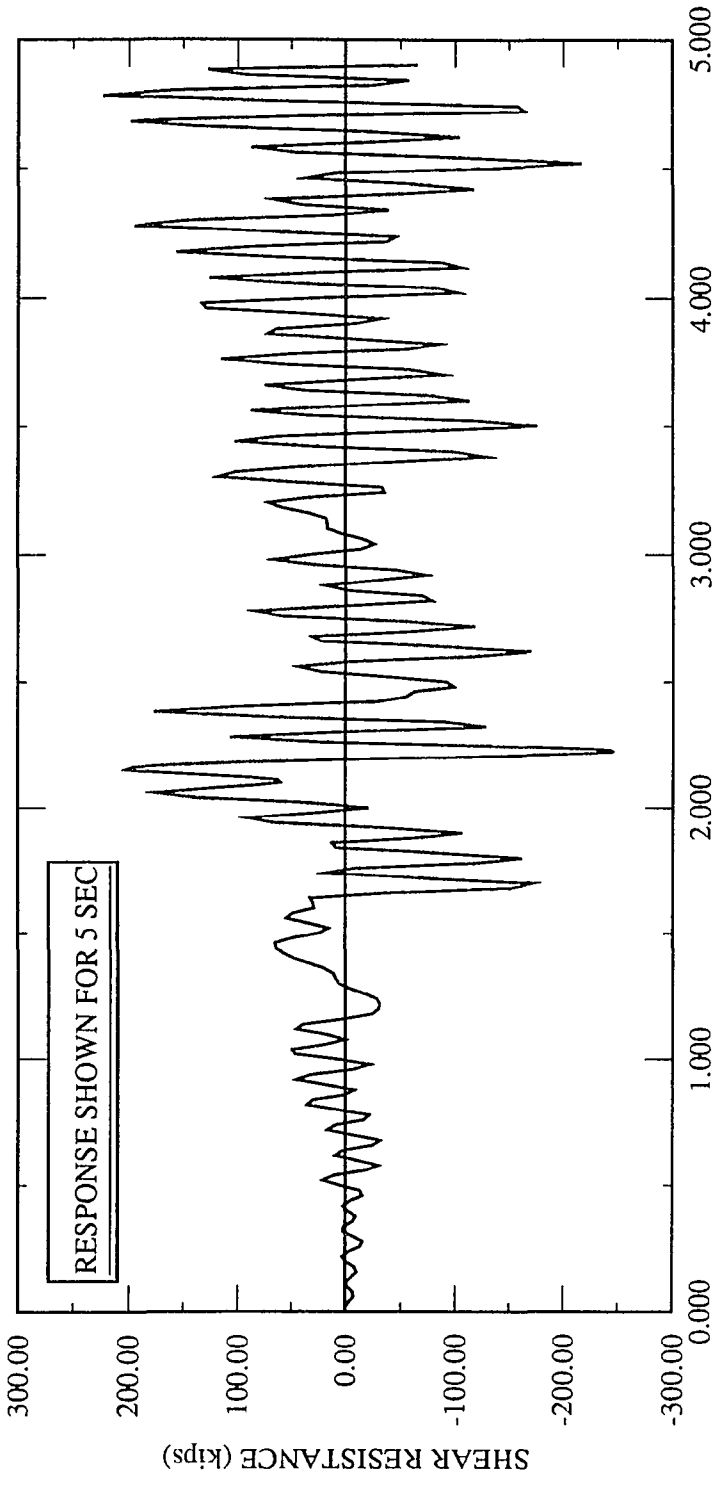

Figure 6.18 Load Time History for 96X64W.R2, Total

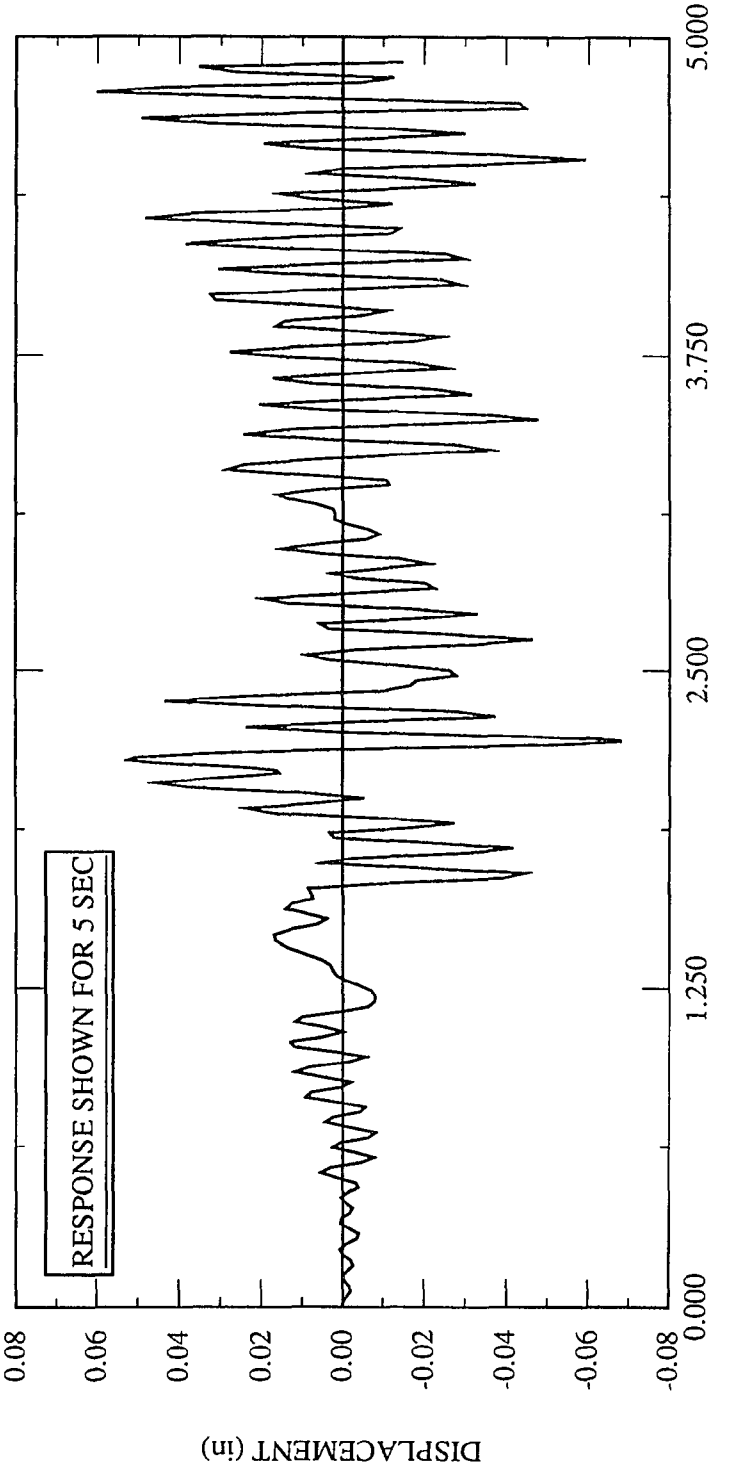

Figure 6.19 Displacement Time History for 96X64W.R2

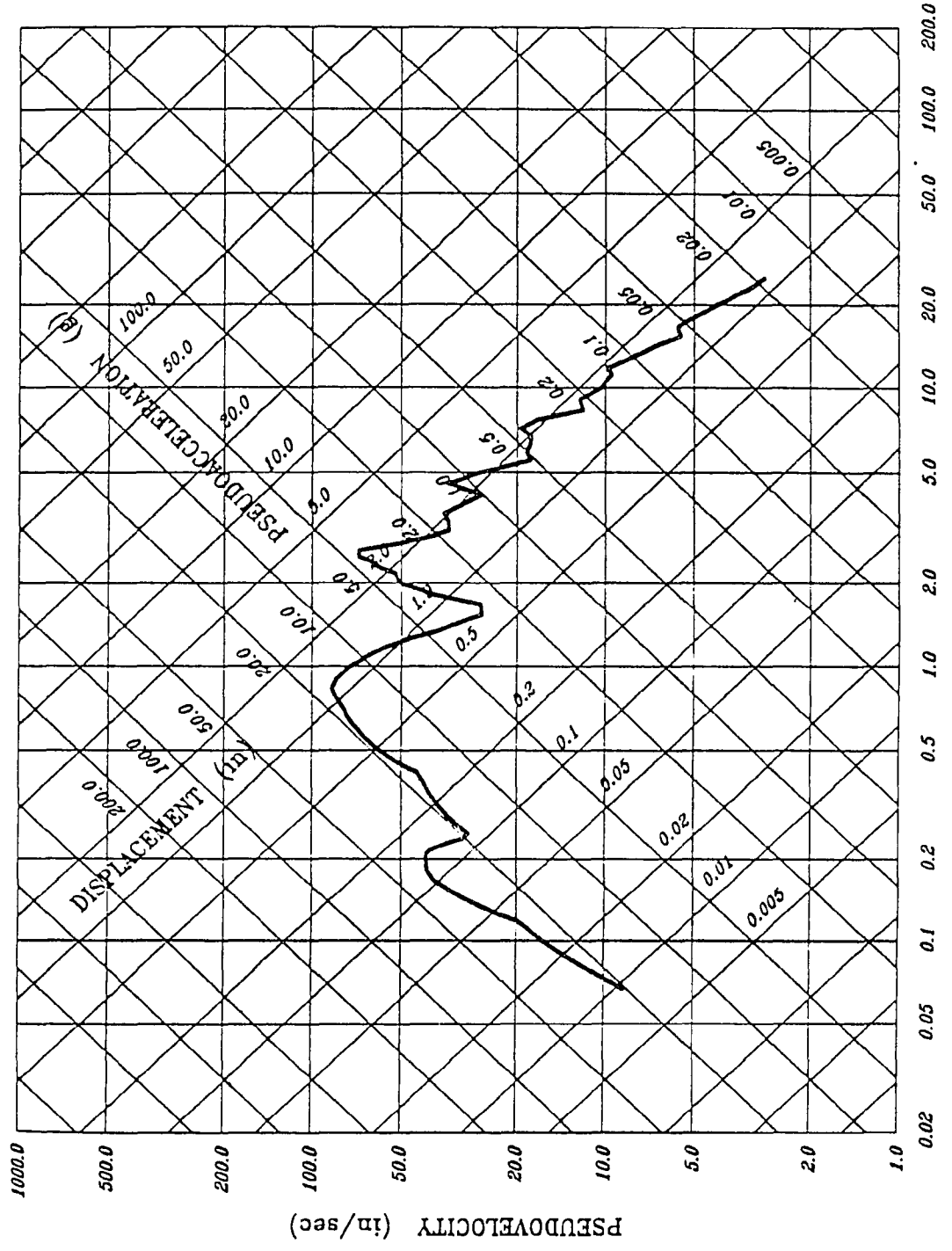

Figure 6.20 Typical Response Spectrum

CHAPTER 7

SUMMARY AND CONCLUSIONS

7.1 Summary

Investigations of structures subjected to moderate to high intensity earthquakes reveal that unreinforced masonry construction is one of the most hazardous types of construction. Several projects have been initiated with the intentions to develop methodologies for evaluation and strengthening of URM structures.

The overall objective of this work was to study inplane behavior of URM walls and corresponding strengthening schemes using analytical models. Several discrete and smeared approaches for modeling the joint bond failure URM structures were examined followed by the suggested analytical approach. Steps for incorporation of the suggested approach in a general purpose software were presented. The validity of the analytical model was demonstrated by solving different problems at element as well as structure level and comparing answers with experimental and analytical results.

Behavior of several URM walls under vertical compression and lateral load was studied. Explanation for some of the observed events in load-deflection curve was given based on analytical model used in this study. Two strengthening schemes for URM walls were analysed. A comparative evaluation was made regarding the effectiveness of these strengthening schemes in increasing strength and stiffness. Nonlinear dynamic analysis was performed on URM wall and two strengthening schemes.

7.2 Conclusions

Joints in URM structures can be represented using uncoupled springs in normal and shear direction at each end of the joint element. The stiffness of the springs can be calculated from material and geometric properties of the joint. Alternatively, they can be evaluated as described in references [23, 43]. For correct estimate of stresses, staggered mortar joints should be continued further (pseudo joints) into the adjacent blocks using material properties of the blocks.

Comparison of results obtained from suggested analytical model and fine mesh model confirms the validity of the suggested approach. Required CPU for the suggested model was 100 times lesser than that for the fine mesh model. Nonlinear analysis shows that analytical formulation of joints using springs and simple bond failure surface with non-associative flow rule can predict response and failure mode of URM wall with reasonable accuracy, when compared with experimental results. Different events observed in experimental load-deflection curve for URM structures can be explained based on the plasticity model used in this study.

Interface conditions between wall and frame plays important role in strengthening of URM walls using steel frame. The assumption of perfect bond conditions at the interface significantly increases the contribution of frame in resisting lateral load. Such a behavior is beneficial as steel frame is additional structural system used to strengthen URM walls. Careful attention should be given to the axial stiffnesses of frame and wall. Total compressive stress will be distributed based on the axial stiffness. If frame axial stiffness is very high compared to wall axial stiffness, most of the compressive stress will go to the frame. This is detrimental to

the overall performance of the system as masonry strength will reduce significantly because of lack of compressive force. Total increase in strength of the combined system over the original URM wall is marginal in such a case. The increase in strength due to addition of steel frame is almost nullified by the decrease in masonry strength due to lack of precompression. Full capacity of steel frame is not utilized and failure occurs due to extensive cracking of URM wall. If compression on the total system is increased so that failure mode of masonry wall in the combined frame-wall system is similar to that of URM wall alone, the performance of the system improves significantly. The increase in strength of the combined system over original URM wall is also more as compared to the first case. Yielding of steel frame occurs when combined system fails due to extensive cracking of wall.

Bracing system is a very effective way to increase strength of URM walls. At the failure of the combined system due to extensive cracking of URM wall, yielding of diagonal bracing bars is noticed. Thus, full capacity of bracing bars is utilized in the combined system. Performance of the bracing system is greatly dependent on the buckling of compression members. Shear strength based on buckling load should be checked while designing the sections for bracing systems.

For the same amount of steel used in force resisting members, increase in shear strength due to addition of bracing system is much more as compared to that due to addition of frame. Increase in strength is very important because of brittle behavior of URM walls. Ductility requirement is inversely proportional to strength. Thus, availability of higher strength using bracing system requires lower ductility demand.

The suggested analytical approach can be effectively utilized in predicting

dynamic response of structural systems with nonlinearity in the form of bond failure of joints. If system exhibits brittle characteristics, the nonlinear response can be effectively predicted using response spectra. This is particularly important to engineers interested in examining the viability of structural systems.

7.3 Recommendations for Further Research

Strength of URM walls is strongly dependent on the vertical compression. Changes in vertical compression can significantly reduce the strength as already shown in this work. Ground motions in vertical direction can cause dramatic change in the vertical compression on URM walls. Code guidelines for earthquake loading neglects the effects of vertical component of the ground acceleration based on the assumption that vertical component is small and always smaller as compared to horizontal components of ground acceleration. However, measurements of ground motions during past earthquakes indicates that vertical acceleration can reach values comparable to horizontal accelerations and may even exceed these accelerations [52]. Thus, it will be of great practical interest to evaluate the response of URM walls and corresponding retrofitting schemes under combined vertical and horizontal motions.

One of the major problems associated with the performance of URM buildings is the lack of ductility of masonry systems. Generally, attempt is made to increase the strength of URM systems by addition of other structural systems. Required increase in strength is significantly high because of lack of ductility of URM walls, making the overall project expensive. Rehabilitation projects can be very economical if ductility of existing structural systems can be increased instead of strength.

URM walls are very weak under out of plane loading. This is again due to presence of joints causing bond failure at the interface of brick and mortar. Damage to life and property due to out of plane collapse of URM walls is substantial. The analytical model used in this study can be employed for studying out of plane bending of URM walls. A section of the wall can be analysed under plane strain condition using the same modeling technique as described in this work. The failure in such cases can occur either at the base or at mid-height depending on the vertical compression and height of the wall. Effectiveness of various strengthening schemes can also be evaluated.

REFERENCES

1. Abboud B., Hamid A., and Harris H., "Small-Scale Modeling of Concrete Block Masonry Structures," ACI Structural Journal, Vol. 87, No. 2, March-April, 1990.

2. ABK, "Methodology for Mitigation of Seismic Hazards in Existing Unreinforced Masonry Buildings," TR-04 & TR–08, 250 North Nash Street, El Segundo, CA 90245.

3. Abolhassan Astaneh et. al., "Preliminary Report on the Seismological and Engineering Aspects of the October 17, 1989 Santa Cruz (Loma Prieta) Earthquake," UCB/EERC 89/14, October 1989.

4. ACI 530–88/ASCE 5–88, "Building Code Requirements for Masonry Structures".

5. ADINA, "Theory and Modeling Guide," ADTR-87, Watertown, MA 02172.

6. Ali S. and Page A., "A Failure Criterion for Mortar Joints in Brickwork Subjected to Combined Shear and Tension," Masonry International, No. 9, December 1986.

7. Ali S. and Page A., "Finite Element Model for Masonry Subjected to Concentrated Loads," ASCE, Journal of Struct. Engg., Vol 114, No. 8, August, 1988.

8. ANSYS, "Engineering Analysis System," Swanson Analysis Systems Inc., Rev 4.1A, Houston, Pennsylvania 15342.

9. Applied Technology Council, " A Handbook for Seismic Evaluation of Existing Buildings," ATC–22, 3 Twin Dolphin Drive, Suite 275, Redwood City, California 94065.

10. Bathe K. J., "Finite Element Procedures in Engineering Analysis," Prentice-Hall, Englewood Cliffs, 1982

11. Bathe K. J. and Chaudhary A., "A Solution Method for Planar and Axisymmetric Contact Problems," International Journal of Numerical Methods in Engineering, 1985, Vol. 21, pp 65–88.

12. Buragohain D. N. and Shah V. L., "Curved Isoparametric Interface Surface Element," ASCE, Journal of Structural Division, Vol. 104, ST1, Jan 1978, pp 205–209.

13. Bush Thomas et. al., "Observations on Two Seismic Strengthening Schemes for Concrete Frames," Earthquake Spectra, Vol. 7, No. 4, pp 511–527, 1991.

14. Cook R. D. and Al- Abdulla J. K., "Some Plane Quadrilateral "Hybrid" Finite Elements," AIAA, Vol. 7, No. 11, Nov. 1969.

15. Crotty and Wardle, "Boundary Integral Analysis of Piecewise Homogenous Media with Structural Discontinuities," International Journal of Rock Mechanics Mining Science & Geomechanics, Vol. 22, No. 6, pp 419–427, 1985.

16. Cundall P. A. UDEC, "A Generalized Distinct Element Program for Modelling of Jointed Rock," U. S. Arm European Research Office and Defence Nuclear Agency, Contract DATA 37–39–C-0548, 1980.

17. Cundall P. A. and Hart R. D., "Development of Generalized 2–D and 3–D Distinct Element Programs for Modelling Jointed Rock," Itasca Consulting Group, Misc. Paper SL-85–1, U. S. Army Corps of Engineers, 1985.

18. Deppe K., "The Whittier Narrows, California Earthquake of October 1, 1987–Evaluation of Strengthened and Unstrengthened Unreinforced Masonry in Los Angeles City," Earthquake Spectra, Vol. 4, No. 1, pp 157–180, 1988.

19. Desai C. S. and Nagaraj B. K., "Modeling for Cyclic Normal and Shear Behavior of Interfaces," ASCE, Journal of Engineering Mechanics, Vol. 114, No. 7, pp 1198–1217 Sept. 1986.

20. Dhanasekar M., Kleeman P. and Page A., "Biaxial Stress-Strain Relations for Brick Masonry," Journal of Struct. Engg. Vol 111, No. 5, May 1985.

21. Dhanasekar M., Page A. W., "The Influence of Brick Masonry Infill Properties on the Behavior of Infilled Frames," Proc. Inst. Civil Engrs, Part 2, June 1985.

22. Epperson G. S. and Abrams D. P., "Nondestructive Evaluation of Masonry Buildings," Document No. 89–26–03, Advanced Construction Technology Center, University of Illinois at Urbana-Champaign, Urbana, Illinois 61801.

23. Goodman R. E., Taylor R. L. and Brekke T. L., "A Model for Mechanics of

Jointed Rock," Proceedings, ASCE, Journal of Soil Mechanics and Foundations Division, SM3, pp 637–658, May 1968.

24. Gulkan P., et. al., "Seismic Testing of Single-Story Masonry Houses," ASCE, Journal of Struct. Engg., Vol. 116, No. 1, Jan 1990.

25. Hegemier G., et. al., "Full Scale Simulated Seismic Testing of Reinforced Masonry Structures," Sixth Meeting of the U.S.- Japan TCCMAR, Port Lulow, Washington, U.S.A. August, 1990.

26. Hrennikoff A., "Solution of Problems of Elasticity by the Framework Method," Proceedings of ASME, pp A-169–A-175, 1941.

27. Katona M., "A Simple Contact Friction Interface Element with Application to Buried Culverts," International Journal for Numerical and Analytical Methods in Geomechanics, Vol. 7, pp 371–384, 1983.

28. Kyle W. and Frank R., "Influence of Vertical Compressive Stress on Shear Resistance of Concrete Block Masonry Walls," NSBIR 84–2929, U. S. Department of Commerce, Oct. 1984.

29. Kyle W. and Frank R., "Influence of Aspect Ratio on Shear Resistance of Concrete Block Masonry Walls," U. S. Dept. of Commerce National Bureau of Standards, National Engineering Laboratory, Center for Building Technology, Gaithersburg, MD 20899, Jan 1985

30. Kyle W. and Frank R., "Influence of Block and Mortar Strength on Shear Resistance of Concrete Block Masonry Masonry Walls," NSBIR 85–3143, U. S. Department of Commerce Apr. 1985.

31. Kyle W. and Frank R., "Influence of Mortar Bedding on Masonry Prism Behavior, NSBIR 86–3467," U. S. Department of Commerce, Feb. 1987.

32. Langenbach Randolph, "Earthquakes: A New Look at Cracked Masonry," Civil Engineering, Vol 62, No. 11, pp 56–59, Nov. 1992.

33. Los Angeles Municipal Code, "Earthquake Hazard Reduction in Existing Buildings," Ordinance No. 154807, Approved Jan 1981.

34. Maksoud Ayman and Drysdale R. G., "Numerical Modeling of Masonry Walls," 6th Canadian Masonry Symposium, Vol 2, pp 801–813, June 1992.

35. McCormick C. W., "Plane Stress Analysis," Proceedings of ASCE, Journal of Structural Division, Vol. 89, 4, pp 37–54, Aug. 1963.

36. McHenry D., " A Lattice Analogy for the Solution of Stress Problems ," Journal of Institution of Civil Engineers, No. 2, pp 59–82, Dec. 1943.

37. Mehta S. S. and Saadeghvaziri M. A., "Analytical Evaluation of Joint Stiffness in URM Structures," 6th Canadian Masonry Symposium, Vol. 1, pp 109–117, June 1992.

38. Mengi Y. and McNiven H., "A linear Mathematical Model for the Seismic In-plane behavior of Brick Masonry Walls, " Earthquake Engineering and Structural Dynamics, Vol 12, 1984.

39. Mengi Y. and McNiven H., "A Mathematical Model for the Inplane Nonlinear Earthquake Behavior of Unreinforced Masonry Walls," Earthquake Engineering and Structural Dynamics, Vol. 18, 1989.

40. Naraine K. and Sinha S., "Loading and Unloading Stress-Strain Curves for Brick Masonry," ASCE, Journal of Struct. Engg., Vol. 115, No. 10, October 1989.

41. Ngo D. and Scordelis A. C., " Finite Element Analysis of Reinforced Concrete Beams," ACI Journal, pp 152–162, March 1967.

42. Okamoto N. and Nakazawa M., "Finite Element Incremental Analysis with Various Frictional Conditions," International Journal for Numerical Methods in Engineering, 14, pp 337–357, 1979.

43. Page A. W., "Finite Element Model for Masonry," ASCE, Journal of Struct. Division, Vol. 104, No. ST8, August, 1978.

44. Page A., Kleeman P. and Dhanasekar M., "An Inplane Finite Element Model for Brick Masonry," New analysis techniques for Structural Masonry, Chicago, Illinois, September 1985.

45. Page A. W., "Quality Control in Masonry Construction-The Lessons from the New Castle Earthquake," 6TH Canadian Masonry Symposium, pp 711–723, 1992.

46. Pande G. N. et. al., "Equivalent Elastic Moduli for Brick Masonry," Computers

and Geomechanics, 8 pp 243–265, 1989.

47. Pande G. N., Beer G., Williams J. R., "Numerical Methods in Rock Mechanics," TA 706.P34, Wiley1990.

48. Pian H. H., " Derivation of Element Stiffness Matrices by Assumed Stress Distributions," AIAA, Vol. 2, No. 7, 1333–1336, July 1964.

49. Pian T. H. and Tong P., "Basis of Finite Element Methods for Solid Continua," International Journal for Numerical Methods in Engineering, Vol. 1 , pp 3–28, 1969.

50. "Repair and Retrofit of Existing Structures," Phil M. Ferguson Structural Engineering Laboratory, The University of Texas at Austin, PMFSEL Report No. 87–6, pp 44–49.

51. Rizzo F. J. and Shippy D. J., "A Formulation and Solution Procedure for the General Non-Homogenous Elastic Inclusion," International Journal of Solids and Structures, Vol. 4, pp 1161–1179, 1968.

52. Saadeghvaziri M. A. and Foutch D. A., "Inelastic Response of R/C Bridges under Horizontal and Vertical Earthquake Motions," Department of Civil Engineering, University of Illinois at Urbana-Champaign, SRS 540, UILU-ENG-88–2003.

53. Saadeghvaziri M. A. and Mehta S. S., "Finite Element Model for Unreinforced Masonry Structures," Conference on Non-linear Finite Element Methods, SPLIT Sweansea, Sept. 1991.

54. Saliba J. E., Alakkad R. S. and Sawaya G. E., "Use of Anisotropic Behavior in Masonry," 6th Canadian Masonry Symposium, Vol 2, pp 687–694, June 1992.

55. Seible F. et al., "Nonlinear Analysis of Reinforced Concrete Masonry Subassemblages," Proceedings of Fifth North American Masonry Conference, Vol 1, University of Illinois at Urbana-Champaign, June 1990.

56. Schafer H., "A Contribution to the Solution of Contact Problems with the Aid of Bond elements," Computer Methods in Applied Mechanics and Engineering, No. 6, pp 335–354, 1975.

57. Sharma K. G. and Desai C. S., "Analysis and Implementation of Thin-Layer

Element for Interfaces and Joints," Journal of Engineering Mechanics, Vol. 118, No. 12, pp 2442–2463, December 1992.

58. Takayanagi T. and Schnobrich W., "Computed Behavior of Reinforced Concrete Coupled Shear Wall," Structural Research Series No. 434, UILU-ENG-76–2024.

59. URS/John A. Blume and Associates, "Techniques for Seismically Rehabilitating Existing Buildings," A report Prepared for Federal Emergency Management Agency, 150 Fourth St, San Francisco, CA 94103.

60. Zienkiewicz O. C. and G. N. Pande, "Time Dependent Multilaminate Model of Rocks- A Numerical Study of Deformation and Failure of Rock Masses," International Journal of Numerical and Analytical Methods in Geomechanics, Vol. 1, 219–247, 1977.

61. Zienkiewicz O. C., "The Finite Element Method," McGraw-Hill, London, 1987.

APPENDIX 1

EXPLANATION OF USER DEFINED ELEMENT

User defined element is identified by STIF100 in the ANSYS program. There are two key options associated with STIF100.

The first key option, KEYOPT(1) is used to identify orientation of the element. KEYOPT (1) equal to 1 means shear springs are in X-direction and normal springs are in Y-direction. KEYOPT(1) equal to 3 means normal springs are in X-direction and shear springs are in Y-direction.

The second key option KEYOPT(2) is used to identify the type of the joint element. KEYOPT(2) equal to 1 indicates that joint element is pseudo joint between two bricks. This can be used to detect splitting of bricks based on principal tension if nonlinear material properties are specified. KEYOPT(2) equal to 2 indicates mortar joints. Bond failure criteria will be used to detect failure of joints in nonlinear analysis when this option is selected. Numbering of all STIF100 elements should start from bottom left and proceed in anticlockwise direction.

Six real constants are required for each type of the joint element discussed above. They are tensile strength, initial strain (normally zero), thickness, length, **a, b** in the same order.

The first value is used when material failure based on principal tension is to be modeled. The second term is not used. Thickness and length of joint are used in calculation of stiffness matrix. Last two terms **a** and **b** are used to define initial bond failure as:

$$\tau = (a \times \sigma) + b$$

Two linear properties, Modulus of Elasticity and Poisson ratio are used for calculation of stiffness matrix. Four nonlinear material properties are required to define rest of the bond failure surface shown in Fig. 2.4. They start from 13 to 16 on NL command. The first one C13=100 indicates user defined plasticity. C14 =**at** and C15=**bt** defines bond failure in tension and shear. C16 = **f** defines coefficient of friction for subsequent failure curve. These nonlinear material properties should be specified for material property number (MAT)=3.

Bond failure equation in tension and shear is

$$\tau = bt - (at \times \sigma)$$

Subsequent failure curve is

$$\tau = f \times \sigma$$

APPENDIX 2

SAMPLE INPUT DATA FOR ANSYS RUN WITH USER DEFINED ELEMENT

Input details for a problem using joint element is given in this appendix. The model generated is shown in Fig. 4.3.

```
1 /PREP7
2
3 /TITLE,INPUT DATA FOR NONLINEAR DYNAMIC ANALYSIS
4 KAN,4
5 KAY,5,2
6 KAY,9,1
7 KNL,1
8 ALPHAD,0.7
9 BETAD,0
10 GAMMA,0.05,40
11 /PBC,ALL,2
12
13 ET,1,42,,,,,,1
14 ,2,100,1,1
15 ,3,100,1,2
16 ,4,100,3,2
17 ,5,21,,,4
18
19 EX,1,2.41E06
20 NUXY,1,0.16
21 EX,2,2.41E06
22 NUXY,2,0.16
23 EX,3,1.21E06
24 NUXY,3,0.16
```

```
25 EX,4,1.21E06
26 NUXY,4,0.16
27
28 NL,3,13,100,-0.5,580,0.65
29 ,4,13,100,-0.5,580,0.65
30
31 R,2,1000,0,0.8,8.0
32 ,3,10000,0,0.8,8.0,0.65,580
33 ,4,10000,0,0.8,8.0,0.65,580
34 ,5,10.36
35
36 N,1
37 ,2,,8
38 ,3,,8.8
39 NGEN,12,2,2,3,1,0,8.8
40 NDELE,25
41 NGEN,2,24,1,24,1,8
42 NGEN,2,24,25,48,1,0.8
43 NGEN,12,48,25,96,1,8.8
44 NDELE,577,600
45
46 TYPE,1
47 REAL,1
48 MAT,1
49 E,1,25,26,2
50 EGEN,12,2,1
51 EGEN,12,48,1,12,1
52
```

```
53 TYPE,2
54 REAL,2
55 MAT,2
56 E,2,26,27,3
57 EGEN,6,4,145
58 E,52,76,77,53
59 EGEN,5,4,151
60 EGEN,6,96,145,155
61
62 TYPE,3
63 REAL,3
64 MAT,3
65 E,4,28,29,5
66 EGEN,5,4,211
67 E,50,74,75,51
68 EGEN,6,4,216
69 EGEN,6,96,211,221,1
70
71 TYPE,4
72 REAL,4
73 MAT,4
74 E,25,49,50,26
75 EGEN,12,2,277
76 EGEN,11,48,277,288
77
78 NRSEL,x,0
79 D,ALL,ALL
80 NALL
```

```
81
82 NRSEL,X,104.8
83 CPSIZE,24
84 CP,1,UX,ALL
85 CP,2,UY,ALL
86 F,ALL,FX,-4000
87 TYPE,5
88 REAL,5
89 E,553
90 EGEN,24,1,409
91
92 /PBC,ALL,0
93 EPLOT
94 NALL
95 EPLOT
96 ITER,-40,40,40
97 KRF,1
98 KBC,1
99
100 KNL,1
101 AFWRITE
102 FINISH
103 /EOF
```

***********ANSYS EXECUTION AND EXPLANATION OF INPUT DATA**********

NEW TITLE= INPUT DATA FOR NONLINEAR TRANSIENT DYNAMIC ANALYSIS

ANALYSIS TYPE= 4 (NONLINEAR TRANSIENT DYNAMIC ANALYSIS)

INITIAL VELOCITY AND ACCELERATION ZERO (KAY(5)=2)

USE FULL NEWTON-RAPHSON SOLUTION PROCEDURE (KAY(9)=1)

NON-LINEAR ANALYSIS - SUPPLY NON-LINEAR PROPERTIES

MASS MATRIX DAMPING MULTIPLIER= 0.70000

STIFFNESS MATRIX DAMPING MULTIPLIER= 0.

NEWMARK AMPLITUDE DECAY FACTOR= 0.50000E-01 USE UP TO 40 EQUILIBRIUM ITERATIONS (IF NECESSARY)

ALL BOUNDARY CONDITION PLOT KEY = 2

ELEMENT TYPE 1 USES STIF 42 KEYOPT(1-9)= 0 0 0 0 0 0 0 0 0 INOPR= 1 NUMBER OF NODES= 4

ISOPAR. STRESS SOLID, 2-D

CURRENT NODAL DOF SET IS UX UY TWO-DIMENSIONAL STRUCTURE

ELEMENT TYPE 2 USES STIF100 KEYOPT(1-9)= 1 1 0 0 0 0 0 0 0 INOPR= 0 NUMBER OF NODES= 4

USER DEFINED ELEMENT

CURRENT NODAL DOF SET IS UX UY TWO-DIMENSIONAL STRUCTURE

ELEMENT TYPE 3 USES STIF100 KEYOPT(1-9)= 1 2 0 0 0 0 0 0 0 INOPR= 0 NUMBER OF NODES= 4

USER DEFINED ELEMENT

CURRENT NODAL DOF SET IS UX UY TWO-DIMENSIONAL STRUCTURE

ELEMENT TYPE 4 USES STIF100 KEYOPT(1-9)= 3 2 0 0 0 0 0 0 0 INOPR= 0 NUMBER OF NODES= 4

USER DEFINED ELEMENT

CURRENT NODAL DOF SET IS UX UY TWO-DIMENSIONAL STRUCTURE

ELEMENT TYPE 5 USES STIF 21 KEYOPT(1-9)= 0 0 4 0 0 0 0 0 0 INOPR= 0 NUMBER OF NODES= 1

GENERAL MASS

CURRENT NODAL DOF SET IS UX UY TWO-DIMENSIONAL STRUCTURE

MATERIAL 1 COEFFICIENTS OF EX VS. TEMP EQUATION C0 = 2410000.

PROPERTY TABLE EX MAT= 1 NUM. POINTS= 2 TEMPERATURE DATA TEMPERATURE DATA -9999.0 0.24100E+07 9999.0 0.24100E+07

MATERIAL 1 COEFFICIENTS OF NUXY VS. TEMP EQUATION C0 = 0.1600000

PROPERTY TABLE NUXY MAT= 1 NUM. POINTS= 2 TEMPERATURE DATA TEMPERATURE DATA -9999.0 0.16000 9999.0 0.16000

MATERIAL 2 COEFFICIENTS OF EX VS. TEMP EQUATION C0 = 2410000.

PROPERTY TABLE EX MAT= 2 NUM. POINTS= 2 TEMPERATURE DATA TEMPERATURE DATA -9999.0 0.24100E+07 9999.0 0.24100E+07

MATERIAL 2 COEFFICIENTS OF NUXY VS. TEMP EQUATION C0 = 0.1600000

PROPERTY TABLE NUXY MAT= 2 NUM. POINTS= 2 TEMPERATURE DATA TEMPERATURE DATA -9999.0 0.16000 9999.0 0.16000

MATERIAL 3 COEFFICIENTS OF EX VS. TEMP EQUATION C0 = 1210000.

PROPERTY TABLE EX MAT= 3 NUM. POINTS= 2 TEMPERATURE DATA TEMPERATURE DATA -9999.0 0.12100E+07 9999.0 0.12100E+07

MATERIAL 3 COEFFICIENTS OF NUXY VS. TEMP EQUATION C0 = 0.1600000

PROPERTY TABLE NUXY MAT= 3 NUM. POINTS= 2 TEMPERATURE DATA TEMPERATURE DATA -9999.0 0.16000 9999.0 0.16000

MATERIAL 4 COEFFICIENTS OF EX VS. TEMP EQUATION C0 = 1210000.

PROPERTY TABLE EX MAT= 4 NUM. POINTS= 2 TEMPERATURE DATA TEMPERATURE DATA -9999.0 0.12100E+07 9999.0 0.12100E+07

MATERIAL 4 COEFFICIENTS OF NUXY VS. TEMP EQUATION C0 = 0.1600000

PROPERTY TABLE NUXY MAT= 4 NUM. POINTS= 2 TEMPERATURE DATA TEMPERATURE DATA -9999.0 0.16000 9999.0 0.16000

NONLINEAR PROPERTIES FOR MATERIAL 3 NUM. POINTS= 48 SLOC= 13 100.00 -0.50000 580.00 0.65000 0. 0.

NONLINEAR PROPERTIES FOR MATERIAL 4 NUM. POINTS= 48 SLOC= 13 100.00 -0.50000 580.00 0.65000 0. 0.

REAL CONSTANT SET 2 ITEMS 1 TO 6 1000.0 0. 0.80000 8.0000 0. 0.

REAL CONSTANT SET 3 ITEMS 1 TO 6 10000. 0. 0.80000 8.0000 0.65000 580.00

REAL CONSTANT SET 4 ITEMS 1 TO 6 10000. 0. 0.80000 8.0000 0.65000 580.00

REAL CONSTANT SET 5 ITEMS 1 TO 6 10.360 0. 0. 0. 0. 0.

NODE 1 KCS= 0 X,Y,Z= 0. 0. 0.

NODE 2 KCS= 0 X,Y,Z= 0. 8.0000 0.

NODE 3 KCS= 0 X,Y,Z= 0. 8.8000 0.

SET IS SELECTED NODES IN RANGE 2 TO 3 IN STEPS OF 1 GEOMETRY INCREMENTS ARE 0. 8.8000 0.

DELETE SELECTED NODES IN THE RANGE 25 TO 25 BY 1

GENERATE 2 TOTAL SETS OF NODES WITH INCREMENT 24 SET IS SELECTED NODES IN RANGE 1 TO 24 IN STEPS OF 1 GEOMETRY INCREMENTS ARE 8.0000 0. 0.

GENERATE 2 TOTAL SETS OF NODES WITH INCREMENT 24 SET IS SELECTED NODES IN RANGE 25 TO 48 IN STEPS OF 1 GEOMETRY INCREMENTS ARE 0.80000 0. 0.

GENERATE 12 TOTAL SETS OF NODES WITH INCREMENT 48 SET IS SELECTED NODES IN RANGE 25 TO 72 IN STEPS OF 1 GEOMETRY INCREMENTS ARE 8.8000 0. 0.

DELETE SELECTED NODES IN THE RANGE 577 TO 600 BY 1

ELEMENT TYPE SET TO 1

REAL CONSTANT NUMBER= 1

MATERIAL NUMBER SET TO 1

ELEMENT 1 1 25 26 2

GENERATE 12 TOTAL SETS OF ELEMENTS WITH NODE INCREMENT OF 2 SET IS SELECTED ELEMENTS IN RANGE 1 TO 1 IN STEPS OF 1 NUMBER OF ELEMENTS= 12

GENERATE 12 TOTAL SETS OF ELEMENTS WITH NODE INCREMENT OF 48 SET IS SELECTED ELEMENTS IN RANGE 1 TO 12 IN STEPS OF 1 NUMBER OF ELEMENTS= 144

ELEMENT TYPE SET TO 2

REAL CONSTANT NUMBER= 2

MATERIAL NUMBER SET TO 2

ELEMENT 145 2 26 27 3

GENERATE 6 TOTAL SETS OF ELEMENTS WITH NODE INCREMENT OF 4 SET IS SELECTED ELEMENTS IN RANGE 145 TO 145 IN STEPS OF 1 NUMBER OF ELEMENTS= 150 ELEMENT 151 52 76 77 53

GENERATE 5 TOTAL SETS OF ELEMENTS WITH NODE INCREMENT OF 4 SET IS SELECTED ELEMENTS IN RANGE 151 TO 151 IN STEPS OF 1 NUMBER OF ELEMENTS= 155

SET IS SELECTED ELEMENTS IN RANGE 145 TO 155 IN STEPS OF 1 NUMBER OF ELEMENTS= 210

ELEMENT TYPE SET TO 3

REAL CONSTANT NUMBER= 3

MATERIAL NUMBER SET TO 3

ELEMENT 211 4 28 29 5

GENERATE 5 TOTAL SETS OF ELEMENTS WITH NODE INCREMENT OF 4 SET IS SELECTED ELEMENTS IN RANGE 211 TO 211 IN STEPS OF 1 NUMBER OF ELEMENTS= 215 ELEMENT 216 50 74 75 51

GENERATE 6 TOTAL SETS OF ELEMENTS WITH NODE INCREMENT OF 4 SET IS SELECTED ELEMENTS IN RANGE 216 TO 216 IN STEPS OF 1 NUMBER OF ELEMENTS= 221

GENERATE 6 TOTAL SETS OF ELEMENTS WITH NODE INCREMENT OF 96 SET IS SELECTED ELEMENTS IN RANGE 211 TO 221 IN STEPS OF 1 NUMBER OF ELEMENTS= 276

ELEMENT TYPE SET TO 4

REAL CONSTANT NUMBER= 4

MATERIAL NUMBER SET TO 4

ELEMENT 277 25 49 50 26

GENERATE 12 TOTAL SETS OF ELEMENTS WITH NODE INCREMENT OF 2 SET IS SELECTED ELEMENTS IN RANGE 277 TO 277 IN STEPS OF 1 NUMBER OF ELEMENTS= 288

GENERATE 11 TOTAL SETS OF ELEMENTS WITH NODE INCREMENT OF 48 SET IS SELECTED ELEMENTS IN RANGE 277 TO 288 IN STEPS OF 1 NUMBER OF ELEMENTS= 408

NRSE FOR LABEL= X BETWEEN 0. AND 0. KABS= 0. TOLERANCE= 0.100000E-05

24 NODES (OF 576 DEFINED) SELECTED BY NRSE COMMAND.

SPECIFIED DISP ALL FOR ALL SELECTED NODES VALUES= 0. 0. ADDITIONAL DOFS=

576 NODES (OF 576 DEFINED) SELECTED BY NALL COMMAND.

NRSE FOR LABEL= X BETWEEN 104.80 AND 104.80 KABS= 0.

TOLERANCE= 0.524000

24 NODES (OF 576 DEFINED) SELECTED BY NRSE COMMAND.

SET MAXIMUM COUPLED NODE SET SIZE TO 24

COUPLED SET= 1 DIRECTION= UX TOTAL NODES= 24

COUPLED SET= 2 DIRECTION= UY TOTAL NODES= 24

MAXIMUM COUPLED SET NUMBER= 2

SPECIFIED FORCE FX FOR ALL SELECTED NODES VALUES= -4000.0 0.

ELEMENT TYPE SET TO 5

REAL CONSTANT NUMBER= 5

ELEMENT 409 553

GENERATE 24 TOTAL SETS OF ELEMENTS WITH NODE INCREMENT OF 1 SET IS SELECTED ELEMENTS IN RANGE 409 TO 409 IN STEPS OF 1 NUMBER OF ELEMENTS= 432

ALL BOUNDARY CONDITION PLOT KEY = 0

576 NODES (OF 576 DEFINED) SELECTED BY NALL COMMAND.

NITTER= -40 NPRINT= 40 NPOST= 40

USE CONVERGENCE AND/OR TIME STEP OPTIMIZATION BOUNDARY CONDITION STEP OR RAMP DEPENDENT UPON KBC COMMAND.

ALL PRINT CONTROLS RESET TO 40 ALL POST DATA FILE CONTROLS RESET TO 40

REACTION FORCE KEY= 1 CALCULATE AND PRINT NODAL AND REACTION FORCES.

STEP BOUNDARY CONDITION KEY= 1

*** NOTE *** NEWTON-RAPHSON SOLUTION OPTION KAY(9) IS SET TO 1. - RECOMMENDED VALUE IS 2.

*** NOTE *** DATA CHECKED - NO FATAL ERRORS FOUND. CHECK OUTPUT FOR POSSIBLE WARNING MESSAGES.

*** PREP7 GLOBAL STATUS ***

TITLE= INPUT DATA FOR NONLINEAR TRANSIENT DYNAMIC ANALYSIS

ANALYSIS TYPE= 4

NUMBER OF ELEMENT TYPES= 5

432 ELEMENTS CURRENTLY SELECTED. MAX ELEMENT NUMBER = 432

576 NODES CURRENTLY SELECTED. MAX NODE NUMBER = 600

MAXIMUM LINEAR PROPERTY NUMBER= 4

NUMBER OF NON-LINEAR PROPERTIES= 2

MAXIMUM REAL CONSTANT SET NUMBER= 5

ACTIVE COORDINATE SYSTEM= 0 (CARTESIAN)

MAXIMUM COUPLED D.O.F. SET NUMBER= 2

NUMBER OF IMPOSED DISPLACEMENTS= 48

NUMBER OF NODAL FORCES= 24

ANALYSIS DATA WRITTEN ON FILE27

NON-LINEAR ANALYSIS - SUPPLY NON-LINEAR PROPERTIES

ALL CURRENT PREP7 DATA WRITTEN TO FILE16 NAME= FILE16.DAT

FOR POSSIBLE RESUME FROM THIS POINT

***** ROUTINE COMPLETED ***** CP = 7.030

/EOF ENCOUNTERED ON FILE18

***** RUN COMPLETED ***** CP= 7.0400 TIME= 15.1639

APPENDIX 3

NUMERICAL PROCEDURE

The finite element discretization process yields a set of simultaneous equations:

$$[K]\{U\} = \{F^{app}\} \tag{A3.1}$$

where:

[K] is stiffness matrix

{U} is set of unknown displacements

$\{F^{app}\}$ is set of applied loads.

If the stiffness matrix [K] is itself a function of the unknown displacements then equation A3.1 is a nonlinear equation. The Newton-Raphson method is an iterative process of solving the nonlinear equations and can be written as [8]

$$[K_n]\{\Delta U\} = \{F^{app}\} - \left\{F_n^{el}\right\} \tag{A3.2}$$

$$\{U_{n+1}\} = \{U_n\} + \{\Delta U\} \tag{A3.3}$$

where:

$[K_n]$ is tangent stiffness matrix

$\{F^{el}\}$ is set of loads corresponding to the element stresses (restoring forces)

The right hand side of the equation A3.2 is the out-of-balance load vector; i.e., the amount the structural system is out of equilibrium. A single solution iteration is depicted graphically in Fig. A3.1 for a single degree-of-freedom model. As can

be seen from this figure, more than one Newton-Raphson iteration is needed to obtain a converged solution. The general algorithm proceeds as follows:

1. Assume $\{U_n\}$, normally the converged solution from the previous step. When n=0 (the first step), $\{U_n\} = \{0\}$
2. Compute updated tangent matrix $[K_n]$ and restoring force $\{F^{el}{}_n\}$ from the configuration $\{U_n\}$.
3. Calculate $\{\Delta U\}$ from equation A3.2
4. Add $\{\Delta U\}$ to $\{U_n\}$ in order to obtain next approximation $\{U_{n+1}\}$
5. Repeat steps 2 to 4 until convergence is obtained.

The solution obtained at the end of the iteration process would correspond to load vector $\{F^{app}\}$. The final converged solution will be in equilibrium; that is, the restoring forces $\{F^{el}\}$ (computed from the current stress state) would equal the applied loads $\{F^{app}\}$. None of the intermediate solutions would be in equilibrium.

If the analysis includes path-dependent nonlinearities such as plasticity, bond failure etc., then the solution process requires that some intermediate steps be in equilibrium in order to correctly follow the load path. This is accomplished effectively by using a step-by-step incremental analysis; i.e., the final load $\{F^{app}\}$ is reached by stepping the load in increments and performing the Newton-Raphson iterations at each step:

$$[K_{m,n}]\{\Delta U_n\} = \{F_m^{app}\} - \left\{F_{m,n}^{el}\right\} \qquad \text{(A3.4)}$$

where:

$[K_{m,n}]$ is tangent matrix for load step m, iteration n

$\{F^{el}{}_{m,n}\}$ is restoring force for load step m, iteration n

$\{F^{app}_m\}$ is total applied force at load step m.

When the stiffness matrix is updated every iteration as indicated equations A3.2 and A3.4, the process is termed as full Newton-Raphson solution procedure. Alternatively, the stiffness matrix could be updated occasionally or not at all. These procedures are called modified Newton-Raphson and Initial Stress Methods, respectively.

Applied Loads: The set of applied loads $\{F^{app}\}$ is defined by:

$$\{F^{app}\} = \left\{F^{nd}\right\} + \{F^{ac}\} + \sum \{F_e^{pr}\} \tag{A3.5}$$

where:

$\{F^{nd}\}$ is applied nodal loads

$\{F^{ac}\}$ is acceleration load vector

$\{F_e{}^{pr}\}$ is element pressure load vector

The applied loads are total loads (not incremental) since they are balanced by the developed element elastic forces $\{F^{el}{}_e\}$

Imposed Displacements: Imposed displacements, while input on a total displacement basis, are handled in an incremental manner at the equation solution level as:

$$\{\Delta U\} = \left[K_{cc}^{-1}\right]\left(-[K_{cs}]\{\Delta U_s\} + \{F^{app}\} - \left\{F_n^{el}\right\}\right) \tag{A3.6}$$

Where $[K_{cc}]$ and $[K_{cs}]$ are partitions of the structure stiffness matrix obtained as:

$$\begin{bmatrix} [K_{cc}] & [K_{cs}] \\ [K_{cs}^t] & [K_{ss}] \end{bmatrix} \begin{Bmatrix} \{U_c\} \\ \{U_s\} \end{Bmatrix} = \begin{Bmatrix} \{F_c^a\} \\ \{F_s^a\} \end{Bmatrix} + \begin{Bmatrix} \{F_c^r\} \\ \{F_s^r\} \end{Bmatrix} \tag{A3.7}$$

Subscript **c** stands for computed values and subscript **s** stands for specified values.

$\{\Delta U_s\}$ is the vector of imposed displacement increments :

$$\{\Delta U_s\} = \{U_{s,n}\} - \{U_{s,n-1}\} \tag{A3.8}$$

with $\{U_{s,n}\}$ and $\{U_{s,n-1}\}$ being the user-specified imposed displacements (total values) at step n and n-1, respectively. When previously free degree of freedom is given an imposed displacement value, the $\{U_{s,n-1}\}$ for that degree of freedom is defined as the displacement solution value at step n-1. Therefore, $\{\Delta U_s\}$ reflects the displacement increment for the previous position n-1 to the new specified position as indicated by $\{U_{s,n}\}$.

Nodal and Reaction Forces: Nodal and reaction forces are simply :

$$\{F_n^r\} = -\left\{F_n^{el}\right\} + \{F^{ac}\} + \{F^{pr}\} \tag{A3.9}$$

That is, the nodal forces are the negative of the element elastic nodal forces, plus acceleration and/or pressure effects if present.

Dynamics: The dynamic equilibrium equation for the Newton-Raphson scheme, using Newmark time integration and including equilibrium iterations, is at time t_{n+1} and equilibrium iteration i:

$$\begin{aligned}\overline{[K_{n+1,i}]}\{\Delta U\} = \{F^{app}_{n+1}\} - \left\{F^{el}_{n+1,i}\right\} + \\ [M]\Big(a_0(\{U_n\} - \{U_{n+1,i}\}) + a_2\left\{\dot{U}_n\right\} + a_3\left\{\ddot{U}_n\right\}\Big) + \\ [C]\Big(a_1(\{U_n\} - \{U_{n+1,i}\}) + a_4\left\{\dot{U}_n\right\} + a_5\left\{\ddot{U}_n\right\}\Big)\end{aligned} \tag{A3.10}$$

where the effective tangent stiffness is

$$\overline{[K_{n+1,1}]} = [K_{n+1,i}] + a_0[M] + a_1[C] \tag{A3.11}$$

and a_j are Newmark constants defined as

$$\begin{gathered}a_0 = \frac{1}{\alpha\Delta t^2}\ ,\ a_1 = \frac{\delta}{\alpha\Delta t}\ ,\ a_2 = \frac{1}{\alpha\Delta t} \\ a_3 = \frac{1}{2\alpha} - 1\ ,\ a_4 = \frac{\delta}{\alpha} - 1\ ,\ a_5 = \frac{\Delta t}{2}\left(\frac{\delta}{\alpha} - 2\right) \\ a_6 = \Delta t(1-\delta)\ ,\ a_7 = \delta\Delta t\end{gathered} \tag{A3.12}$$

α and δ are Newmark Integration Parameters

The approximation to the displacement at time t_{n+1} is

$$\{U_{n+1,i+1}\} = \{U_{n+1,i}\} + \{\Delta U\} \tag{A3.13}$$

The equilibrium iterations are continued till $\{U_{n+1,i}\}$ has converged, at which time new velocities and accelerations are computed and time is advanced to the next time point.

Element Implementation: Various quantities of interest can be written at ele-

ment level, in incremental form as :

$$
\begin{aligned}
[K_{e,n}] &= \int_v [B_n^t][D_n][B_n]\delta v \\
\{\Delta\sigma\} &= [D_n]\{\Delta\epsilon\} \\
\{\Delta\epsilon\} &= [B_n]\{\Delta U\} \\
[\sigma_{n+1}] &= \{\sigma_n\} + \{\Delta\sigma\} \\
\{\epsilon_{n+1}\} &= \{\epsilon_n\} + \{\Delta\epsilon\}
\end{aligned}
\tag{A3.14}
$$

The elemental restoring force is simply :

$$
\left\{F_{e,n}^{el}\right\} = \int_v [B_n^t]\{\sigma_n\}\delta v \tag{A3.15}
$$

tangent matrices and restoring forces are determined by the particular non-linear phenomenon being modeled. The bond failure of joints is expressed in terms of plasticity formulation as discussed in the Chapter 3. In plasticity, the nonlinearity is contained in the stress-strain relationship and is written as:

$$
[D_n] = [D] - \frac{[D]\{b_n\}\{b_n^t\}[D]}{-\psi\{\sigma^t\}\{b_n\} - \omega\{b_n^t\}\{b_n\} + \{b_n^t\}[D]\{b_n\}} \tag{A3.16}
$$

where [D] is elastic stress-strain matrix

ψ, ω and b_n are material parameters depending on plasticity model used. See reference [8] for further discussion.

$[D_n]$ is the elasto-plastic incremental stress-strain matrix which relates the increment in stress to the increment in strain. For the bond failure of joints, $[D_n]$ is computed in routine USERPL, as discussed in chapter 3.

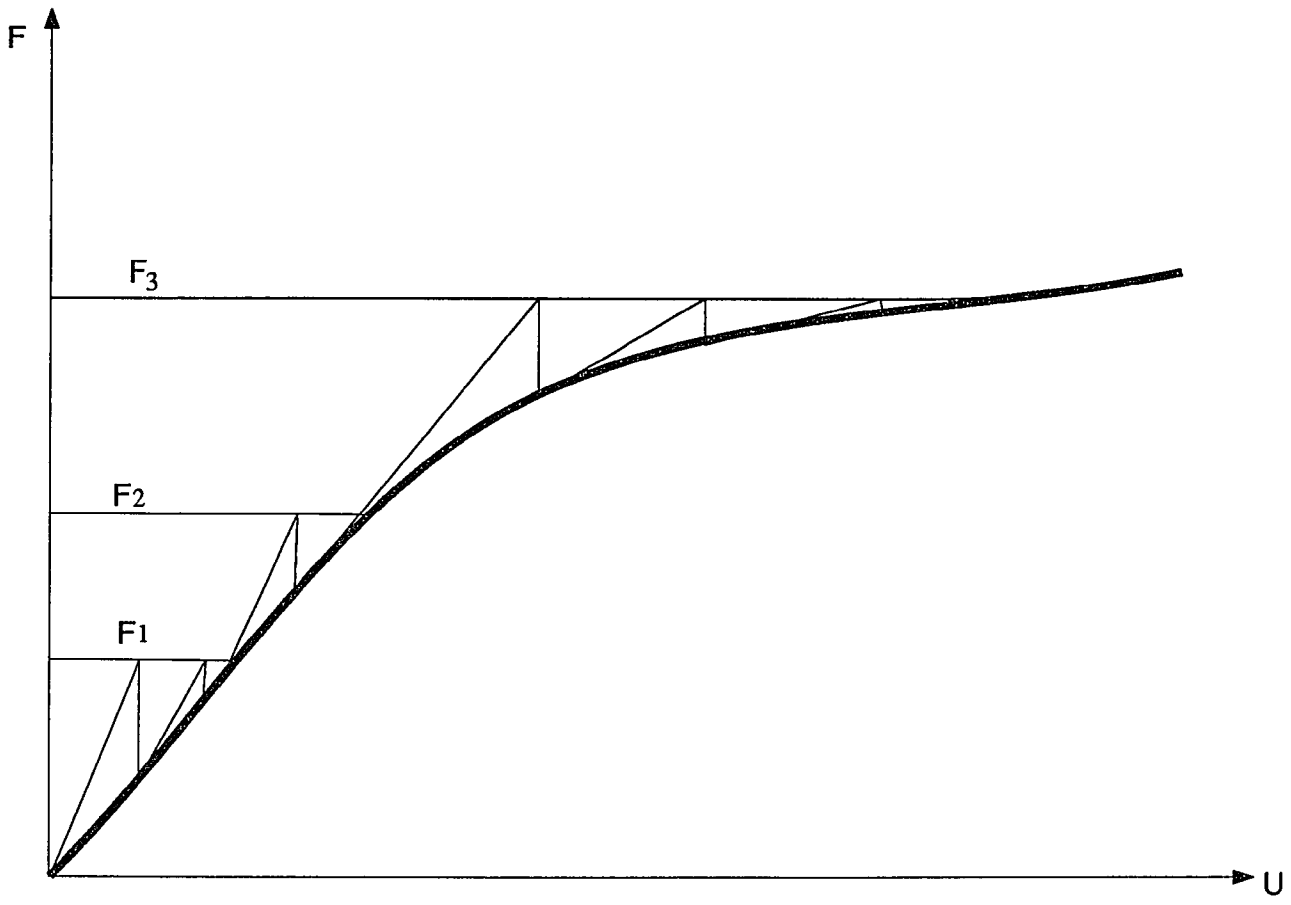

Figure A3.1 Incremental Newton-Raphson Procedure